Escuela Superior de Ingeniería y Tecnología

Escola Tècnica Superior d'Enginyeria Química

Trabajo Final de Máster

Máster en Mecánica de Fluidos Computacional

Optimización del diseño de las estructuras de entrada y salida de un decantador secundario mediante simulaciones CFD.

Secondary clarifier inlet/outlet structures optimization by the use of CFD simulations.

Presentado por: Gómez Rey, Alberto

Director/a: Martorell Masip, Benjamí

Fecha: 23 de Julio de 2019

Contents

Table of Figures

Index of Tables

Resumen

El presente trabajo estudia la influencia del diseño de las estructuras de entrada del fango activo (campana deflectora) y salida de agua tratada (posición y forma del vertedero de salida), en el rendimiento de un decantador secundario para el tratamiento de aguas residuales. El estudio se ha llevado a cabo a través de simulaciones CFD con el software openFoam, en las que se han analizado diferentes combinaciones de estructuras de entrada y salida.

Los resultados obtenidos muestran una gran influencia de estas estructuras en los campos de velocidad y la distribución de sólidos dentro del decantador, influyendo por tanto de manera decisiva sobre el rendimiento del decantador, tanto en lo referente a la extracción de fangos, como en lo que se refiere al contenido de sólidos en suspensión del efluente. Así mismo, se ha observado una gran influencia de los parámetros reológicos del fango y su densidad sobre los campos de velocidad obtenidos en las simulaciones.

Palabras Clave: CFD, openFoam, Decantación secundaria

Abstract

The present work studies the influence of the design of active sludge inlet structure (influent well) and treated water outlet structure (position and shape of effluent weir), in the performance of a secondary clarifier for waste water treatment. The study has been carried out through CFD simulations with the openFoam software, in which different combinations of input and output structures have been analysed.

The obtained results show a great influence of these structures in the velocity fields and the solids distribution inside the clarifier. These structures have shown to be a key factor regarding clarifier performance, both in transport and extraction of sludge, as well as in suspended solids content in the effluent. Results have shown a great dependency of flow fields on sludge density and rheologic properties.

Keywords: CFD, openFoam, Secondary clarification

1. Introduction:

1.1. Background

The goal of water and waste-water treatment, is to remove the pollutants from water to achieve the optimal conditions required for the intended purposes or to be released to the environment with the minimum impact. A big percentage of the pollutants in water and waste-water (WW) are in form of suspended solids, or can be converted from dissolved state into suspended solids by the use of chemicals, or by micro-organisms action.

The removal of the suspended solids from water is based on one of the following physical principles: density differences or particle interception.

Based on density differences, two main processes are used: sedimentation/clarification and flotation. For particle interception two main techniques are used: surface filtration and depth filtration.

The unitary process of clarification consists on the separation of suspended solids from water by gravity differences. This operation is normally performed in open tanks were the water is introduced, usually in an continuous mode, and maintained in laminar flow condition, reducing its velocity in order to allow suspended solids going to the bottom of the tank. In many cases suspended solids concentration and removal is also an important performance feature of the system, as it influences not only clarification performance, but also downstream sludge treatment.

In water treatment engineering, clarification is a very common operation used in several treatment stages of the process [1]:

- Drinking water treatment: clarification is used to remove residual suspended solids usually with the previous addition of chemicals (coagulant and floculant).

- Primary treatment (WW): clarification is used to remove suspended solids in raw waste-water.

- Secondary treatment (WW): clarification is used to remove activated sludge from water, usually this is the last stage of waste-water treatment, previous to the release into water bodies.

- Tertiary treatment (WW): clarification can be used to remove residual suspended solids usually with the previous addition of chemicals (coagulant and floculant).

Due to its spread use in water and waste-water treatment, clarification performance is a key point for the fulfilment of effluent water quality standards, and its correct design and operation can condition the proper performance of all the water treatment plant.

The previous reason joined to the lack of a deep knowledge of the performance of this equipments has motivated the present work. The availability of a such a powerful tool, as CFD can contribute to a better understanding of the flow fields involved in clarification processes.

1.2. Literature review

Several authors have studied clarifier performance by the use of CFD [2]. Kerbs *et al.* [3] suggested some inlet structures to minimize density currents effects, these authors recommended to introduce the mixture sludge water close to the bottom, for secondary clarifiers. They also recommended to implement an extra element, as interception bars or concentric slotted baffles, to reduce the potential energy. Krebs [4] also suggested that the installation of a baffle vertically in the bottom, at the middle of the clarifier length, would improve clarifier performance. Weiss *et al.* [5] implemented an asymmetric clarification model in the commercial solver Fluent 6. This model was used to study the flow field inside a circular clarifier, with special focus on the prediction of the TSS profile versus heigh. Sludge withdrawal was done through almost all the bottom of the clarifier, simulating an hydraulic suction type system. Dahl *et al.* [6] also presented a mathematical model used to simulate the flow field and TSS profiles inside a secondary clarifier.

Brennan developed the code setlingFoam; this code is the predecessor of driftFluxFoam used in the present work. In his thesis [7] Brennan explained the equations that forms the mathematical model and also gave some details about solver algorithm. Apart from model details, the author studied the influence of the rheological properties on the CFD simulations, and compared the simulation results with data obtained in lock exchange experiments. He also made several simulations of 2D and 3D rectangular settling tank, and compared the results with field data.

In the first part of his thesis, J De Clercq [8] made a review of clarifier simulation models, computational methods, and experimental techniques available for field data collection, including among others: velocity measurements, suspended solids, settling velocity, rheology parameters measurement, and particle size distribution. In a second part the author simulated the behaviour of a circular secondary settling tank with Fluent software by the implementation of a 2D axil-symmetric domain. The CFD results were confronted with field

data, TSS and Tracer test measurements. In his simulations J De Clercq found some difficulties with the scrapper simulation. Some other aspects as particle size distribution in the clarifier and sludge rheology properties were studied in his thesis. The author made an interesting experimental study regarding rheology of activated sludge, proposing a modified Herschel-Bulkley model for sludge simulation. He also studied the influence of rheological model on simulation results.

In [9] J De Clercq *et al.*, proposed a new 1D clarifier model. The partial differential equations were converted into a system of ODE, by the division of the clarifier into a number of layers. This model included one dispersion term, and a settling velocity function based on the Cho function [10].

Burt [11], in his thesis, studied the improvement of several circular secondary clarifier performance by the implementation of a center well lower baffle and a peripheral baffle. He used a 2D axis-symmetric model based on a drift-flux model. The author studied the influences of several variables, as turbulence model, sludge rheological properties, sludge transport in the clarifier floor, among others. He simulated a tracer test within the CFD model, and compared the results with data obtained in field test, showing good correlations. He also studied the influence of rheological model on simulations and compared them with the lock exchange test results over a synthetic latex sludge manufactured by himself. Finally he compared the CFD simulation results with experimental data, obtained at field before and after improvement solutions implementation.

1.3. Objectives

The objectives of the present work can be summarized as follows:

- Obtain a detailed insight of secondary clarifier performance, through the use of computational fluid dynamics (CFD) simulations.

- Study the influence of inlet baffle configuration on flow field and clarifier performance.

- Study the influence of effluent weir position and baffle configuration on flow field and clarifier performance.

- Analyse the obtained results in order to derive design recommendations for inlet and outlet internal structures.

2. Secondary clarification

2.1. Sedimentation theory

The objective of particulate matter sedimentation theory is to explain the movement of suspended solids dispersed in a fluid (continuous media), forced by gravity action due to density differences. The characteristics of this behaviour depends on the nature of suspended solids and the fluid within which they are moving. In this work we have considered water as the fluid and activated sludge as the dispersed phase.

Depending on suspended solids concentration and their physiochemical characteristics it can be established the following four different particle settling behaviours in waste-water treatment [1, 12]:

- Type I, discrete non-flocculent particle settling: dilute suspension of particles settle in a independent way with no interaction between them. It happens in low suspended solids concentration suspension as in sand and grit removal. Settling velocity is described by stokes law.

- Type II, flocculate settling: a dilute suspension of particles, due to its physiochemical nature tend to join with each other (flocculate) to form bigger particles that settle faster due to increased mass.

- Type III, hindered or zone settling: intermediate concentration suspension of particles, that interact with each other and form an structured matrix that settle together in a relative fixed position.

- Type IV, compression settling: a high concentrated solids suspension that has settled together in a structured matrix, concentrate further due to compression of the structure by the weight of the particles above them.

In secondary settling tanks, although type II, III and IV can happen, sedimentation type III governs the design [12]. In Type III settling, total suspended solids concentration (TSS) is much higher than in type I and II. Suspended solids, settle as a unit with uniform velocity, maintaining the relative position between them until the sludge blanket reach the bottom. At that time the sludge blanket start compression, increasing TSS, therefore reducing the volume occupied by the sludge.

2.2. Solid flux theory

Kynch [13], proposed the solid flux theory, based on the hypothesis that "at any point in a dispersion the velocity of fall of a particle depends only on the local concentration of particles", until there is an interaction between them, that leads to a density increase (see Figure 2.1). In this way, sedimentation velocity can be calculated from batch experiments at different initial concentration. Data obtained from theses experiments can be used to built a curve for zone settling velocity (v_s) versus suspended solids concentration (X), this is, a settling velocity function (see Figure 2.3).

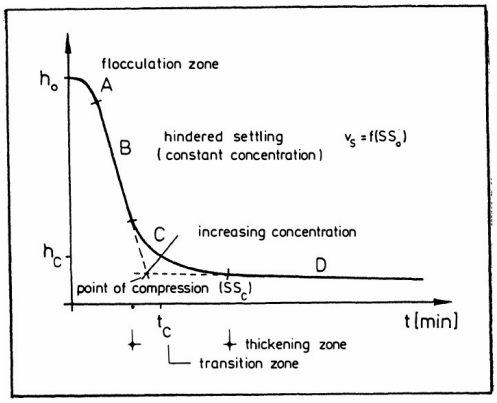

Figure 2.1
Settling curve of an activated sludge suspension (from [18])

Regarding the shape of this function, between the different proposal [7, 10, 14] the openFoam model used in the present work is based on the work of Takács [14].

2.2.1. Settling velocity:

Takács model is represented by the following formula:

$$v_s = v_0 e^{-r_h X^*} - v_0 e^{-r_p X^*} \quad ; \quad \text{with} \, 0 \le v_s \le v'_0 \tag{2.1}$$

where

v_s = settling velocity of the suspension,
v_0 = maximum settling velocity,
$X^* = X - X_{min}$; Xmin minimum attainable suspended solids concentration;
r_h = settling parameter characteristic of the hindered settling zone;
r_p = settling parameter characteristic of low solids concentration.

As It can be seen in Figure 2.2 Takács model distinguish between 4 different settling behaviors, function of suspended solids concentration:

- Region I: starting from 0 up to Xmin TSS, settling velocity is zero, this means that an small solid fraction is not able to settle so it will go away with the clarified effluent water.

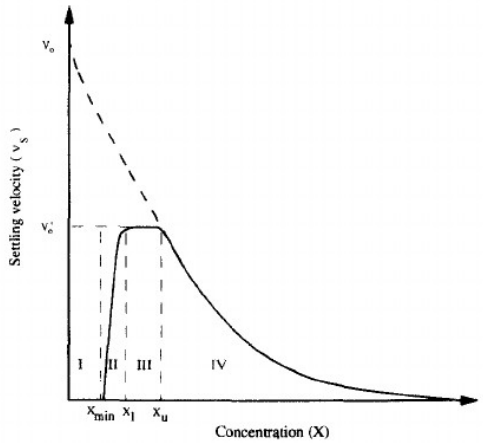

Figure 2.2
Takács settling velocity from [14]

- Region II: once TSS increases over Xmin, the settling velocity increases as TSS increases.

- Region III: settling velocity has reached a maximum, that is maintained in a TSS interval.

- Region IV: after the maximum, settling velocity decays with increasing TSS, until it reaches zero, at high concentration. In this region the settling behavior is identical to Vesiling model.

In openFoam 6, two settling models are available: simple model and general model (see Figure 2.3). General model is similar to Táckacs model, but it doesn't limit the maximum settling velocity [10, 15]. The code used can be located in the following route of the users installation:

"applications/solvers/multiphase/driftFluxFoam/relativeVelocityModels/general/ general.c

The code used in the model for drift velocity of dispersed phase is represented as follows:

```
Udm_ = (rhoc_/rho())*V0_* (exp(-a_*max(alphad_ - residualAlpha_, scalar(0)))
                           - exp(-a1_*max(alphad_ - residualAlpha_, scalar(0))) );
```

(2.2)

where:

Udm_	//relative velocity betwen phases
rhoc_	//continuous phase density
rho_	//mixture density: rho_=alpha1_*rhod_ + alpha2_*rhoc_;
a_	//Velocity exponent for region IV in Figure 2.2
a1_	//Velocity exponent for region II in Figure 2.2
residualAlpha_	//Non settleable suspended solids volumen fraction
V0_	//maximun sedimentation velocity

In reference [6] experimental data shows that settling velocity match Simple model shape. On the other hand in reference [16] sedimentation velocity is reduced at low concentration, so general model seems to be more suitable to describe settling velocity.

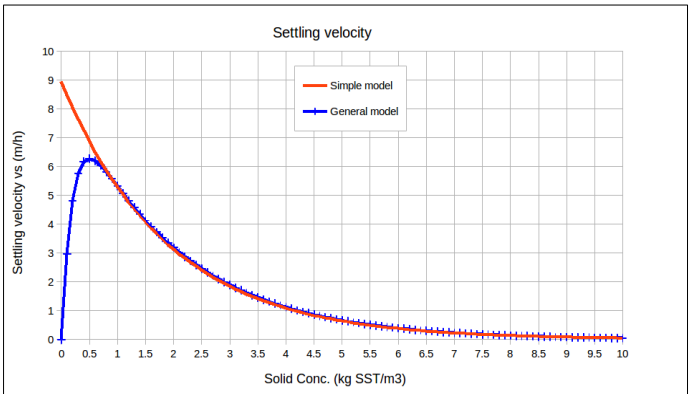

Figure 2.3
Settling velocity models available in openFoam 6

Experimental works show the hypothesis of the reduction in settling velocity at low concentration [9-10, 17-21].

2.2.2. Correlation between SVI and settling velocity

Sludge Volume Index, referred as SVI, is the volume occupied by a gram of sludge after 30 min of sedimentation, measured as ml/g [22]. Several authors [18], have studied the correlation of settling velocity of activated sludge with SVI in order to find a fast and easy way to find sludge settling characteristics. In Figure 2.4 it is shown several settling velocity curves calculated from different authors correlations, as indicated by Härtel and Pöpel [18], for the same SVI. The curves presented in Figure 2.4 are calculated according to Takács model, with $r_p=0.1*r_h$.

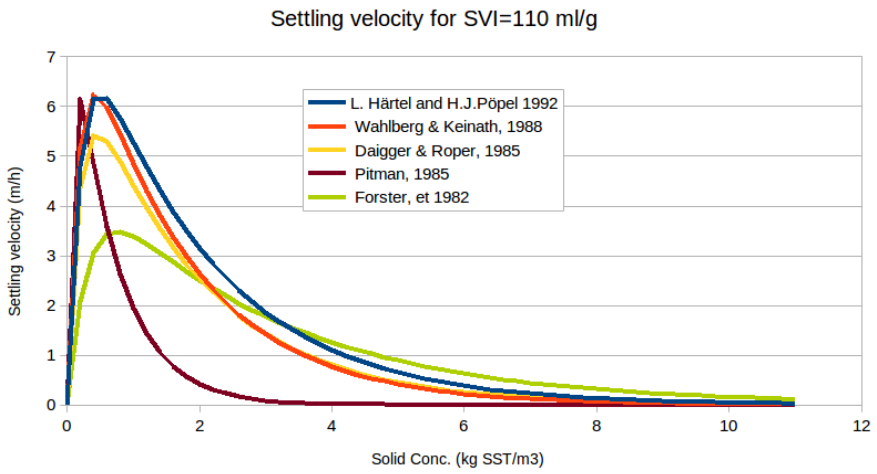

Figure 2.4
Different settling velocities correlations calculated for an activated sludge with SVI=110 ml/g

For the correlations showed before, the one of Härtel and Pöpel [18], will be used in the present study in order to calculate settling velocity of an activated sludge with SVI=110 ml/g.

2.3. Clarifier design approach

Regarding clarifier design procedures, two main streams exist: one based on solid flux theory followed mainly in English language speaking countries (UK, USA), and the other based on empirical correlations from field studies, whose main representatives are Germany and Netherlands, with their corresponding standard ATV and STORA.

The first stream uses solid flux theory to determine the required surface to avoid solid overload. Although it is based on a theoretical description of clarifier performances, that considers also the settling velocities as function of sludge quality, the obtained information is reduced to required area. Return sludge concentration can be also determined, without considering any dilution effect generated by the extraction mechanism or density currents generated. In any case this theory does not give any information about water deep, inlet configuration, baffle arrangements, weir locations, etc… Information regarding effluent suspended solids is not supplied either [23].

German approach (ATV standard) on the other hand is based on empirical relationships that also consider the sludge quality. With this standard is possible to calculate required area clarifier water deep, as well as return sludge concentration including possible diluting efffect of sludge collection mechanism. It also provides guidelines about bottom slopes and scrapper velocities. All this guidelines considers an effluent suspended solid concentration below 20 mg/l [24].

2.4. General characteristics and clarifier types

In previous paragraphs it has shown a brief introduction to solids settling theories, as well as available standards to calculate clarifier main dimensions. However, until the present moment, almost nothing has been mentioned about specific details in clarifier design. At the time of a clarifier design several options must be selected, regarding tank shape, input/output configuration, sludge removal mechanism, weir configuration,… In the Table 2.1 it is shown a variety of combinations that can be usually selected:

Apart from the option indicated in Table 2.1, some other design options are available as weir baffles, etc.. With such a big variety of options it is sometimes difficult to select the most appropriate combination of design factors that drives us to the best design condition. In this

sense apart from experience and testing, CFD tools can provide an essential insight in order to select the best design options. In Figure 2.5 it it shown some different flow patterns.

Tank shape	Inlet position	Water out position	Water out type	Sludge out position	Scrapper type
Circular (or polygonal prism shape)	Center	Peripheral	Weir Or Submerged tube	Center bottom	Mechanical
				All around bottom	Hydraulic suction
		Radial	Weir Or Submerged tube	Center bottom	Mechanical
				All around bottom	Hydraulic suction
	Peripheral	Center	Weir Or Submerged tube	Center bottom	Mechanical
				All around bottom	Hydraulic suction
Rectangular shape	Short wall 1	Short wall 2 (in fornt of wall 1)	Weir Or Submerged tube	Short wall 2 end	Mechanical
				Short wall 1 end	Mechanical
				Middle length	Mechanical
				All around bottom	Hydraulic suction
		1/3 end perpendicular to Short wall 2	Weir Or Submerged tube	Short wall 2 end	Mechanical
				Short wall 1 end	Mechanical
				Middle length	Mechanical
				All around bottom	Hydraulic suction

Table 2.1

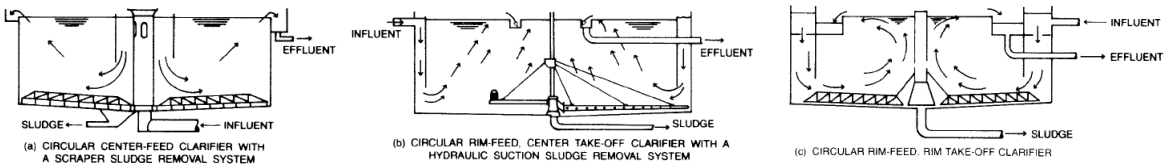

Figure 2.5
Some circular clarifier flow profiles, (from [12]

3. Sludge rheology

Sludge rheology has an important effect on density current decay, what in turn will influence the velocity field inside the clarifier [7] .

Ac. to Ratkovich *et al.* [25], activated sludge is usually modelled using the pseudoplastic power-law or Bingham plastic rheological models. The apparent viscosity which depends among others of TSS content and temperature, is the most critical parameter. In openFoam 6, for driftFluxFoam solver, plastic, slurry and BinghamPlastic models are available. In Figure 3.1 the shear stress / shear strain rate relationships for Newtonian and some non-Newtonianfluids are summarised. In the present work Bingham plastic model has been used with the standard parameters supplied in [7].

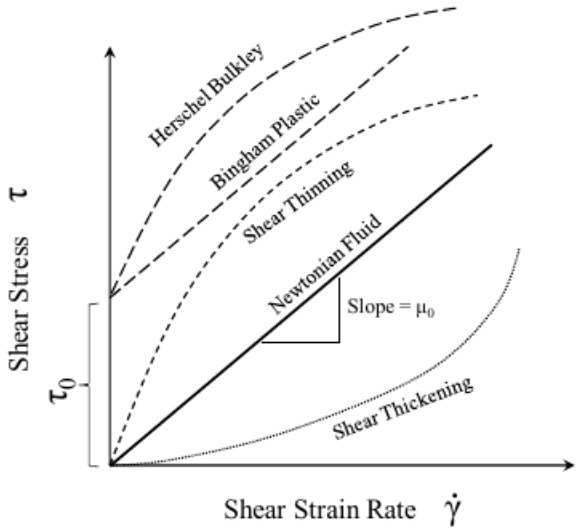

Figure 3.1
Shear stresses-shear strain rate diagram. Adopted from [11]

3.1. Bingham model

In the following paragraphs the Bingham model is described. This derivation has been taken from ref [8] and [11].

Apparent viscosity is calculated as:

$$\mu_m = \tau_{ij} / \dot{\gamma}_{ij} \tag{3.1}$$

where μ_m apparent mixture viscosity
τ_{ij} Stress tensor
$\dot{\gamma}_{ij}$ Strain rate tensor ;

Shear rate is the component of the stain tensor describing velocity gradients perpendicular to velocity direction.

Bingham model

$$\tau_{ij}=\left(\frac{\tau_0}{\dot{\gamma}}+k\right)\dot{\gamma}_{ij};\ \text{for}\ \tau\geq\tau_0$$
$$\dot{\gamma}_{ij}=0;\qquad\text{for}\ \tau<\tau_0 \tag{3.2}$$

Where: $\dot{\gamma}=\sqrt{\frac{1}{2}\dot{\gamma}_{ij}^2}$ Magnitude of the strain rate:

k is a fluid consistency index;
τ_0 plastic yield stress

Models with a yield stress (minimum shear stress required to initiate fluid strain), show an infinite apparent viscosity when the stress applies is below yield stress. To avoid this inconsistency in the flow field, several solutions have been proposed (see [8]).

In the Figure 3.2 it can be seen a real rheogram that shows the non existence of a plastic yield stress. This behaviour can be modelled through the perturbation model, among others.

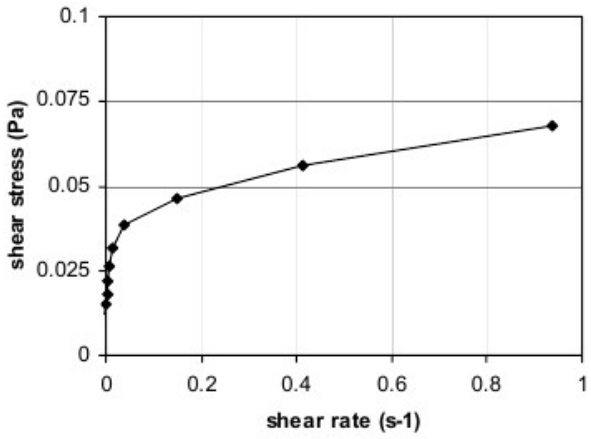

Figure 3.2
Typical rheogram for sludge. From [8]

Implementation of Bingham Model in openFoam 6 can be found in archive "BinghamPlastic.C".

4. Mathematical model of two phase flow

Multiphase flows are present in many engineering applications, in particular we can find many examples in water treatment; for instance: primary and secondary clarification (solid-liquid phases), dissolved air flotation (solid-liquid-gas phases), activated sludge aeration (solid-liquid-gas phases), fluidized bed reactors (UASB) (solid-liquid-gas phases), etc…

The main difficulties in modelling multiphase or multicomponent flows relies on the presence of a deformable moving inter-phase, with fluctuating variables and discontinuities at the inter-phase [2].

In order to describe the performance of this kind of flows, different approaches can be used [7]:

- Euler-Lagrange approach: each particle trajectory of the dispersed phase is tracked individually through the flow domain. The momentum equation is formulated in coordinates that follows the particle trajectory.

- Euler-euler approach [26]: in this approach the phases are treated as a inter-penetrating continua with a connecting inter-phase. The concept of volume of fraction of each phase (α_k) is introduced. The sum of α_k of all phases present is equal to 1.

* Multi phase model: the mathematical description of this model, considers a set of equations (mass, momentum and energy conservation) for each phase separately. An interacting force between phases is introduced in the momentum equation. This interfacial interaction between phases incorporate mathematical complications and uncertainty [27].

* Mixture model (diffusion model): the mathematical description of this model, considers only 1 set of equations (mass, momentum and energy conservation) for the mixture as a whole plus one additional transport equation (Diffusion equation or Dispersed phase continuity equation), which takes account for the concentration changes. Additionally constitutive equations for relative velocities between phases are included. The mixture properties are defined according to the properties of each phase the corresponding phase fraction (α_k) present in the mixture. The drift-flux model is an example of a mixture model that includes diffusion model, slip flow model and homogeneous flow model [28]. The use of the drift-flux model is appropriate when the motions of two phases are strongly coupled [27].

In the case of settling tanks an experimental settling velocity is used to model the relative velocity between solid and liquid phase velocity (see section 2.1).

* The Volume Of Fluid (VOF) model can model two or more immiscible fluids, it considers only considers only 1 set of equations (mass, momentum and energy conservation) plus one additional equation for volumetric fraction tracking, modelled as a scalar transport equation.

In the present work the drift-flux model implemented in the software openFoam [15] will be used. In the following section, only mathematical formulation of this model will be described. Acc. to Ishii *et al.*[28], for most practical applications, the drift-flux model is the best mixture model that is highly developed for normal gravity as well as microgravity conditions.

4.1. Drift-flux model

In the following section the drift flux model equations are presented. The formulation that follow is based on the center of mass and Drift-flux Velocities. These equations are extracted from [1, 15, 28].

4.1.1. Equations of State and Mixture Properties

Phase fractions: $\alpha_1+\alpha_2=1$ (α is volume fraction) (4.1)

Mixture density: $\rho_m=\alpha_1\rho_1+\alpha_2\rho_2$ (4.2)

Mixture pressure: $P_m=\alpha_1 P_1+\alpha_2 P_2$ (4.3)

Velocity for mixture centre of mass: $\boldsymbol{U_m}=\frac{\alpha_2\rho_2\boldsymbol{U_2}+\alpha_1\rho_1\boldsymbol{U_1}}{\rho_m}$ (4.4)

4.1.2. Kinematic Constitutive Equations.

Relative velocity *of phase 1 to phase 2:* $\boldsymbol{U_r}=\boldsymbol{U_1}-\boldsymbol{U_2}$ (4.5)

Diffusion velocity *or* velocity of phase k relative to velocity for mixture centre of *mass:* $\boldsymbol{U_{km}}=\boldsymbol{U_k}-\boldsymbol{U_m}$; k=1,2 phases (4.6)

Introducing (4.2) and (4.6) into (4.4), the following relationship for the diffusion velocity is obtained:

$\alpha_1\rho_1\boldsymbol{U_{1m}}+\alpha_2\rho_2\boldsymbol{U_{2m}}=0$ (4.7)

Only one diffusion velocity is required $\mathbf{U_{km}}$, by a kinematic constitutive equation. The diffusion velocity is defined as:

$$\boldsymbol{U}_{2m}=-\frac{\alpha_1\rho_1}{\alpha_2\rho_2}\boldsymbol{U}_{1m}=-\frac{\alpha_1\rho_1}{\rho_m}(\boldsymbol{U}_1-\boldsymbol{U}_2) \tag{4.8}$$

Drift velocity of the phases:

$$\boldsymbol{U}_{1d}=-\alpha_2\boldsymbol{U}_r \tag{4.9}$$

$$\boldsymbol{U}_{2d}=\alpha_1\boldsymbol{U}_r \tag{4.10}$$

Relationship between the **diffusion velocity** $\boldsymbol{U}_{km}$ and the **drift velocities** $\boldsymbol{U}_{kd}$

$$\boldsymbol{U}_{2m}=\frac{\rho_1}{\rho_m}\boldsymbol{U}_{2d}=-\frac{\alpha_1\rho_1}{\alpha_2\rho_m}\boldsymbol{U}_{1d} \tag{4.11}$$

$$Total\ volumetric\ flux: \quad \boldsymbol{J}=\alpha_k\boldsymbol{U}_k \qquad ; \quad \text{with k:1,2} \tag{4.12}$$

4.1.3. Transport Equations

Mixture Continuity equation:

$$\frac{\partial\rho_m}{\partial t}+\frac{\partial(\rho_m U_{m,i})}{\partial x_j}=0 \tag{4.13}$$

Diffusion equation or Dispersed phase continuity equation:

$$\frac{\partial\alpha_2\rho_2}{\partial t}+\frac{\partial(\alpha_2\rho_2 U_{m,i})}{\partial x_j}=-\frac{\partial(\alpha_2\rho_2 U_{2m,i})}{\partial x_j} \tag{4.14}$$

Mixture momentum equation:

$$\frac{\partial(\rho_m U_{m,i})}{\partial t}+\frac{\partial(\rho_m U_{m,i}U_{m,j})}{\partial x_j}=-\frac{\partial P_m}{\partial x_i} \tag{4.15}$$

$$+\frac{\partial}{\partial x_j}\left[\underbrace{\alpha_k\tau_{k,ij}}_{viscous\ stress\ \tau}+\underbrace{\alpha_k\rho_k u'_{k,i}u'_{k,j}}_{turbulent\ stress\ \tau_t}-\underbrace{\alpha_k\rho_k U_{km,i}U_{km,j}}_{difussion\ stress\ \tau_{dm}}\right]+\rho_m g_{m,i}+\underbrace{M_{m,i}}_{capillary\ force}$$

Where k= 1, 2 (phases 1 and 2)
I,j=1,2,3
M_m: capillary force, that takes into account the surface tension effects as a Momentum sink or source
$u'_{i\,k}$ velocity fluctuation

Diffusion stress: this represents the momentum diffusion due to relative motion between the two phases.

4.1.4. Relative velocity model

Relative velocity model used to describe the slip velocity between solid phase (activated sludge) and water is defined as settling velocity. Settling velocity of the solid phase depends on the suspended solid fraction, and also on sludge characteristics. The details of this settling velocity are presented in section 2.2.1.

4.1.5. Turbulence modelling

In two phase flow the presence of a second phase normally with higher density, makes buoyancy a mayor force that affects turbulent kinetic energy not only its dissipation but also its generation in case of inverted density stratification [7]. In driftFluxFoam turbulence is modelled through a “buoyant modified k-ε model”. The reader can refer to Brennan [7] for further information.

5. Physical model and simulation set up

5.1. Secondary clarifier design

Due to the limited time for the development of the present study only circular clarifier with center well feed, and center sludge purge will be studied. Two positions for effluent outlet weir will be studied: perimeter and 1/3 of diameter. Although we did not find data for Europe, Bender and Crosby declares in [29] that “most activated sludge facilities in the United States uses center-feed, peripheral overflow, circular clarifier”.

As a base point for simulations, the standard ATV-a131 [24] was chosen. This standard is a recognized international protocol that includes design equations and recommendation for activated sludge process design including biological reactor and secondary clarifier.

The geometry must comply the following conditions:

- It must be representative of a real design including size and shape, so obtained results can be used in real designs.

- Time required for each simulation must be short enough, so it is possible to perform a reasonable number of simulations during the time available for this master work.

According to ATV-a131 [24] , the surface overflow rate must be selected depending on the suspended solids concentration (TSS) in the influent, sludge sedimentation characteristics (SVI), and clarifier flow type (horizontal/vertical). This standard considered the clarifier flux predominantly horizontal if:

$$\frac{\text{vertical distance from inlet to water surface}}{\text{horizontal distance from inlet to outlet}} < 1/3$$

In any case, if diameter is less than 20m, clarifier must be designed as vertical flux secondary clarifier. Depending on the mentioned ratio, a maximum sludge loading rate (q_{sv}) must be selected.

In horizontal settling tank flux type, an influent disturbance length is considered in the design. This length is considered equal to side wall depth of the tank. In the design adopted in the present work, the diameter used is 16.4 m (<20m), so vertical flow must be adopted. Nevertheless as Vertical/Horizontal coefficient is equal to 1/3, it has decided to include disturbance length in the adopted diameter.

The following parameters and dimensions have been selected (see Table 5.1):

Secondary clarifier design parameters	
Design Influent flow (m^3/h)	200
Recirculation flow (m^3/h)	150
Total Influent flow to clarifier (m^3/h)	350
Influent Suspended Solids (g/m^3)	3.28
SVI (ml/g)	105
Sludge volume loading rate q_{SV} (l/m^2h)	400
Surface overflow rate q_A (m/h)	1.16
Required total diameter (m)	16.30
Adopted total diameter (m)	16.40
Required total vertical height at side (m)	3.42
Adopted total vertical height at side (m)	3.50

Table 5.1

The operation conditions of the designed clarifier have been verified by the solid flux theory. In Figure 5.1 we show two solid flux curves:

- Black line represents solid flux line for an activated sludge with SVI=105. Settling parameters have been calculated according to Härtel and Pöpel correlation [18] (see chapter 2.2). The calculated settling values are: v0=9.24 m/h, rh=0.51, r=10*rh (see ec (2.1))

- Gray line represents solid flux line for an activated sludge with same SVI, but the settling parameters have been adapted to ec (2.2), were the solid content is expressed in volume fraction. So in this case settling parameters are: V0_=9.24 m/h, a=524, r=10*rh.

Blue line represents the underflow rate line. If this line does not cross solid flux curve for a concentration greater to influent concentration, then the system is not overloaded. As it is shown in Figure 5.1 the system is operating very close to the critical condition, so the safety margin is almost zero. Under these conditions, depending on the hydraulic structures design the system can suffer a failure condition, with the lack of capacity for enough sludge removal.

In the Figure 5.2 the general dimensions of model rev1.1_refined_9 are shown. Apart from the modifications to influent center well, baffles and outlet weir, all other general dimensions are the same for all the studied models.

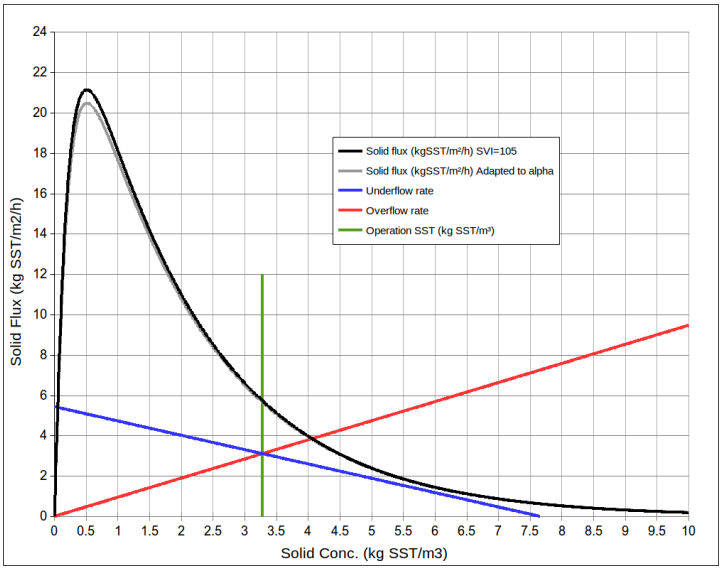

Figure 5.1
Solid flux representation for the system design conditions

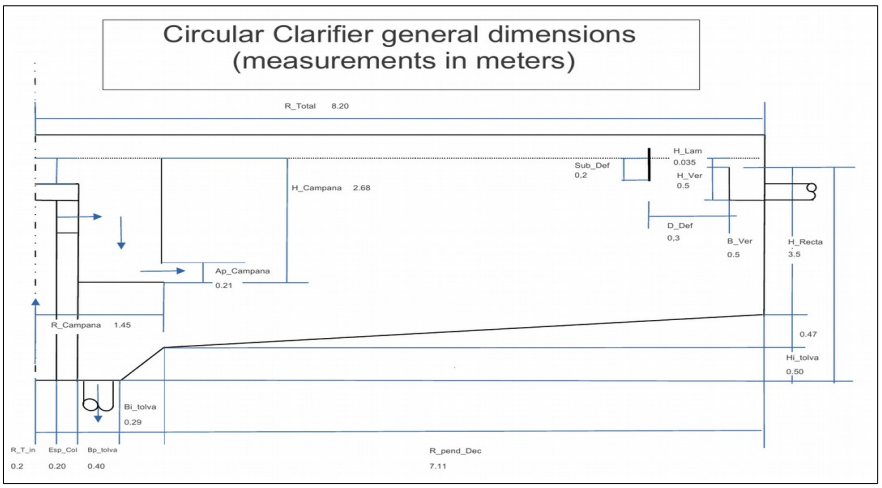

Figure 5.2
Clarifier model dimensions

5.2. Experiment matrix for simulations

In the Table 5.2 it is shown the experimental matrix with the different simulations to be performed. The objective is to cover different number of combinations of inlet-outlet structures in order to find the design with the best performance, this matrix has been adapted during the study according to the results obtained in the simulations.

		Weir				
		Shape: Standard-inside **Position:** Perimeter **Additional baffle:** NO	**Shape:** Standard-outside **Position:** Perimeter **Additional baffle:** Double angle Position middle	**Shape:** Standard-outside **Position:** Perimeter **Additional baffle:** Double angle Position up	**Shape:** Standard-inside **Position:** 1/3 diameter **Additional baffle:** NO	**Shape:** Standard-outside **Position:** Perimeter **Additional baffle:** Single angle Position up
Center well + Influent baffle	**Center well:** Straight-Narrow **Center lower baffle:** Horizontal-Normal	rev1.1_refined9				
	Center well: Straight-Narrow **Center lower baffle:** Horizontal-Long	rev6_refined10	rev6_1_refined10	rev6_2_refined10	rev6_3_refined10	
	Center well: Straight-Narrow **Center lower baffle:** Horizontal-Normal + Inclined Baffle	rev2_refined9				
	Center well: Straight-Narrow **Center lower baffle:** Horizontal-Long **Middle baffle:** vertical 1	rev12_refined10				
	Center well: Straight-Narrow **Center lower baffle:** Horizontal-Long **Middle baffle:** vertical 2	rev12_1_refined10				
	Center well: Straight-Narrow **Center lower baffle:** NO	rev4_refined9				
	Center well: Straight-wide **Center lower baffle:** NO	rev7_refined10_1				
	Center well: Straight-wide-Short **Center lower baffle:** NO	rev10_refined10				
	Center well: Straight Narrow +Inclined end 1 **Center lower baffle:** Horizontal-Short + Inclined Baffle 1	rev3_refined9				
	Center well: Straight Narrow +Inclined end 1 **Center lower baffle:** Horizontal-Short + Inclined Baffle 2	rev9_refined10				
	Center well: Straight Narrow +Inclined end 2 **Center lower baffle:** Horizontal-Short + Inclined Baffle 1	rev11_refined10		rev11_2_refined10	rev11_3_refined10	Rev11_4_refined10
	Center well: Straight Narrow +Inclined end 2 **Center lower baffle:** Horizontal-Short + Inclined Baffle 3					Rev11_5_refined10
	Center well: Straight Narrow +Inclined end **Center lower baffle:** NO	rev5_refined9				

Table 5.2
Experiment matrix

6. Modelling

6.1. Software

For the development of the present study the following software has been used:

* **gmsh**: version gmsh-4.2.3-Linux64, for geometry and mesh development

* **openFoam**: version openFoam 6 (this work was started with version 3.0; however, due to issues in the relative velocity model, it was decided to upgrade to the latest version).The solver used is driftFluxFoam.

* **ParaView**: version 5.4.0 64 bit, for post-processing.

* LibreOffice Version: 6.2.3.2

All the software packages used in the present study are openSource and free licence software.

6.2. Initial and Boundary conditions (B.C.) implementation

Due to limited computational resources, it was decided to simulate the system in 2D, with axil-symmetric boundary condition in z plane. The geometry is specified as a wedge of angle 2º, and 1 cell thick.

Figure 6.1 shows names for model 1.1_rev9. These names are the same for all the models apart from those cases where additional baffles have been included. In Table 6.1 boundary conditions are specified for all the patches. In the following paragraphs some of the more remarkable features are mentioned:

For 2D axil-symmetry simulation, wedge boundary condition is used in both symmetry planes, for all variables.

Free surface of secondary clarifier can be modelled with slip boundary condition in all variables except p_rgh.

Velocity (flow) is fixed in *inlet* and *Outlet_Sludge*, while in *Outlet_Water* velocity is calculated through the use of “pressureInletOutletVelocity” boundary condition.

All physical walls, apart form *Pend_Dec*, are treated with no slip condition, so velocity is fixed as 0.

A fixed translating velocity, was imposed to the the bottom of the clarifier (*Pend_Dec*) in order to simulate the bottom scrapper, that move the sludge from all the surface up to the hopper.

Pressure: driftFluxFoam solver uses p_rgh, defined as: p_rgh = p-rho*gh;

Pressure B.C. is fixed as fixedFluxPressure is all the patches except, symmetry planes, and Outlet_Water. According to openFoam Users Manual [30] “This boundary condition is used for pressure in situations where zeroGradient is generally used, but where body forces such as gravity and surface tension are present in the solution equations”. See also [31].

Alpha.sludge defines the suspended solids contents, as a volumetric fractions. For the simulations performed the following inlet value has been used:

$$[MLSS] = 3.28\frac{g_{sludge}}{l_{total}}; \quad \Rightarrow alpha.slude = \frac{3.28\left(g_{sludge}/l_{total}\right)}{1042\left(g_{sludge}/l_{sludge}\right)} = 0.00315\frac{l_{sludge}}{l_{total}}\left(volume\ fraction\right)$$

Regarding turbulence model, wall functions were used, apart from inlet/outlet boundary conditions (see Table 6.1).

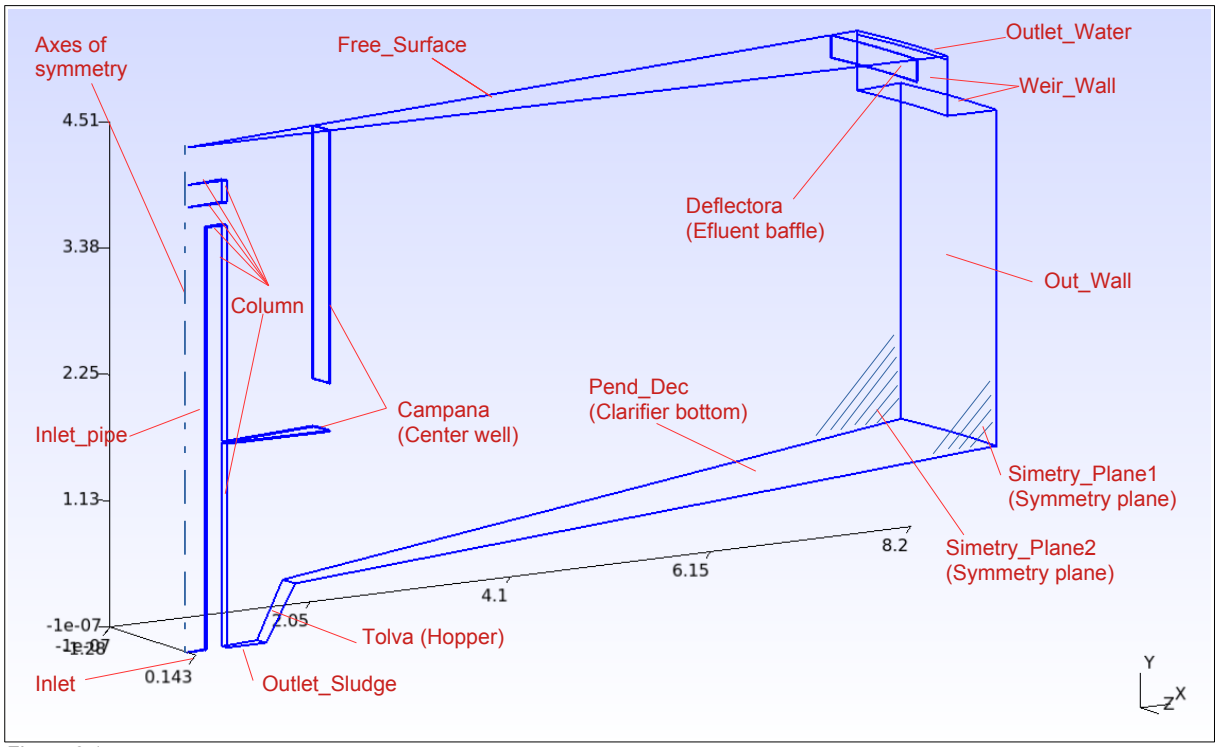

Figure 6.1
Model 1.1_rev9, patch names

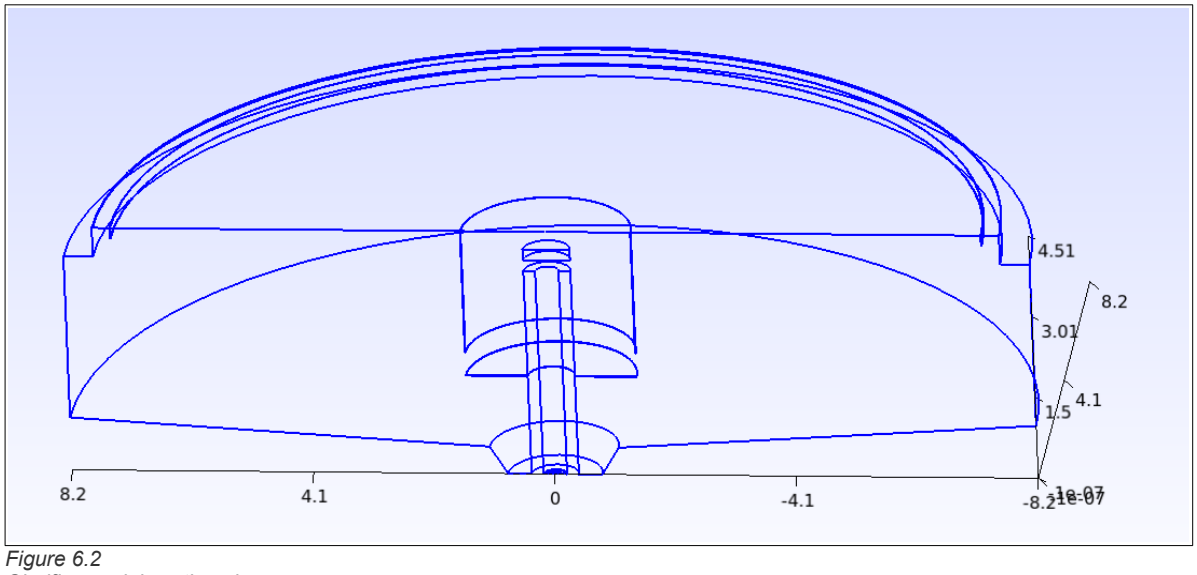

Figure 6.2
Clarifier model section view

Patch name	U	p_rgh	alpha.sludge	k	ε	μ_t
Simetry_Plane1	wedge	wedge	wedge	wedge	wedge	wedge
Simetry_Plane2	wedge	wedge	wedge	wedge	wedge	wedge
Inlet	type fixedValue; value uniform (0 0.7737 0);	type fixedFluxPressure; value uniform 0;	type fixedValue; value uniform 0.00315;	type fixedValue; value uniform 0.000259;	type fixedValue; value uniform 1.973e-07;	type calculated; value $internalField;
Free_Surface	slip	type fixedFluxPressure; value uniform 0;	slip	slip	slip	slip
Column	type fixedValue; value uniform (0 0 0);	type fixedFluxPressure; value uniform 0;	zeroGradient;	type kqRWallFunction; value $internalField;	type epsilonWallFunction; value $internalField;	type nutkWallFunction; value $internalField;
Inlet_pipe	type fixedValue; value uniform (0 0 0);	type fixedFluxPressure; value uniform 0;	zeroGradient;	type kqRWallFunction; value $internalField;	type epsilonWallFunction; value $internalField;	type nutkWallFunction; value $internalField;
Campana	type fixedValue; value uniform (0 0 0);	type fixedFluxPressure; value uniform 0;	zeroGradient;	type kqRWallFunction; value $internalField;	type epsilonWallFunction; value $internalField;	type nutkWallFunction; value $internalField;
Outlet_Sludge	type fixedValue; value uniform (0 -0.02763107 0);	type fixedFluxPressure; value uniform 0;	type inletOutlet; inletValue uniform 0;	type inletOutlet; inletValue uniform 0.000259;	type inletOutlet; inletValue uniform 1.973e-07;	type calculated; value $internalField;
Tolva	type fixedValue; value uniform (0 0 0);	type fixedFluxPressure; value uniform 0;	zeroGradient;	type kqRWallFunction; value $internalField;	type epsilonWallFunction; value $internalField;	type nutkWallFunction; value $internalField;
Pend_Dec	type translatingWallVelocity; U (-0.003 0.0 0.003); value uniform (-0.003 0.0 0.003);	type fixedFluxPressure; value uniform 0;	zeroGradient;	type kqRWallFunction; value $internalField;	type epsilonWallFunction; value $internalField;	type nutkWallFunction; value $internalField;
Out_Wall	type fixedValue; value uniform (0 0 0);	type fixedFluxPressure; value uniform 0;	zeroGradient;	type kqRWallFunction; value $internalField;	type epsilonWallFunction; value$internalField;	type nutkWallFunction; value $internalField;
Weir_Wall	type fixedValue; value uniform (0 0 0);	type fixedFluxPressure; value uniform 0;	zeroGradient;	type kqRWallFunction; value $internalField;	type epsilonWallFunction; value $internalField;	type nutkWallFunction; value $internalField;
Outlet_Water	type pressureInletOutletVelocity; value uniform (0 0 0);	type fixedValue; value uniform 0;	zeroGradient;	type zeroGradient;	type zeroGradient;	type calculated; value $internalField;
Deflectora	type fixedValue; value uniform (0 0 0);	type fixedFluxPressure; value uniform 0;	zeroGradient;	type kqRWallFunction; value $internalField;	type epsilonWallFunction; value $internalField;	type nutkWallFunction; value $internalField;

Table 6.1
Model boundary conditions

6.3. Equations discretization schemes

In order to configure the simulation, tutorial tank3D (available in openfoam6/tutorials/multiphase/driftFluxFoam/RAS/tank3D) was used as starting point. Although this case works properly with the default discretization schemes of tutorial case in version 3.0, it didn't work properly in version 6. Simulation started but after some steps, deltaT started decreasing, until system crashed. After some optimization test stable discretization parameters were found. These are specified in third column of Table 6.2 .

	tank3D	**rev1.1_refined9**
ddtSchemes	Euler	Euler
gradSchemes	Gauss linear	Gauss linear
divSchemes		
div(rhoPhi,U)	Gauss linearUpwind grad(U)	Gauss linearUpwind grad(U)
div(tauDm)	Gauss linear;	Gauss linear;
"div\(phi,alpha.*\)"	Gauss vanLeer;	Gauss vanLeer;
"div\(phirb,alpha.*\)"	Gauss linear;	Gauss linear;
div(rhoPhi,k)	Gauss limitedLinear 1;	**Gauss upwind;**
div(rhoPhi,epsilon)	Gauss limitedLinear 1	**Gauss upwind;**
div(((rho*nuEff)*dev2(T(grad(U)))))	Gauss linear;	Gauss linear;
laplacianSchemes	Gauss linear corrected;	Gauss linear corrected;
interpolationSchemes	linear;	linear;
snGradSchemes	corrected;	corrected;

Table 6.2

Comparative discretization schemes between tutorial tank3D and the model used in the present study.

6.4. Mesh implementation and mesh independence analysis

Model geometry as well as mesh implementation was developed with the software gmsh. Acc. to "Gmsh Reference Manual" [32], "Gmsh is a three-dimensional finite element grid generator with a build-in CAD engine and post-processor". This software was used to perform geometries and mesh. Meshing tool allowed structured and unstructured meshing (or a mixture of both) in 1D, 2D and 3D, with an important control over the mesh generation process.

In the present work a mixture of structured and unstructured mesh was used. The starting point was half of the axil-section view of the clarifier. From the global clarifier domain, it was generated 2 additional layers to the inside of the domain in order to stablish an structured mesh in the walls and patches, and an unstructured mesh inside the domain. Between them a transition unstructured domain (yellow mesh in Figure 6.3) was added in order to control more accurately both: the mesh size at the wall and the mesh size in the bulk

liquid, inside domain. In Figure 6.3 this features can be appreciated. In annex III, there is an example of an archive created to generate the geometry and mesh in the present job.

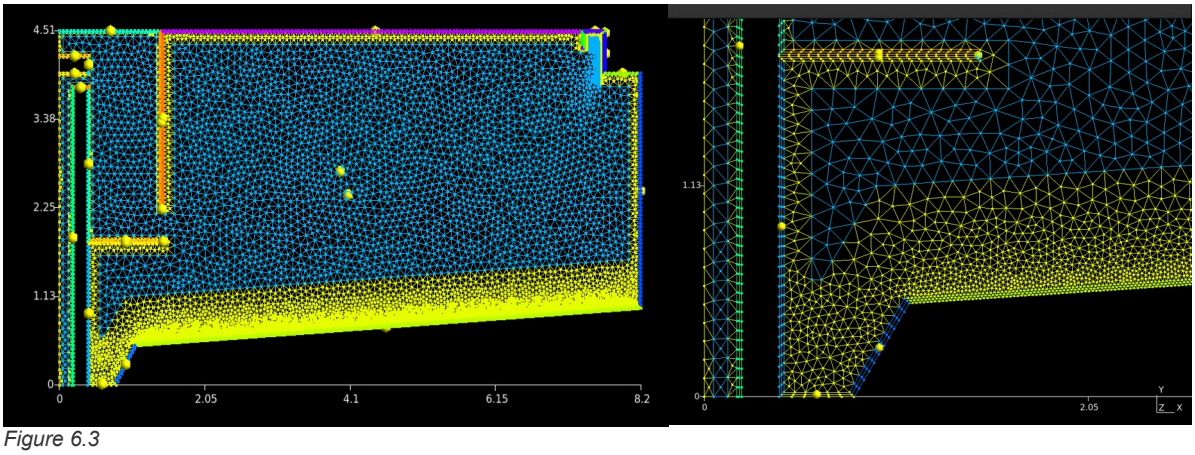

Figure 6.3
Model rev1.1_refined9: mesh layers detail, left: general view., rigth: sludge hopper detail.

6.4.1. Mesh independence analysis

In order to perform a mesh independence analysis case ”rev6_refined10” was selected. From this case mesh size was refined (case ”rev6_refined11_1”), obtaining the results shown inTable 6.3. Refined mesh has more than double number of cells, while maximum cell volume is almost the same, minimum volume cell is reduced one order of magnitude.

Figure 6.4 illustrates the differences between both meshed. From Figure 6.5 to Figure 6.8 we can see the comparative results of the simulation for coarse and refined mesh, under the same simulation conditions. In general solid contours, velocity contours and turbulence kinetic energy contours shows a similar shape for both cases. We can focus mainly in two differences:

- Low solids profile: in Figure 6.6 we can see a small difference in the TSS cloud located in the top section, of the last half part of the clarifier. While coarse model shows a alpha around 3.1 e-05 in that area, refined model shows an alpha around 5.0 e-05.

- Flow at the entrance from the well to the open area: in Figure 6.7 and Figure 6.8 we can see a difference in the flow field just in the entrance of the sludge form the well to the open area of the clarifier. In refined model the current that moves the sludge to the hopper at the bottom of the tank (at x=2 m) goes up and impact with the currents from center well. This phenomenon happens in both simulations, but in refined model the deviation of the incoming current is more pronounced. In respect to the flow field in the rest of the clarifier, not only the shape but also the magnitude is similar in both cases.

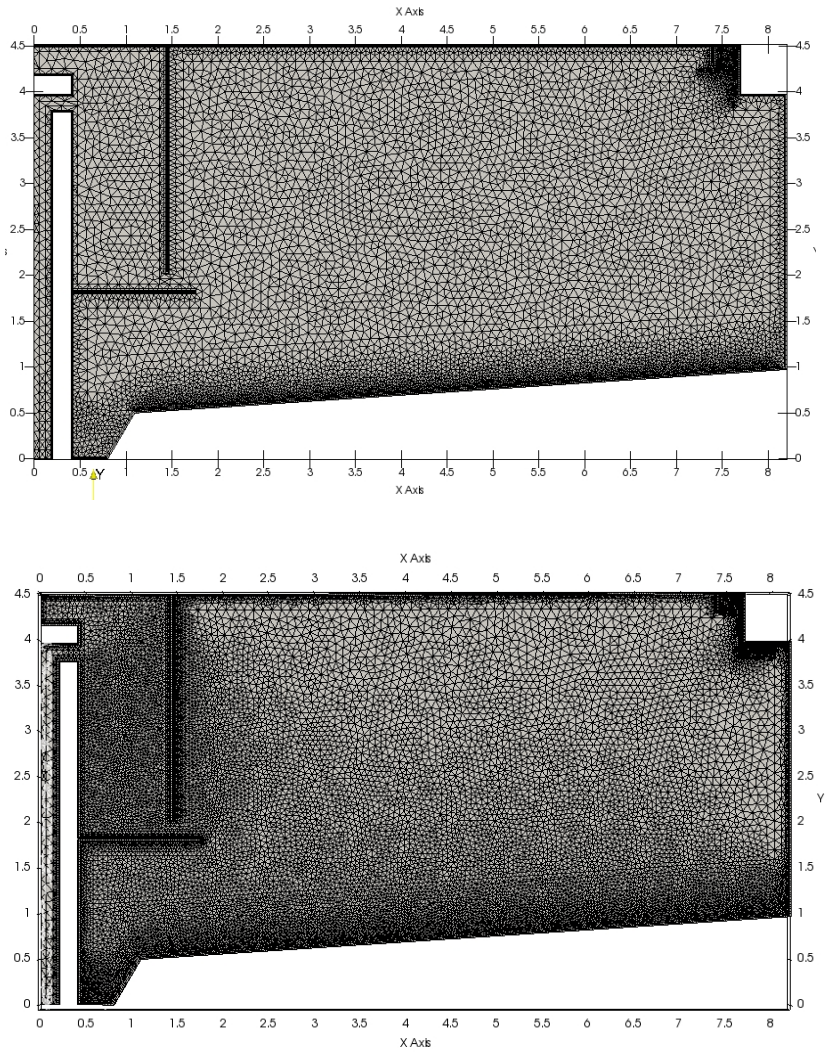

Figure 6.4
Case rev6_refined10 mesh (top) and case rev6_refined11_1 mesh(bottom)

Regarding simulation time, coarse model took 4472 real seconds to simulate 1000 sec, while refined mesh, took 21880 real seconds to simulate the same period, this means 4.9 times more for refined version.

Considering the original objective of simulating the maximum number of combinations inside the experimental frame fixed for this work, it was decided to use the "coarse mesh" version for the development of all the simulations. In view of the obtained results for both meshed presented, the results from a quantitative point of view should be taken with care. In any case in view of the complexity of the mathematical model used to describe activated sludge sedimentation, as well as the uncertainty about numerous model parameters, an

experimental verification of the obtained results is required before consider the same as valid. Specially if reliable quantitative data are required.

Mesh stats	rev6_refined10 (coarse)	rev6_refined11_1(refined)
points:	19059	39114
faces:	57999	123437
cells:	16165	34636
Min volume	3.29069e-07	4.55601e-08
Max volume	0.00178495	0.00179006
Total volume	4.28393	4.28393
Mesh non-orthogonality Max:	54.5483	49.8874
Mesh non-orthogonality average:	15.0132	12.9139
Max skewness	2.34614	2.14228

Table 6.3
Main Mesh parameters for original and refined model

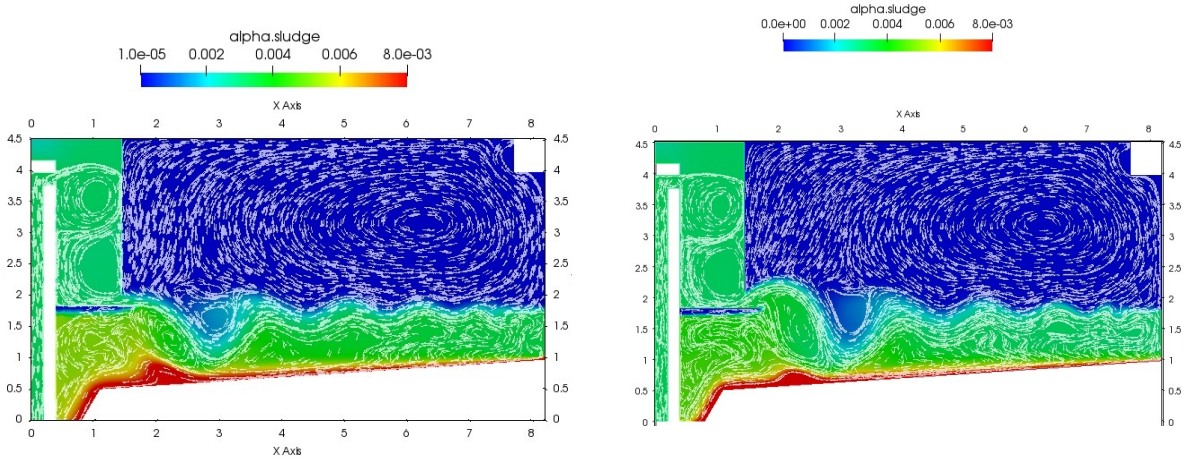

Figure 6.5
Low range TSS contour, left case rev6_refined10, right case rev6_refined11_1

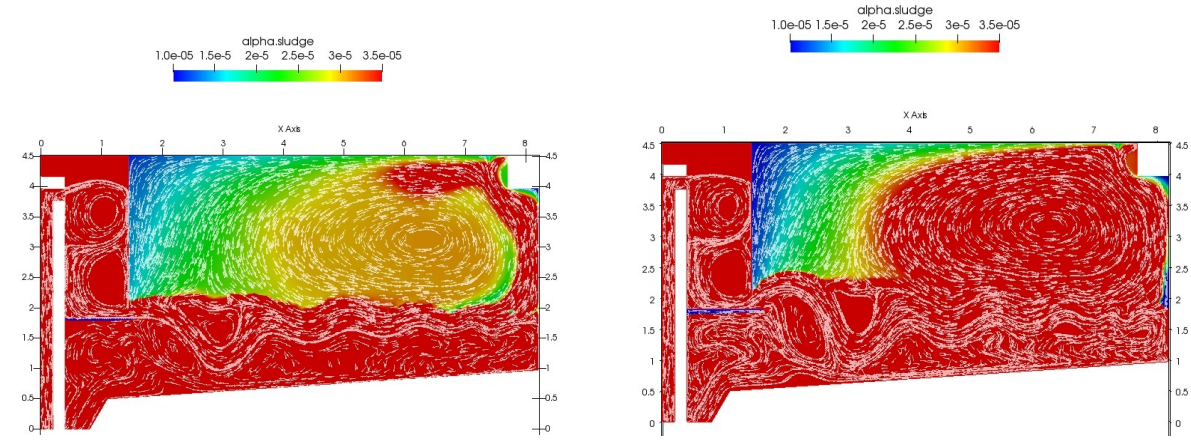

Figure 6.6
Low range TSS contour, left case rev6_refined10, right case rev6_refined11_1

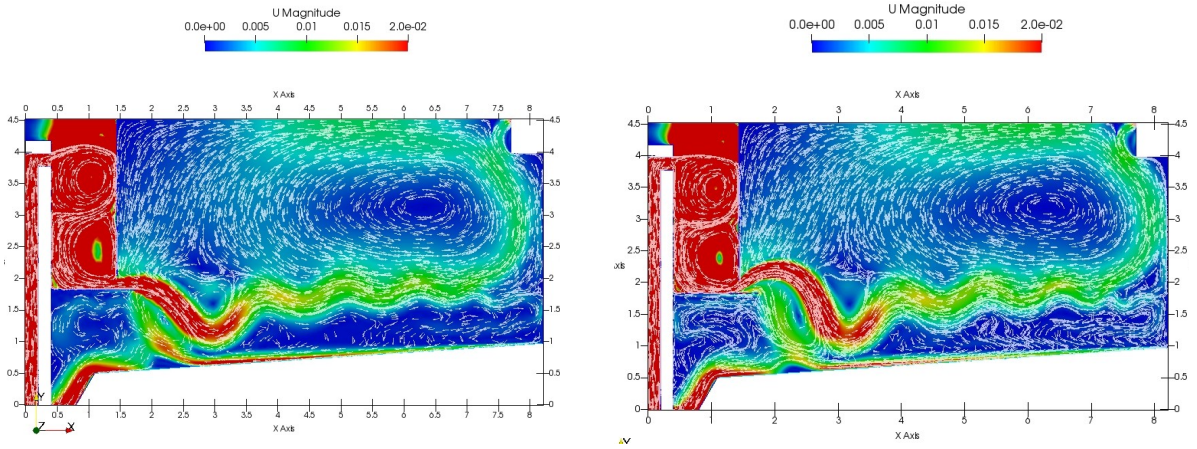

Figure 6.7
Velocity contour, left case rev6_refined10, right case rev6_refined11_1

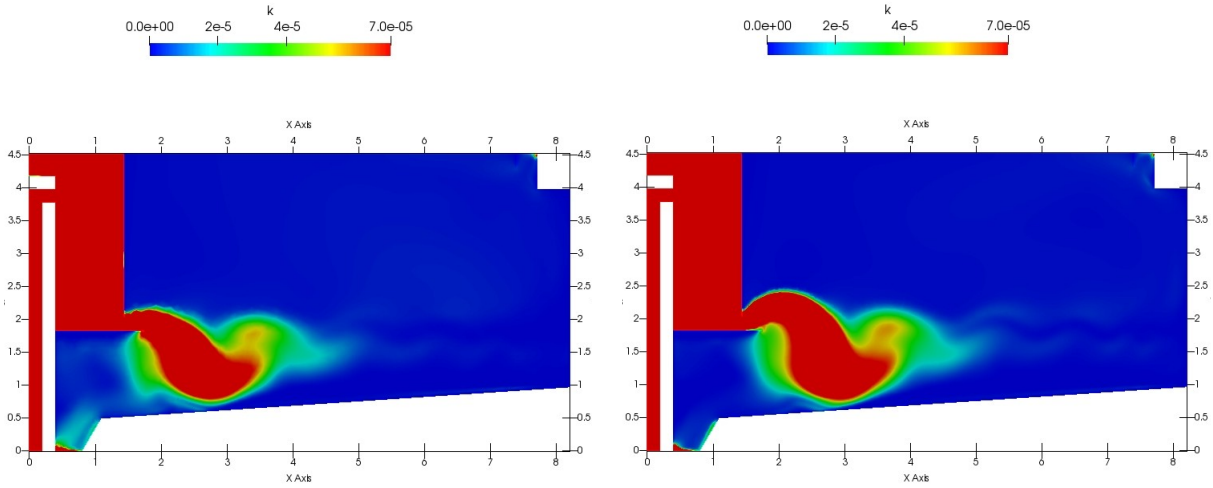

Figure 6.8
Turbulence Kinetic energy, left case rev6_refined10, right case rev6_refined11_1

7. Results and analysis

In annex I, we have included figures of solid contours, velocity contours (including stream lines) and turbulence kinetic energy contours, for all the simulations specified in Table 5.2.

The first step that we have followed in data analysis is to check stationary conditions for the specific simulation results. To perform that, we have made a mass balance for water and sludge. In this balance total flow and Total Suspended Solids through Inlet, Outlet_Sludge, and Outlet_Water patches were calculated. With these values it was verified that inlet mass flow is equal to outlet mass flow, so no accumulation is present in the system, hence stationary condition were reached (refer to annex II, for calculation details).

	Simulated time (sec)	Q_ef (m3/h)	SST_ef (g/l)	SST_purge Objetive (g/l)	SST_purge Sim (g/l)	% SST purge recovery	Q purge (m3/h)	Sludge blanket heigth (m)
rev1.1_refined9	18000	199.97	0.034	7.614	7.518	98.74%	149.97	2.0712
rev2_refined9	18500	199.97	0.051	7.591	7.645	100.72%	149.97	1.584
rev3_refined9	18000	199.97	0.035	7.613	7.380	96.94%	149.97	1.992
rev4_refined9	22200	199.97	0.003	7.656	3.644	47.60%	149.97	2.8896
rev5_refined9	18000	199.97	0.005	7.652	3.675	48.02%	149.97	0
rev6_refined10	18000	199.97	0.032	7.616	7.621	100.05%	149.97	2.028
rev7_refined10	18500	199.97	0.018	7.635	5.060	66.27%	149.97	0
rev6_1_refined10	18300	199.97	0.028	7.622	7.750	101.68%	149.97	1.9728
rev6_2_refined10	26000	199.97	0.029	7.620	7.556	99.16%	149.97	1.992
rev6_3_refined10	22800	199.97	0.020	7.633	7.688	100.72%	149.97	2.0064
rev9_refined10	18000	199.97	0.020	7.632	4.779	62.62%	149.97	2.6928
rev10_refined10	19300	199.97	0.001	7.657	4.835	63.15%	149.97	0
rev11_refined10	18000	199.97	0.018	7.636	7.123	93.29%	149.97	2.0928
rev11_2_refined10	18000	199.97	0.024	7.627	7.236	94.87%	149.97	2.1456
rev11_3_refined10	24100	199.97	0.015	7.640	7.060	92.41%	149.97	2.1864
rev11_4_refined10	37800	199.97	0.016	7.638	6.810	89.15%	149.97	2.1024
rev11_4_refined11		0.00	0.000	#DIV/0!	0.000	#DIV/0!	0.00	
rev11_5_refined10	29200	199.97	0.024	7.627	7.625	99.97%	149.97	1.9824
rev12_refined10	18000	199.97	0.042	7.603	7.589	99.83%	149.97	2.1792
rev12_1_refined10	20600	199.97	0.021	7.631	7.613	99.75%	149.97	1.9056

Table 7.1
Simulations mass balance results

In the Table 7.1, the mass balance results are shown. In red we present several simulation results in which stability was not reached in the simulated time. In black we present simulation results that reached steady state in the simulated time.

In Figure 7.1 we can see TSS profile along a vertical line placed at R=5m, for all the simulated cases. Sludge height and concentration determines sludge inventory in the clarifier, as well as sludge retention time. Sludge retention time is important to avoid de-nitrification and subsequently floating sludge in the clarifier that can disturb effluent quality.

So, less sludge height implies more sludge storage capacity for peak flow events, and less sludge retention time with less risk of undesired de-nitrification.

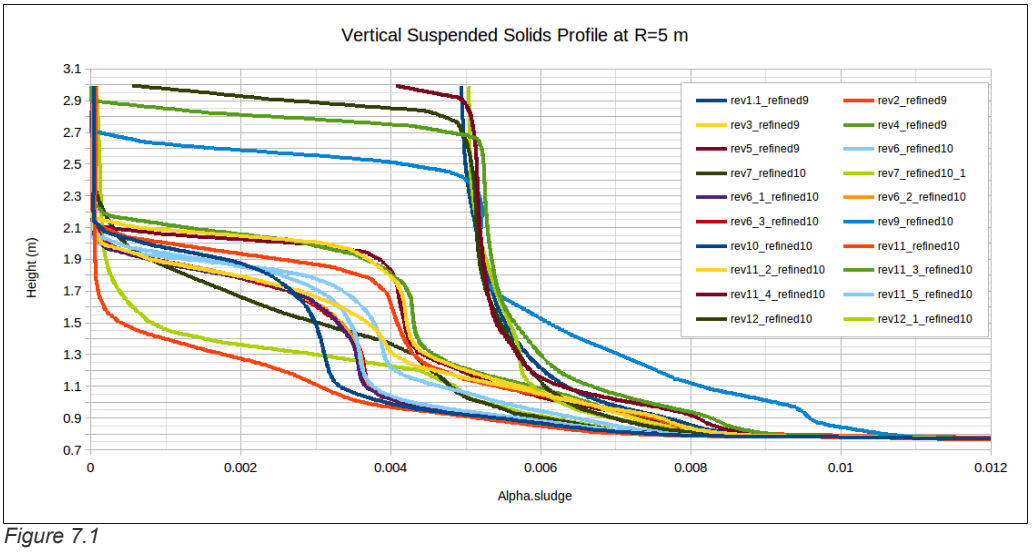

Figure 7.1
TSS profile along clarifier height, at a distance of R=5 m

7.1. Cases were steady state was not reached:

In order to analyse the causes of failure to reach the steady state of some hydraulic configurations we can focus on one of them. In Figure 7.2, we have a case were no influent well lower baffle is installed. As we can see in the velocity contour plot, the inlet flow hits the influent well and falls straight up to the bottom of the clarifier. At that point the current impact the sludge hopper and returns in ascending direction up to the middle of the tank height. After that, a defined narrow current is redirected up to the peripheral wall, where hits the same and splits into two different fractions: one to the top of the surface, where the weir is installed, and the other to the bottom where the sludge is moved again to the hopper.

We can interpret that two phenomena are happening, in one hand there exists a short circuit, so the influent is redirected to outlet pipe, without previous thickening. On the other hand the thickened sludge that is moved from all the bottom wall to the sludge hopper, can not reach the outlet pipe inside the hopper because the turbulence inside the hopper acts as a barrier for this movement. These phenomena can be appreciated also in other inlet configurations without center well lower baffle, see Figure 10.10 or Figure 10.14 in annex I, for reference.

Although we can find references in literature [33] which corroborate that short-circuit happens in full scale real installations, it is not clear that the intensity of the phenomenon found in the simulation is according to reality. This doubt is supported by the fact that there

are many installations operating with center feed, center sludge withdrawal but without center well lower baffle.

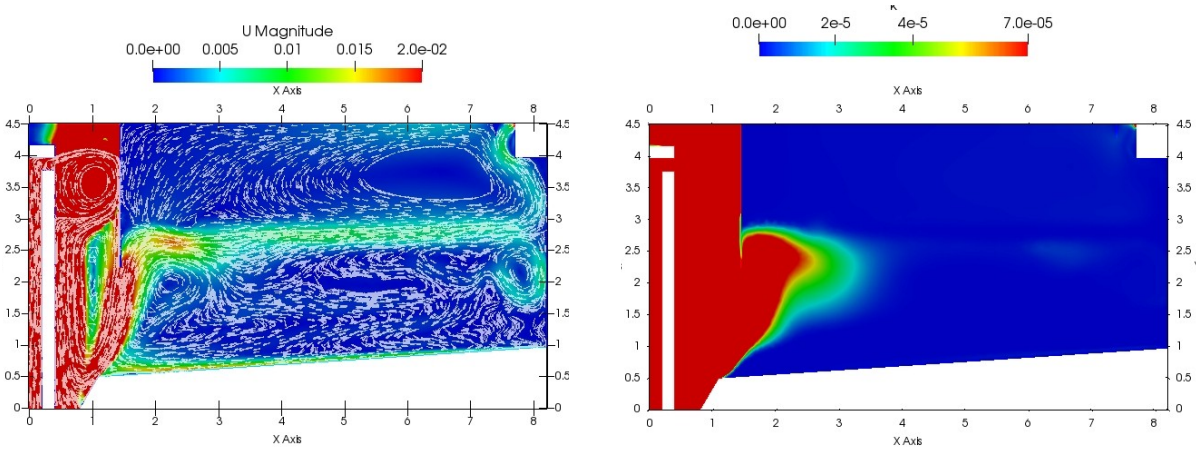

Figure 7.2
Case "rev4_refined9", velocity contour (left), Turbulence Kinetic Energy k (right)

In order to explain the mentioned issue some hypothesis are postulated:

- Improper selection of sludge rheological parameters. The influence of rheological properties in sludge recirculation system short-circuit will be analyse later in section 7.3.1.

- System overload: as can be seen in Figure 5.1, according to solid flux theory the operation point of the system although apparently not overloaded, is almost at the limit. The influence of operation point in sludge recirculation system short-circuit will be analyse in section 7.3.2.

- Improper simulation of sludge transport mechanism (scrapper movements simulation). As mentioned in section 6.2, sludge scrapper stimulation has been implemented as a moving bottom wall. So the scraper blades that in real systems moves the sludge up to the hopper are not implemented in the actual simulations. Although some authors (see [8]), has modelled scrapper blades in a 2D model, that option was not studied in present work due to time limitations.

One interesting characteristic that we appreciate in overloaded simulations (see for example case rev5_refined9 (in annex I) is that the density current tends to rise above the sludge layer. Also the turbulence generated in sludge blanket is not strong enough to transport the sludge from sludge blanket up to effluent weir. We can appreciate that the velocity magnitude of the horizontal velocity current that goes to the outer wall is lower in these cases that in cases as rev3_refined9 or rev6_refined10. This is apparently caused by

the energy dissipation in the incoming section of the clarifier. Dissipation is higher in simulations were sludge transport failure has happened.

7.2. Steady state simulation results:

In this section we are going to focus on simulation results that have reached steady state, in order to analyse the influence of design parameter for inlet and outlet configuration on sludge blanket height and effluent suspended solid profile in clarified water. The different options studied are summarized in Figure 7.3:

In Figure 7.4 we can see the velocity profile for two different inlet well configurations: straight well with lower baffle and inclined end well with lower baffle, both with peripheral weir. In this figure we can appreciate how the mixture sludge/water, enters the clarifier and generates an strong density current. After that, the current is redirected to the clarifier perimeter wall, where it hits the wall and rises to the surface. Finally the current comes back to the center of the clarifier. Depending on the position of the center well baffles, this flow current falls more or less sharply up to the bottom of the clarifier. Apart from that, the general flow field characteristics are very similar in both cases even with different inlet configurations, especially the density current that moves to the perimeter.

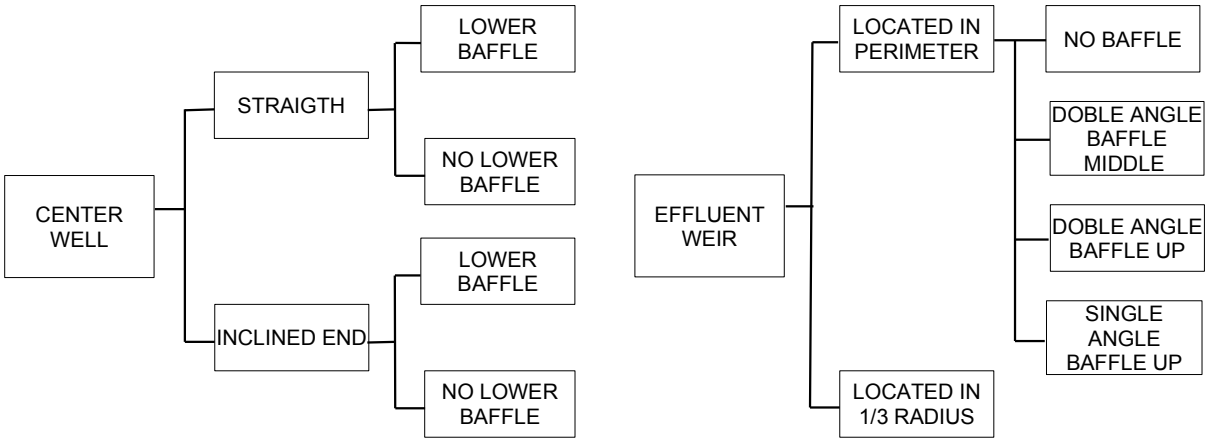

Figure 7.3

The position of the baffles has two main targets:

- Avoid interference of inlet density current with the sludge in the hopper.

The sludge in the hopper must be thickened in order to be able to remove the necessary quantity to maintain the solid balance in the clarifier without sludge accumulation. Several bottom baffle has been simulated.

- Avoid the drag of the sludge from the sludge blanket up to the weir. To get this objective is important to dissipate as much energy as possible with the inlet configurations. Several strategies can be followed:

* Stop the density current that goes to the perimeter (see Figure 10.36 and Figure 10.38). This kind of baffles was implemented in [29].

* Redirect the current back to the center of the clarifier, avoiding the current to raise directly from the wall to the effluent weir. To achieve this different perimeter baffles were proposed, see [12]. In the present study apart from the weir wall located inside the side wall, two more different options were simulated: see Figure 10.34, Figure 10.28 in annex I (double angle baffle was simulated at 2 different heights).

* Place the effluent weir inside the clarifier, instead of in the perimeter.

In the following paragraphs only the result of simulations without short-circuit will be analysed (black lines in Table 7.1).

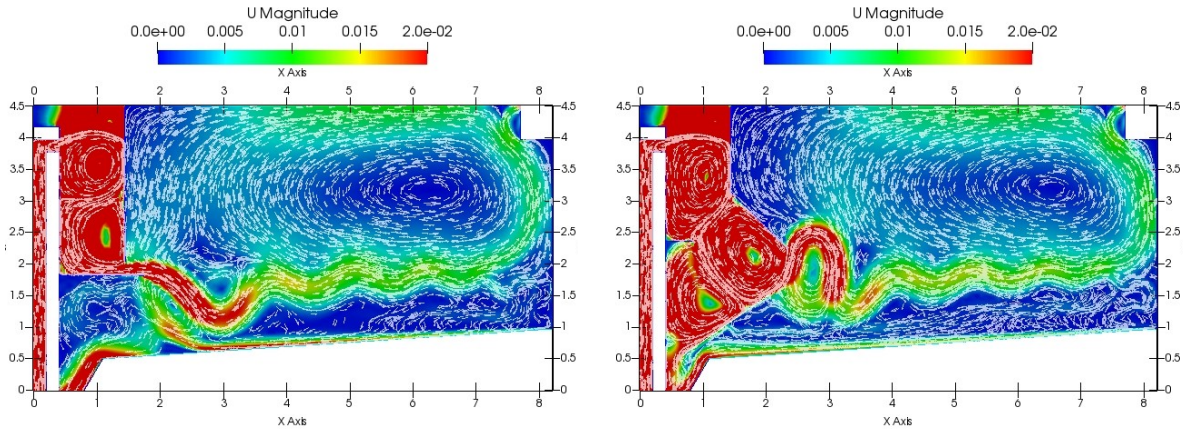

Figure 7.4
Velocity contour for simulation case "rev6_refined10" (left) and case rev3_refined9 (right)

7.2.1. Inlet structures results analysis

In general, from simulated cases that reached steady state, there are no important differences in sludge blanket height. There are two exceptions case rev2_refined9 and rev12_1_refined10, where the sludge blanket is about 0.5 below the other cases. Case rev12_1_refined10 will be analysed in section 7.2.2.

In model rev2_refined9 the inclined baffle contributes to dissipate the incoming turbulent kinetic energy in hopper area, and on the other hand density current generated by Influent

water/sludge mixture is redirected far away the sludge hopper thanks to the additional inclined baffles (see Figure 7.5). This current promotes TSS dragging up to the effluent weir. As a consequence of that, effluent TSS are the highest of all tested simulations.

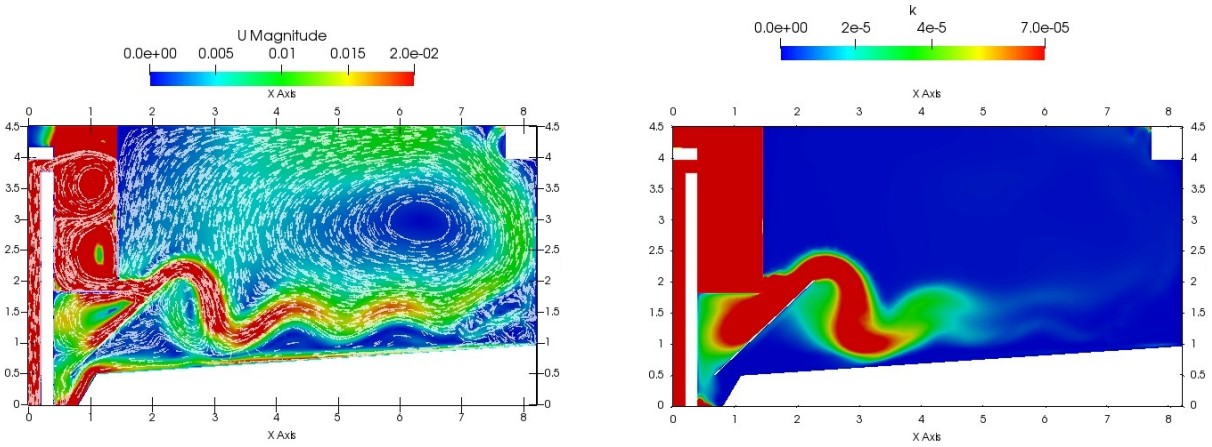

Figure 7.5
DecCircular3D_rev2_refined9: Left: U magnitude contour / Right: k contour

Regarding lower baffle option, the model studied in rev9_refined10, and rev11_refined10 (Center well: straight Narrow + Inclined end), shows a big dependency of size and position of lower baffle, changing from a successful behaviour in model rev11_refined10 to a risky behaviour in model rev9_refined10, where short-circuit is almost imminent due to the turbulence generated in the hopper area by the incoming water/sludge current (see Figure 7.6). This turbulence prevents the sludge transport from the clarifier bottom up to the sludge hopper. However, in model rev11_refined10 this phenomenon is reduced by moving the bottom baffle to the center of the clarifier. Due to that sensitivity to baffle position and size this configuration should be used with care.

On the other hand, models rev1.1_refined9 and rev6_refined10, were simulated with the shape recommended by ATV [24]. Two options are evaluated, in the first one the diameter of the lower baffle is the same of the inlet well. In the second one the lower baffle extend 1.2 times the radius of the center well, and the open space between vertical well and horizontal baffle is 0.5 times. Apparently results do not show any important difference regarding velocity currents (see Figure 7.7). The more remarkable difference is related to center well opening size. In model rev6_refined10 this opening is higher; this causes a greater recirculation of water from the clarifier open area to inside center well. Finally it should be noted that effluent suspended solid concentration are similar in both models, 34 mg/l versus 32 mg/l (Table 7.1).

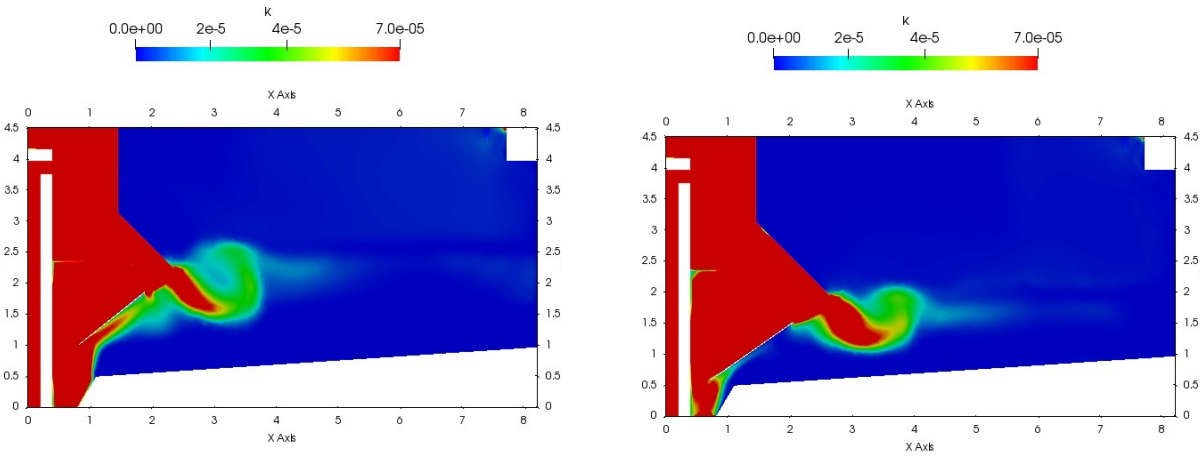

Figure 7.6
k contour: Left: DecCircular3D_rev9_refined10 / Right: DecCircular3D_rev11_refined10

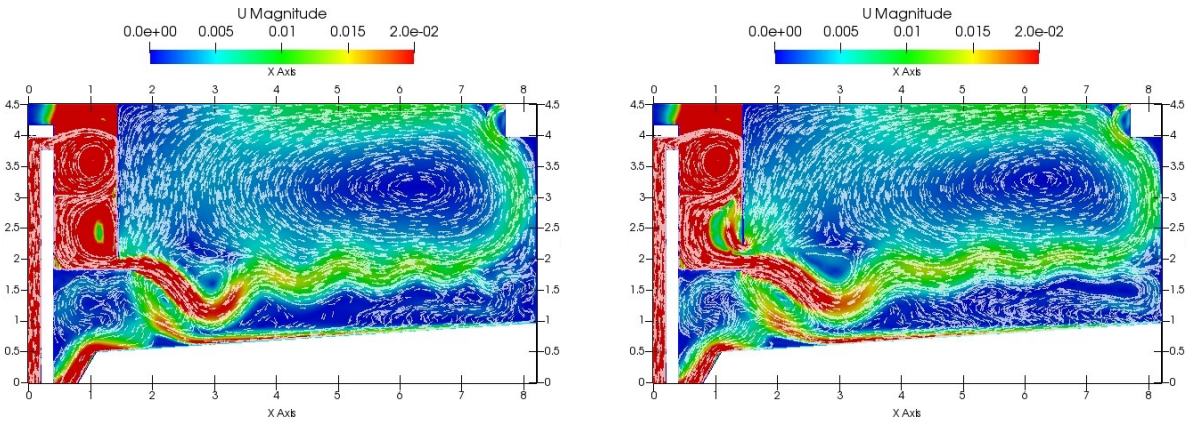

Figure 7.7
U magnitude contour: Left: DecCircular3D_rev1.1_refined9 / Right: DecCircular3D_rev6_refined10

7.2.2. Perimeter vertical ring result analysis

In model rev12_refined10 and rev12_1_refined10, a vertical ring baffle was introduced at a distance of R/2, from clarifier center. This configuration was used by Crosby (see [34]) for the retrofit of existing installations. The ring baffle is located 0.24 m over tank bottom, to allow sludge scrapper to transport the sludge up to the hopper. On the other hand 2 heights have been used, 1 meter in model rev12 and 1.5 m hight in model rev12_1.

In figure Figure 7.8 velocity contour is shown for both models. In case with 1 meter high baffle, the heigh of the baffle disturbs density current, but disturbance is not enough to change notably the velocity profile inside clarifier, compared with velocity profile without ring baffle (see Figure 7.7). However if baffle high is increased up to 1.5 m high, velocity profile changes. Baffle almost stops the density current from the influent, so that density current still travels up to the wall but the rebound with the wall generates a current at a closer distance to the bottom. This phenomenon reduces the drag of solids up to the effluent weir compared to other cases (see Figure 10.11, Figure 10.35 and Figure 10.37 in annex I). In model rev12_1 (see Figure 10.37 in annex I) it can be seen an small area close to effluent weir, where alpha.sludge is around 2.5 e-5 (TSS=26 mg TSS/L). In model rev12 however, effluent weir area is over TSS>36 mg TSS/L.

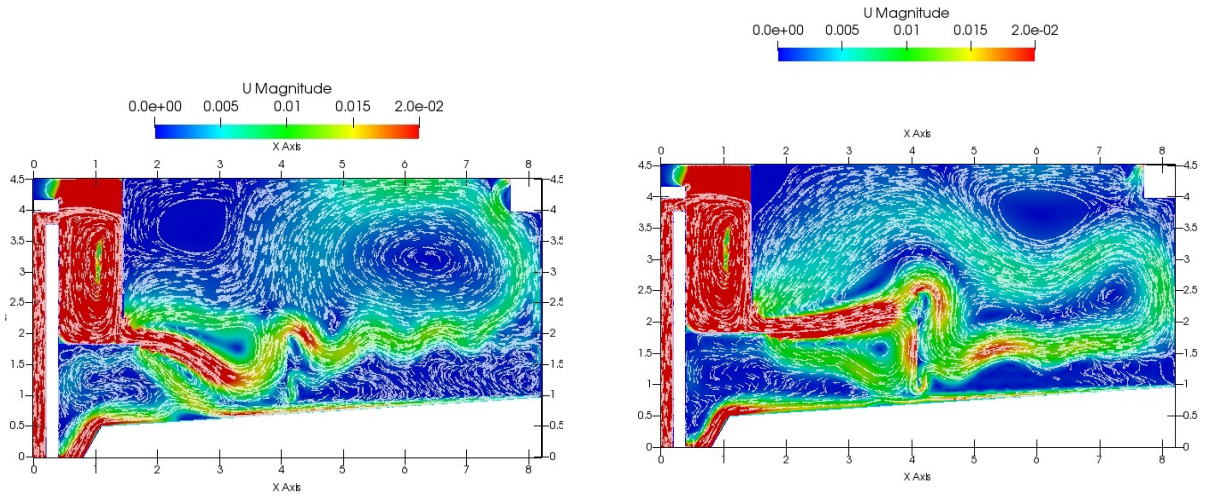

Figure 7.8
Velocity contour: case rev12_refined10 (left) and case rev12_1_refined10 (right).

It is worthy to note that in model rev12_1_refined10 the sludge blanket at R=5 m, this is, after ring baffle position (see Figure 7.1) is maintained very low, so baffle is effective in confining sludge near the centrer of the clarifier. Its interesting to note that efficiency of 1 m high baffle (rev12) is limited compared with the model of 1.5 m baffle (rev12_1).

7.2.3. Weir baffles and weir position

Regarding weir baffle and weir location impact on clarifier performance, three options were studied for straight narrow center well (cases rev6_) and for Straight narrow + inclined end center well (cases rev11_) (see Table 5.2). Although all figures are available in annex_I, we are going to include here some of them for clarity.

Inlet structure: straight inlet well+ lower baffle:

From Figure 7.9 to Figure 7.16 different baffle configurations and weir locations are shown for the straight + lower baffle inlet structure. As we can see in those figures, baffles located in the outside wall are not able to modify sufficiently the flow field, and solids content of the effluent are not significantly influenced.

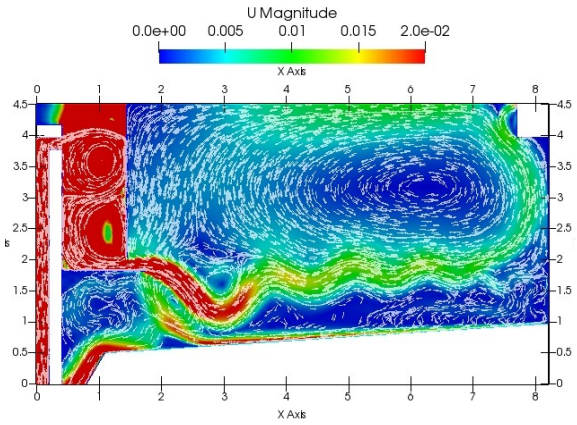

Figure 7.9
rev6_refined10 (velocity profile)

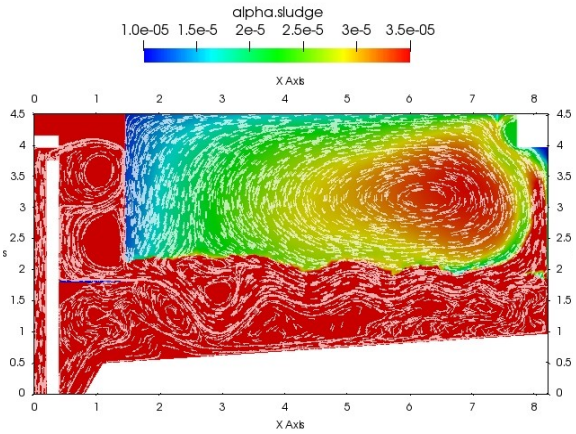

Figure 7.10
rev6_refined10 (TSS profile)

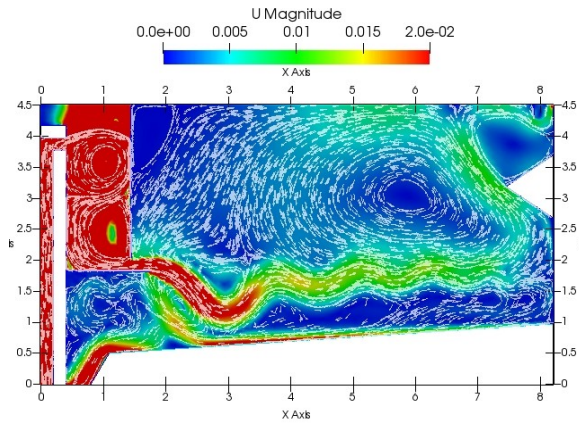

Figure 7.11
rev6_1_refined10 (velocity profile)

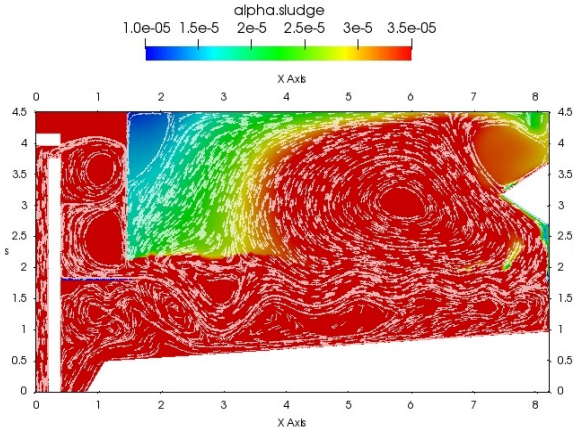

Figure 7.12
rev6_1_refined10 (TSS profile)

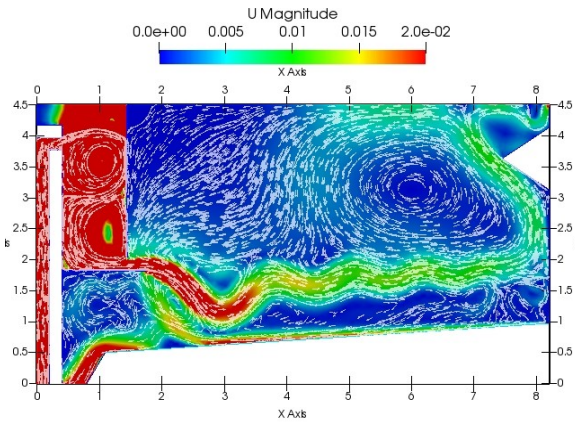

Figure 7.13
rev6_2_refined10 (velocity profile)

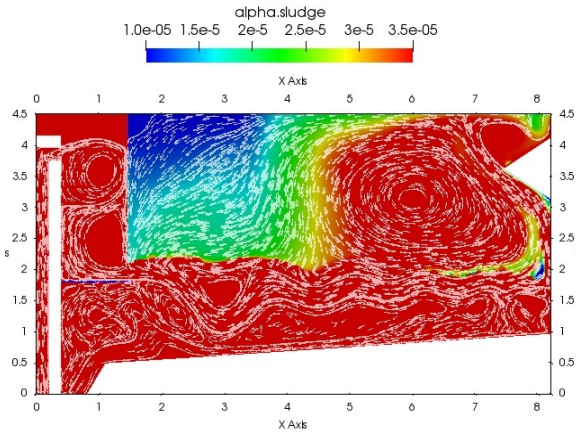

Figure 7.14
rev6_2_refined10 (TSS profile)

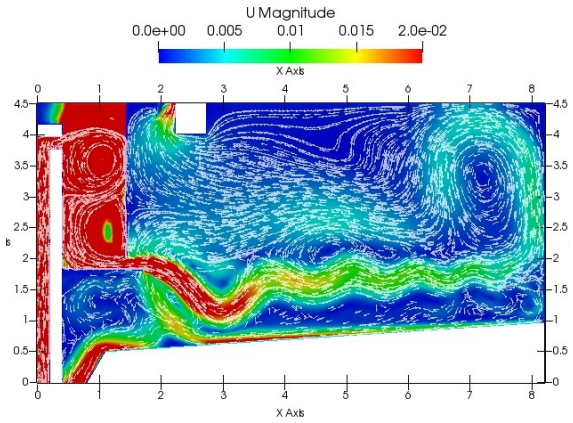

Figure 7.15
rev6_3_refined10 (velocity profile)

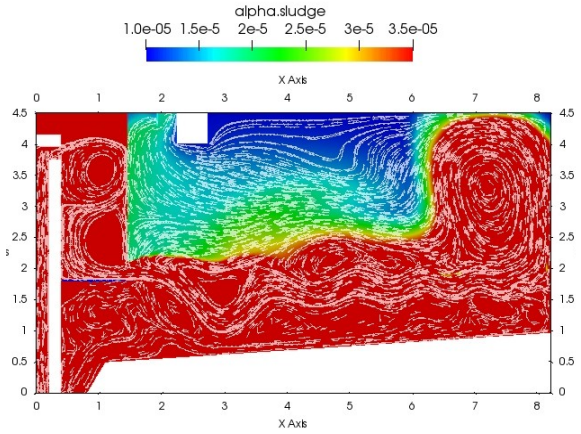

Figure 7.16
rev6_3_refined10 (TSS profile)

However the results obtained for model rev6_3 are more interesting: the weir located inside the clarifier has an important impact on effluent suspended solids content. the solids content has been reduced up to 20 mg/l (Table 7.1) this is a 37% of solid content reduction compared with the original model (rev6).

In Figure 7.16, the solids contour clearly shows how the solid content near the weir area is considerable lower than close to the wall. This means that even with the higher velocity, close to the weir, the influence of the density current is minimized due to the position of the weir. The higher weir velocity in this model is justified by the lower weir length available due to radial position of the same.

Inlet structure: Straight narrow + inclined end, center well:

From Figure 7.17 to Figure 7.24 different baffle configurations and weir locations are shown for the straight narrow + inclined end center well inlet structure. Unlike what happened in the previous studied case, in this case peripheral baffle noticeably influence solid content in weir area. Specifically from both baffles studied the one in model rev6_11_4, produced better results.

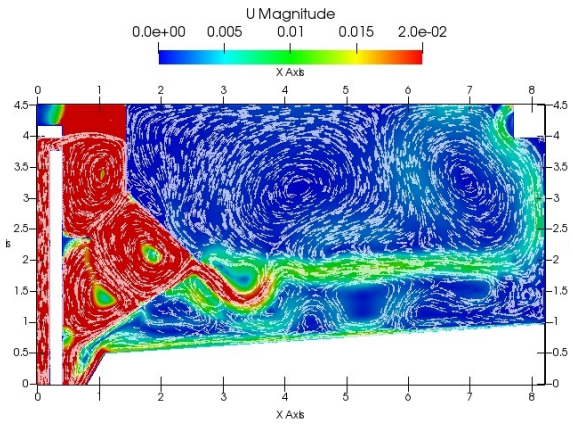

Figure 7.17
rev6_11_refined10 (velocity profile)

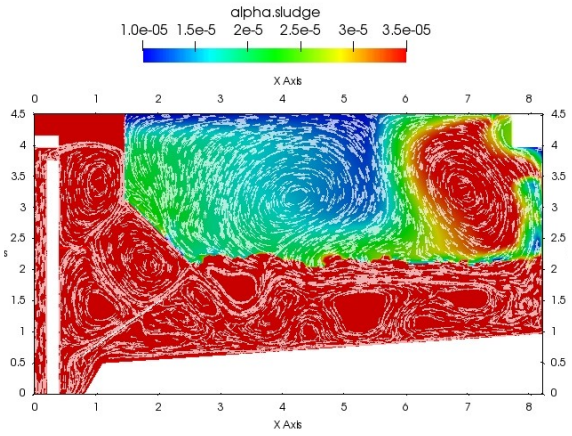

Figure 7.18
rev6_11_refined10 (TSS profile)

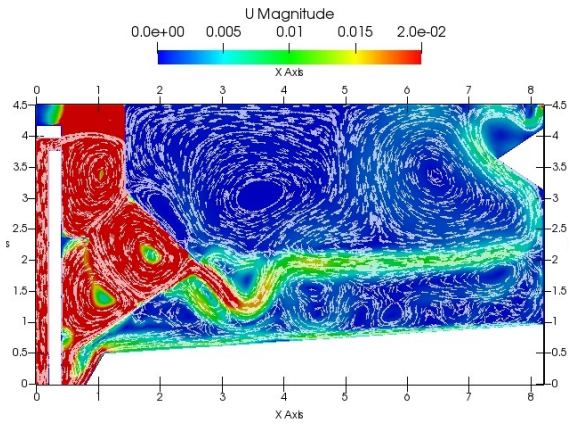

Figure 7.19
rev6_11_2_refined10 (velocity profile)

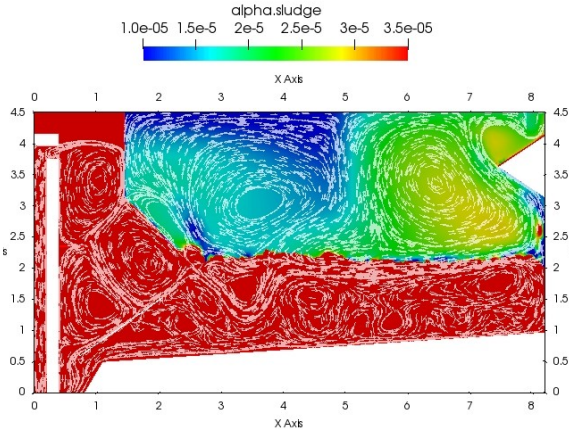

Figure 7.20
rev6_11_2_refined10 (TSS profile)

Although data displayed in Table 7.1 do not show a big improvement in effluent TSS, solid profiles figures shows that in base model (rev6_11) there is an area of alpha>3.5e-5, very close to the effluent weir. However in the other models the TSS concentration in this

area is reduced to alpha values below 2.5e-5 (28% percentage reduction). From both baffle models, the second one (rev6_11_4) shows better results. On the other hand the model with the weir inside the clarifier (rev6_11_3) also shows good results. Differences in effluent TSS between the last two options mentioned are not significant.

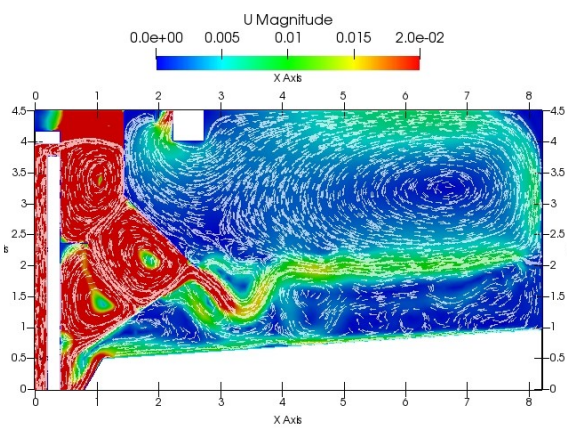

Figure 7.21
rev6_11_3_refined10 (velocity profile)

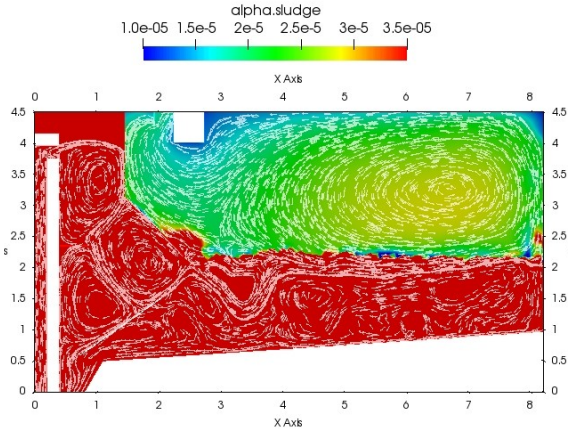

Figure 7.22
rev6_11_3_refined10 (TSS profile)

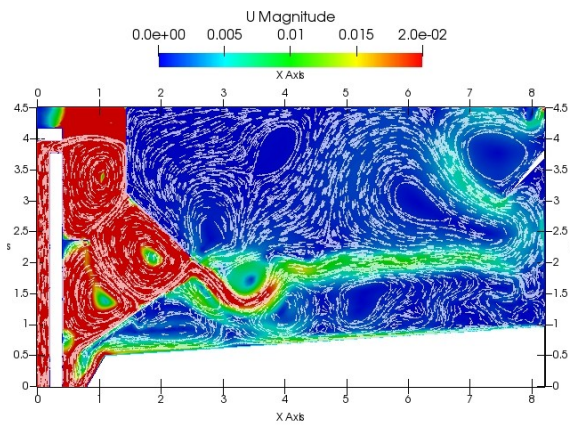

Figure 7.23
rev6_11_4_refined10 (velocity profile)

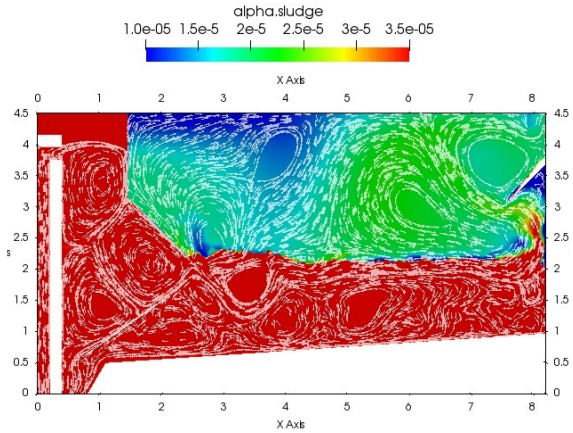

Figure 7.24
rev6_11_4_refined10 (TSS profile)

7.3. Sludge transport failure: hypotheses verifications

7.3.1. Influence of sludge rheology on simulation results

In this section we are going to study the influence of some rheological parameters on clarifier performance, in order to verify whether these properties could be the cause of the failure in transporting the sludge up to the sludge hopper. As mentioned by Clercq in [8], sludge rheology can greatly influence flow field developed in the clarifier. In Figure 7.25 it is shown the differences in flow field inside sludge hopper for two different rheological properties set.

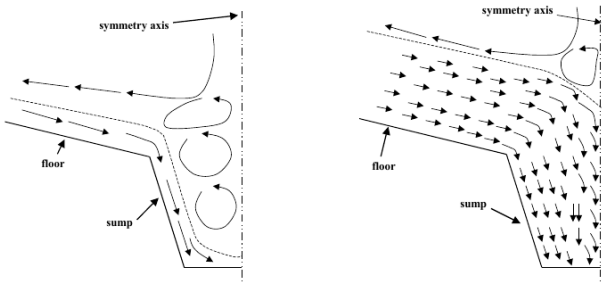

Figure 7.25
Scheme of velocity field near sump for rheologies without (left) and with (right) yield stress. Only half a cross-section of the sump is shown (from [8])

From case “rev4_refined9”, as a starting point, we modified different parameters of the rheology model (see Table 7.2). After some “small” parameters changes without remarkable results it was decided to adopt the values used in “dahl” tutorial available in openFoam 6. The implementation of these new parameter (t=164600 s) resulted in a different flow field, where the short circuit disappeared, and the sludge reached the hopper easily. In Figure 7.26 alpha sludge with velocity streamlines is shown for time t=14800 s, and t=177600 s. It is also interesting to note the difference in kinetic energy dissipation between both cases (Figure 7.27). Density current over extension due to low turbulence energy dissipation was mentioned in [7].

Among others, solids density for both models shows a great difference. While default value used in present work is 1042 kg/m^3 (acc. to [7]), “dahl” tutorial default value is 1996 kg/m^3. We have found a wide variety of results in bibliography, for example: Burt [11] used a value of 1445 kg/m^3, for dried sludge density. According to the correlation shown in [6] the calculated value for dried sludge density is 2119 kg/m^3. De Clercq [8] reported a dry solids density of 1750 kg/m^3 for a mixture of biomass-zeolite.

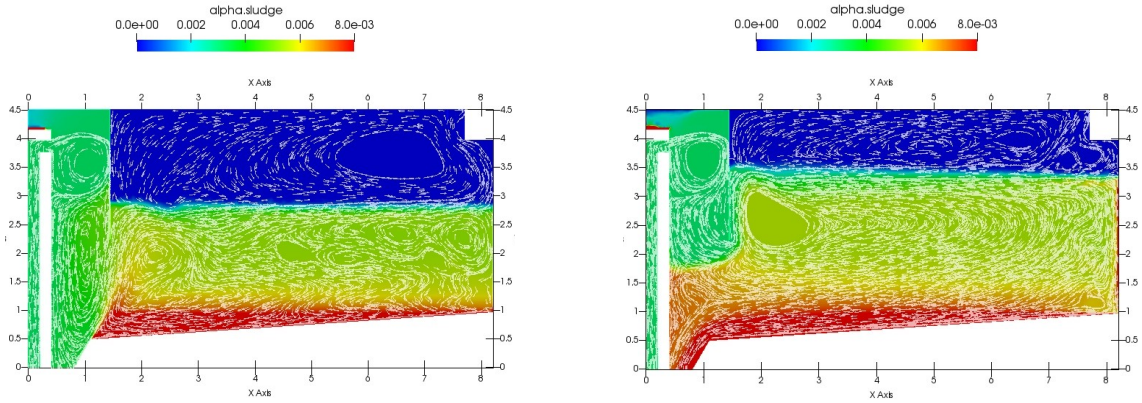

Figure 7.26
Alpha sludge contour for model rev4_refined9_2: Left t=14800 seconds (sludge level going up due to shortcircuit). Right t=177600 seconds (sludge level going down).

t	coeff	exponent	BinghamCoeff	BinghamExponent	muMax	Density	Comments
Original	2.3143E-04	1.7926E-01	7.8450E-07	95.25	10	1042	
0	2.3143E-04	1.7926E-01	8.2373E-07	95.25	10	1042	No changes, short circuit present
3900	2.3143E-04	1.7926E-01	8.6295E-07	95.25	10	1042	No changes, short circuit present
10100	2.3143E-04	1.7926E-01	9.0218E-07	95.25	10	1042	No changes, short circuit present
14500	2.3143E-04	1.7926E-01	9.4140E-07	95.25	10	1042	No changes, short circuit present
46400	2.3143E-04	1.7926E-01	9.4140E-07	95.25	10	1042	No changes, short circuit present
52100	2.3143E-04	1.7926E-01	1.0199E-06	95.25	10	1042	No changes, short circuit present
66700	2.3143E-04	1.7926E-01	1.0983E-06	95.25	10	1042	No changes, short circuit present
70700	2.3143E-04	1.7926E-01	1.1768E-06	95.25	10	1042	No changes, short circuit present
92400	2.3143E-04	1.7926E-01	7.8450E-06	95.25	10	1042	No changes, short circuit present
99300	2.3143E-04	1.7926E-01	7.8450E-05	95.25	10	1042	No changes, short circuit present
111100	2.3143E-03	1.7926E-01	7.8450E-07	95.25	10	1042	No changes, short circuit present
123900	2.3143E-02	1.7926E-01	7.8450E-07	95.25	10	1042	No changes, short circuit present
145601	2.3143E-02	1.7926E-01	7.8450E-07	95.25	100	1042	No changes, short circuit present
147600	2.3143E-04	1.7926E-01	7.8450E-07	95.25	10	1020	No changes, short circuit present
156800	2.3143E-04	1.7926E-01	7.8450E-06	95.25	10	1042	No changes, short circuit present
164600	2.3143E-04	1.7926E+02	5.9660E-04	1050.8	10	1996	Values of Dahl tutorial, Flow field change, short circuit NOT present
177800	2.3143E-04	1.7926E+02	5.9660E-04	1050.8	10	1042	Flow field change, short circuit NOT present

Table 7.2
Rheology parameters at different times for model rev4_refined9_2

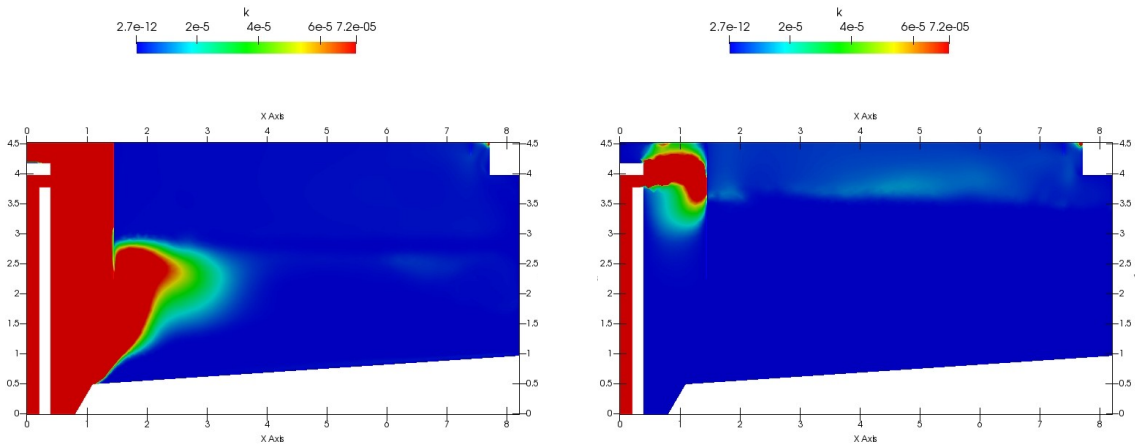

Figure 7.27
Turbulence kinetic energy contour k for model rev4_refined9_2: Left t=14800 seconds. Right t=177600 seconds.

In order to distinguish between rheological and density effects on the simulation results, we performed 3 simulations (see Table 7.3):

Simulation 1	Simulation 2	Simulation 3
Rheological parameters acc. to Dhal (see parameter of t=177800 s in Table 7.2) Low density Model: rev4_refined9_2_0; t=16599 s	Rheological parameters acc. to Dhal (see parameter of t=164600 s in Table 7.2) High density Model: rev4_refined9_2_0; t=21300 s	Rheological parameters acc. to Brennan (see parameter of t=original in Table 7.2) High density Model: rev4_refined9_2_2; t=21600 s

Table 7.3

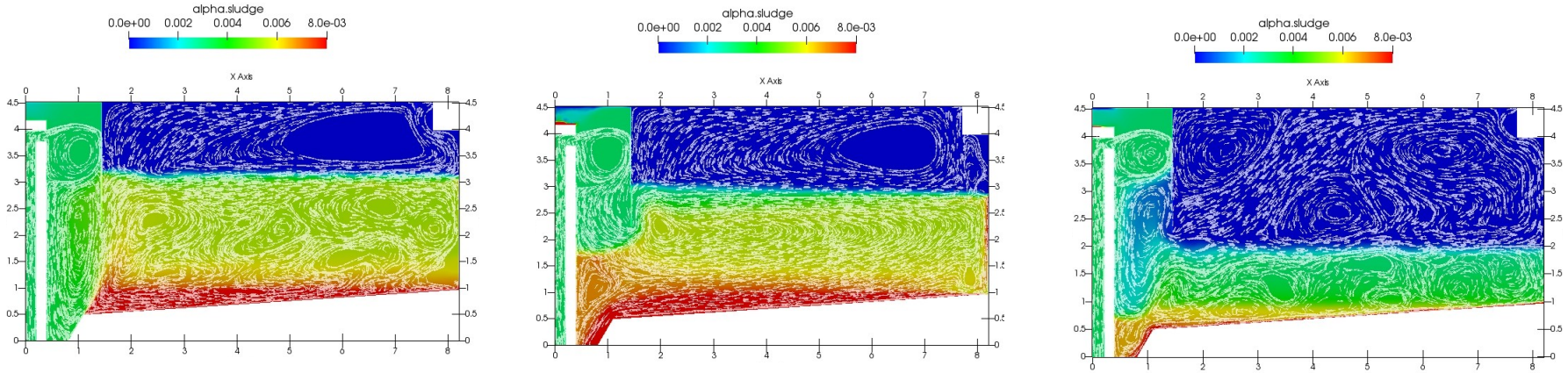

Figure 7.28
SS_profile: Simulation 1 / Simulation 2 / Simulation 3 (see Table 7.3)

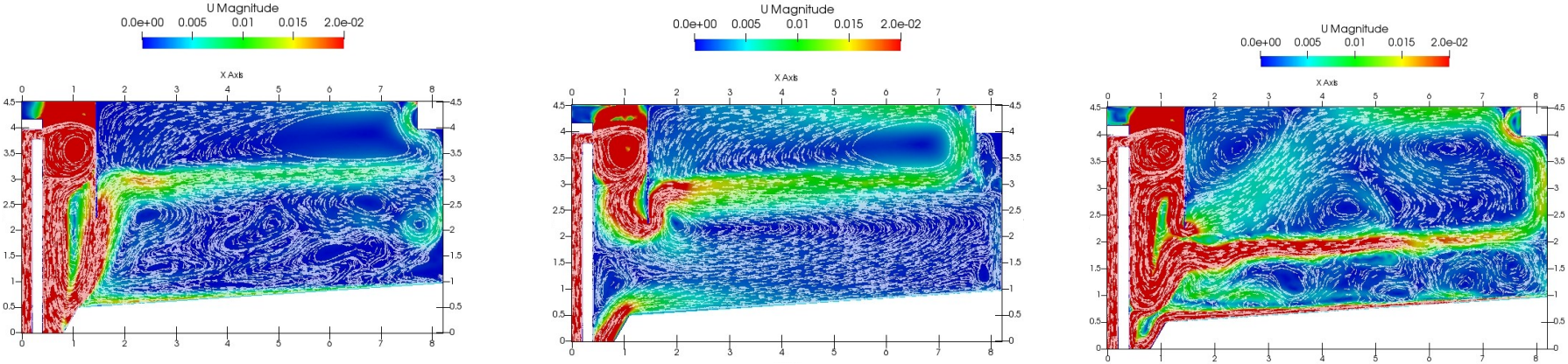

Figure 7.29
U_profile: Simulation 1 / Simulation 2 / Simulation 3 (see Table 7.3)

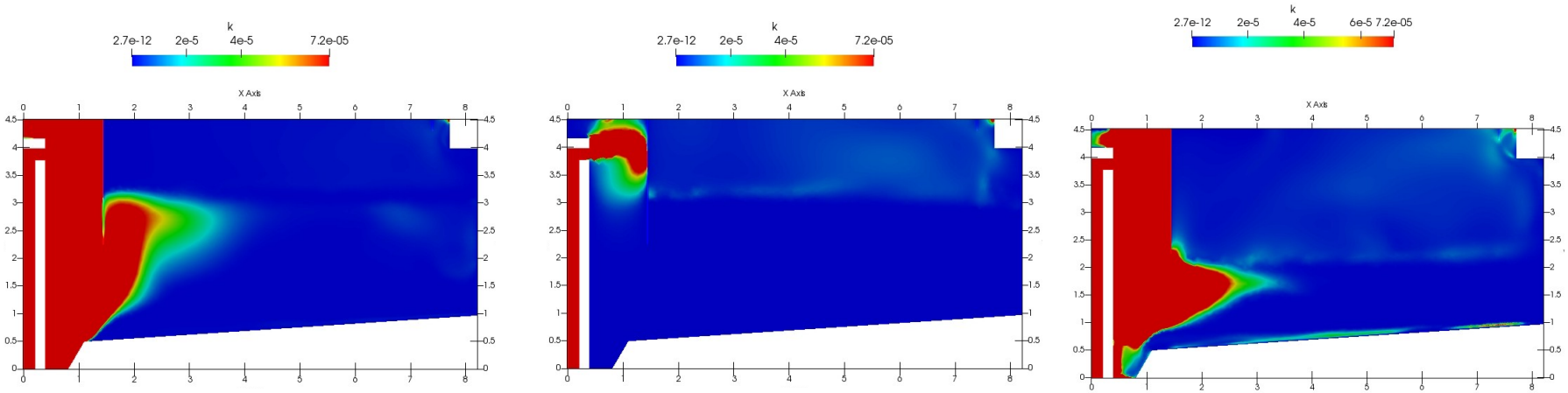

Figure 7.30
k_profile: Simulation 1 / Simulation 2 / Simulation 3 (see Table 7.3)

The results of the three simulations area shown in Figure 7.28 to Figure 7.30:

First of all it is interesting to note that in simulations with density=1996 kg/m^3, short-circuit is not present. As can be seen in ec. (2.2), density directly affects relative velocity between phases, an increase in dispersed phase density increases relative velocity at high TSS ranges.

Regarding flow field, in both simulations with higher dispersed phase density, the velocity current (density current) generated from the inlet well, has more intensity and consequently it reaches the outer wall with higher velocity. Velocity is higher in the simulation 3, showing less turbulent kinetic energy dissipation (this is confirmed in Figure 7.30). Also it is interesting to note in the simulation 3, the higher velocity in the bottom of the clarifier, which moves the sludge up to the hopper. Remember that moving wall velocity is the same in all simulations. Finally we want to highlight the current that returns to inlet well in sim 3. Although this current is also present in other cases (see for example Figure 10.2) its magnitude is higher in sim 3.

Regarding turbulence kinetic energy we can see in Figure 7.30, a great difference between simulation 1 and 2. Also it is interesting ot see in sim 3, how in the sludge hopper the turbulence kinetic energy is lower than sim 1 in some areas. This issue is related to the capacity of this model to transport the sludge up to the hopper.

7.3.2. Influence of operation point on simulation results

In order to check the hypothesis of system overload, the following simulations were performed:

- Recirculation flow increase from 150 m^3/h up to 240 m^3/h. With this action the slope of the underflow rate is increased, so the system operation point is further from overload point. (Case rev4_refined9_3)

As is is shown in Figure 7.31, the short-circuit still is present, and sludge fail to reach the sludge hopper.

- Inlet flow reduced from 200 m³/h to 100 m³/h, and recirculation flow equal to 120 m³/h. (Case rev4_refined9_5). As shown in Figure 7.32, under these conditions the sludge reaches the hopper, but still the incoming flow falls directly on the hopper, which apparently still hinders the entry of sludge into the hopper. According to the mass balance the TSS recovery is 99.38%, so the system is under stationary conditions.

If we compare velocity contour of original simulation (see Figure 7.33) with reduced velocity simulation (see Figure 7.34), we see that the velocity magnitude is smaller just in the area were the sludge reach the hopper for the second case. This reduced velocity allows the sludge to reach the hopper.

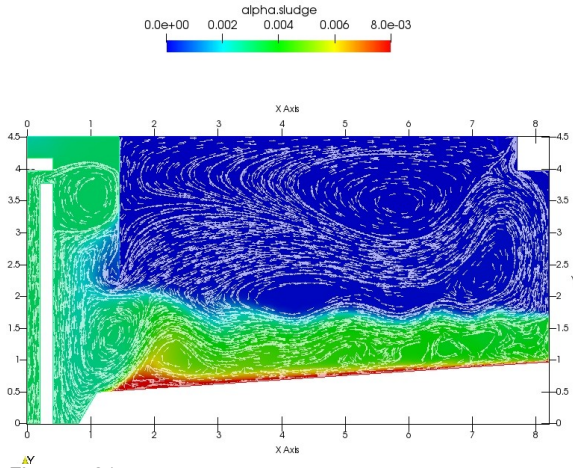

Figure 7.31
Case rev4_refined9_3, TSS contour

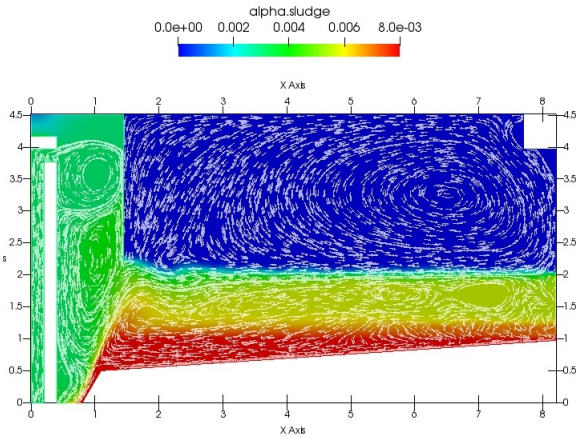

Figure 7.32
Case rev4_refined9_5, TSS contour

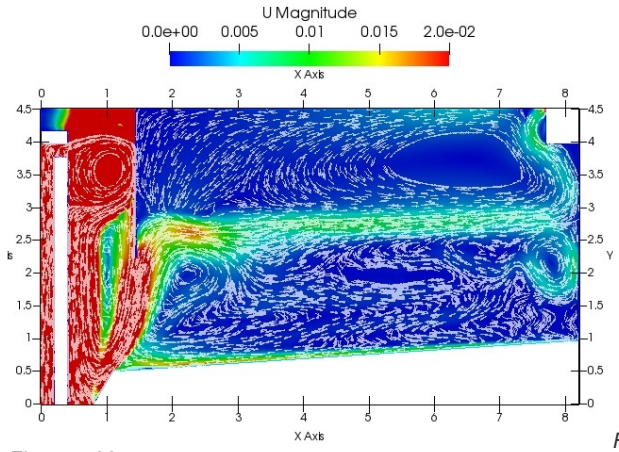

Figure 7.33
Case rev4_refined9, velocity contour

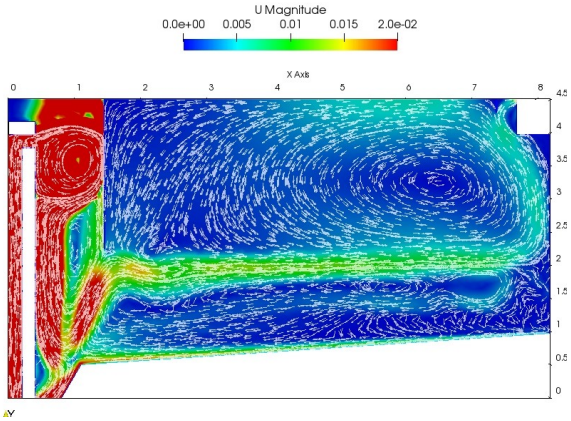

Figure 7.34
Case rev4_refined9_5, velocity contour

Also in Figure 7.34 we see the density current that moves horizontally over the sludge blanket, from inlet up to the wall. Once the current hits the wall, it is redirected up to the weir area located in the top side of the wall. So still in reduced flow simulation, the flow field in the bulk area of the clarifier is similar to other cases.

8. Summary and conclusions

In view of the results obtained in the present work we can get the following conclusions.

- Inlet structure has an important role in avoiding sludge short circuit, and energy dissipation:

Simulations have shown that density current generated just in the entrance from the center well to the clarifier main volume, can promote problems in sludge transport up to the hopper that can end in a clarifier total failure.

In this respect it is very important, in clarifier with center feed and center sludge purge configurations, to provide any kind of inlet bottom baffle that avoid an hydraulic short circuit and excess of turbulence in the sludge hopper.

From the several studied systems the influent well bottom baffle of cases rev6_refined10 and rev12_refined10, are the most reliable. Although other configurations have shown better results in some cases (see case rev3_refined9), they suffer from more sensitivity to size and position, what also suggests that they will be more sensitive to flow variations or system overloads.

- Effluent weir baffle can significantly reduce effluent TSS concentration

Simulations results show how the inlet density current moves directly to the outer wall in a narrow section flow current. For configurations with effluent weir in the peripheral wall, this current can transport an excess of sludge directly to the treated water reducing the clarifier performance.

To avoid this phenomenon several configurations have shown their efficiency. In particular the one used in case rev11_4 has evidenced best results. The peripheral baffle redirects the density current from outer wall, again to the center of the clarifier. As the water leaves the tank in the perimeter top side, part of the redirected current is separated from the main stream and goes to the effluent weir. This current combinations reduces the efluent TSS content due to the presence of a reduced velocity area close to the effluent weir.

- Effluent weir position can significantly reduce effluent TSS concentration

Simulations have exhibited good results for all cases with the effluent weir located at 1/3 R from the clarifier inlet. Even with the higher weir load, TSS content in treated water has been reduced significantly. As it happens in the cases with weir located in the perimeter, in this case also the influent current goes directly from the center weel up to the peripheral wall.

At that point the current is redirected back to the center but velocity magnitude is reduced so the TSS transported by the water current to the effluent weir are also reduced significantly.

- Rheological properties and sludge density have a great impact on simulation results

Sludge rheological properties and density are key points in kinematic energy dissipation and flow field on clarifier. From simulations performed, the following can be deducted:

Rheological properties have a great impact on turbulence kinetic energy disipation, however density is the parameter that most influences the sludge transport to sludge hopper.

Given the previous results, it follows that it is important to study the sludge properties experimentally, in order to obtain reliable simulation results. In any case we can expect that the inlet structure designed to dissipate turbulent kinetic energy of an activated sludge with low viscosity and low density, will have also a positive effect over a system operated with a higher viscosity or density sludge, as general pattern (not intensity) of flow field is similar even with different density and rheological parameters, apart form the differences already highlighted.

8.1. Future work

Considering the complexity of the currents developed in the clarifier and the 3D nature of the turbulence phenomenon, it would be very interesting to extend the simulations study to 3D models. A 3D model would also allow the implementation of a more realistic model for the simulation of sludge scrapper. This issue would be important in order to analyse the effect on the scrapper on the sludge transport an its relationship with sludge short-circuit.

On the other hand, although from a qualitative point of view, results shown are in consonance with simulation results of other authors [8, 11] in view of the complexity of the mathematical model used to describe activated sludge sedimentation, as well as the uncertainty about numerous model parameters, an experimental verification of the obtained results should be made in order to verify the quantitative validity of the same.

Regarding the development of design guidelines, more cases should be studied in order to find the best design solution. Also it is very important to make simulations at different scales and operating conditions in order to find adimensional parameters that allows the implementation of the design guidelines, that fits different model sizes and operating conditions.

9. Bibliography:

[1] Metcalf and Eddy, Inc., Tchobanoglous, George, Burton, Flanklin L., and Stensel, H. David, *Wastewater Engineering Treatment and Reuse*, Fourth Edition. McGraw-Hill, 2003.

[2] P. Krebs, "Success and shortcomming of clarifier modelling," *Water Science and Technology*, vol. 31, no. 2, pp. 181–191, 1995.

[3] P. Krebs, D. Vischer, and W. Gujer, "Inlet-Structure Design for Final Clarifiers," *Journal of Environmental Engineering*, vol. 121, no. 8, pp. 558–564, Aug. 1995.

[4] P. Krebs, "The Hydraulics of Final Settling Tanks," *Water Science and Technology*, vol. 23, no. 4–6, pp. 1037–1046, Feb. 1991.

[5] M. Weiss, B. Gy. Plosz, K. Essemiani, and J. Meinhold, "CFD modelling of sludge sedimentation in secondary clarifiers," *WIT Transactions on Engineering Sciences: Advances in Fluid Mechanics VI*, vol. 52, pp. 509–518, 2006.

[6] Dahl, C, Larsen, T, and Petersen, O, "Numerical modelling and measurement in a test secondary settling tank." Water Science and Technology, Vol. 30 No. 2, pp 219-228, 1994.

[7] D. Brennan, "The Numerical Simulation of Two-Phase Flows in Settling Tanks," PhD Thesis, Imperial College of Science, Technology and Medicine, London, 2001.

[8] B. De Clercq, "Computational fluid dynamics of settling tanks: development of experiments and rheological, settling and scrapper submodels," PhD Thesis, Ghent University, Ghent, 2003.

[9] J. De Clercq, M. Devisscher, I. Boonen, P. A. Vanrolleghem, and J. Defrancq, "A new one-dimensional clarifier model - verification using full-scale experimental data," *Water Science and Technology*, vol. 47, no. 12, pp. 105–112, Jun. 2003.

[10] S. H. Cho, F. Colin, M. Sardin, and C. Prost, "Settling velocity model of activated sludge," *Water Research*, vol. 27, no. 7, pp. 1237–1242, Jul. 1993.

[11] D. Burt, "Improved Design of Settling Tanks Using an Extended Drift Flux Model," PhD Thesis, University of Bristol, Bristol, 2010.

[12] Clarifier Design Task Force of the Water Environment Federation, *Clarifier Design*, Second Edition. WEF, 2005.

[13] G. J. Kynch, "A theory of sedimentation," *Transactions of the Faraday Society*, vol. 48, p. 166, 1952.

[14] I. Takacs, "A dynamic model of the clarification-thickening process," *Water Research*, vol. 25, no. 10, pp. 1263–1271, Oct. 1991.

[15] G. Holzinger, "OpenFOAM A little User-Manual." 15-Jun-2018.

[16] C. P. Dahl, "Numerical Modelling of Flow and Settling in Secondary Settling Tanks," PhD Thesis, ATV project EF-359, Aalborg University, Copenhagen, Denmark, 1993.

[17] H. Laikari, *Simulation of the sludge Blanket of a vertical Clarifier in Activated Sludge Process*. Helsinki, 1987.

[18] L. Härtel and H. J. Pöpel, "A Dynamic Secondary Clarifier Model including Processes of Sludge Thickening," *Water Science and Technology*, vol. 25, no. 6, pp. 267–284, Mar. 1992.

[19] F. Mahdavi Mazdeh, "Investigating flocculation and discrete settling behaviour of activated sludge by means of particle size analysis," Master's dissertation, Ghent University, Ghent, 2014.

[20] D.-H. Li and J. J. Ganczarczyk, “Stroboscopic determination of settling velocity, size and porosity of activated sludge flocs,” *Water Research*, vol. 21, no. 3, pp. 257–262, Mar. 1987.

[21] W. A. S. K. Mancell-Egala, D. J. Kinnear, K. L. Jones, H. De Clippeleir, I. Takács, and S. N. Murthy, “Limit of stokesian settling concentration characterizes sludge settling velocity,” *Water Research*, vol. 90, pp. 100–110, Mar. 2016.

[22] E. Torfs, I. Nopens, M. K. H. Winkler, P. A. Vanrolleghem, S. Balemans, and I. Y. Smets, in *Experimental methods in wastewater treatment, T6: Settling test*, M. C. M. van Loosdrecht, P. H. Nielsen, C. M. Lopez-Vazquez, and D. Brdjanovic, Eds. London: IWA Publishing, 2016, pp. 235–262.

[23] AE Ozinsky and GA Ekama, “Secondary settling tank modelling and design Part1: review of theoretical and practical developments,” *Water SA*, vol. 21, no. 4, Oct. 1995.

[24] ATV-DVWK Specialist Committees KA 5 and and KA 6., “ATV-DVWK-A 131E Dimensioning of Single-Stage Activated Sludge Plants.” GFA Publishing Company of ATV-DVWK Water, Wastewater and Waste, May-2000.

[25] N. Ratkovich *et al.*, “Activated sludge rheology: A critical review on data collection and modelling,” *Water Research*, vol. 47, no. 2, pp. 463–482, Feb. 2013.

[26] “ANSYS Fluent Theory Guide Relsease 15.0.” ANSYS, Inc., Nov-2013.

[27] Ishii, M., “One dimensional drift flux model and constitutive equations for relative motion between phases in various two phases flow regimes.” Water Reactor Safety Research--Analysis Development (NCR-4), Oct-1977.

[28] M. Ishii and T. Hibiki, *Thermo-fluid dynamics of two-phase flow*. New York, N.Y: Springer Science+Business Media, 2006.

[29] Bender, Jon and Crosby, Robert M., “Hydraulic Characteristics of Activated Sludge Secondary Clarifiers.” EPA-600/S2-84-131, Sep-1984.

[30] Christopher J. Greenshields, “OpenFOAM UserGuide version 6.” OpenFOAM Foundation Ltd., 10-Jul-2018.

[31] Christopher J. Greenshields, “OpenFOAM Programmers Guide Version 3.0.1.” OpenFOAM Foundation Ltd., CFD Direct Ltd., 13-Dec-2015.

[32] Christophe Geuzaine and Jean-François Remacle, “Gmsh Reference Manual The documentation for Gmsh 4.1.3.” 23-Jan-2019.

[33] James M. Montgomery, “Critical literature review an research needed on Activated Sludge Secondary Clarifiers.” EPA-600/2-87/075, Sep-1987.

10. ANNEX I: Results

rev1.1_refined9

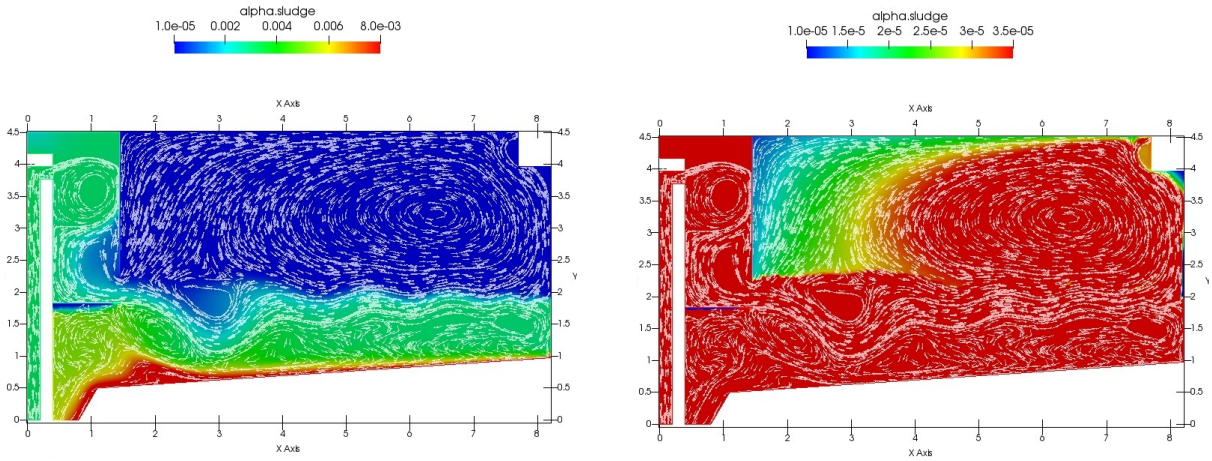

Figure 10.1
Alpha sludge contour (Left High TSS scale / Right Low TSS scale)
rev1.1_refined9

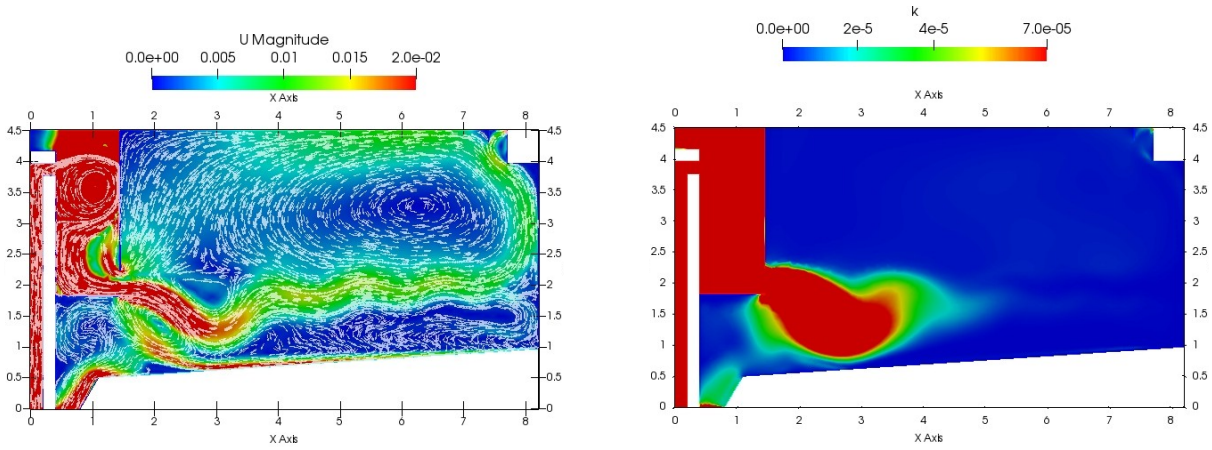

Figure 10.2
Left: U magnitude contour Right: k contour
rev1.1_refined9

rev2_refined9

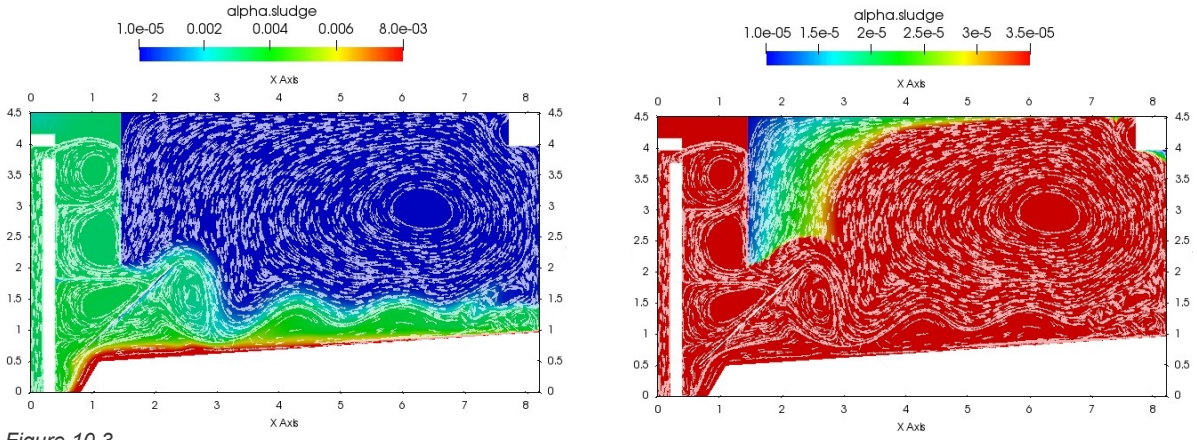

Figure 10.3
Alpha sludge contour (Left High TSS scale / Right Low TSS scale)
rev2_refined9

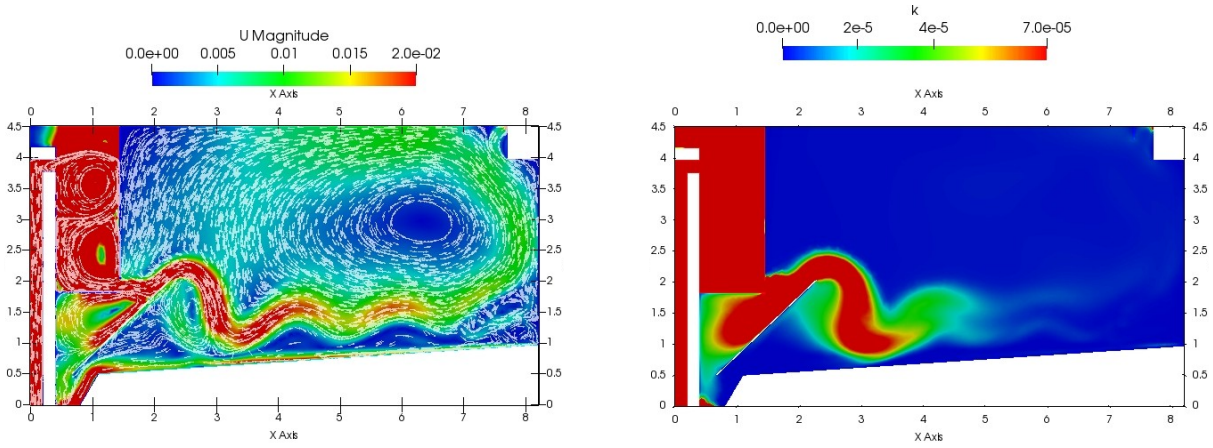

Figure 10.4
Left: U magnitude contour Right: k contour
rev2_refined9

rev3_refined9

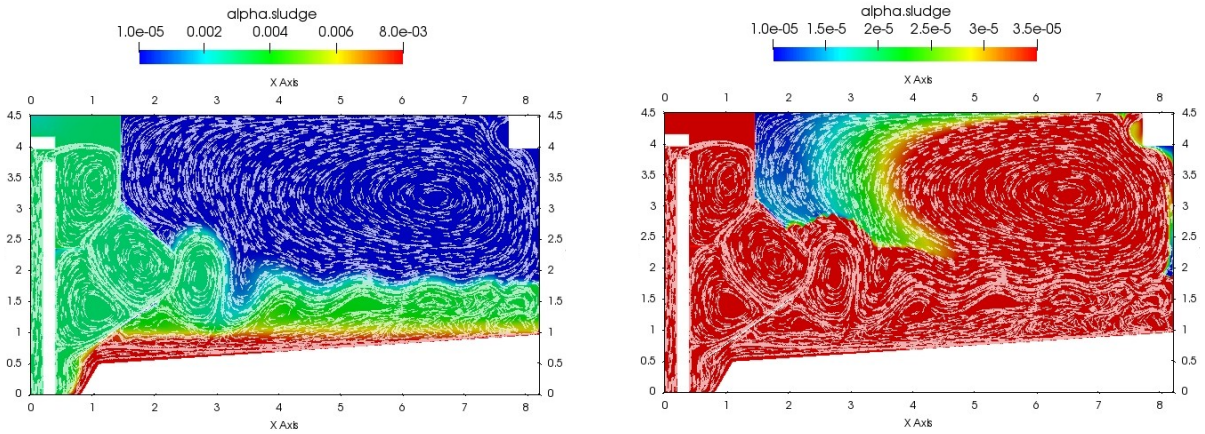

Figure 10.5
Alpha sludge contour (Left High TSS scale / Right Low TSS scale)
rev3_refined9

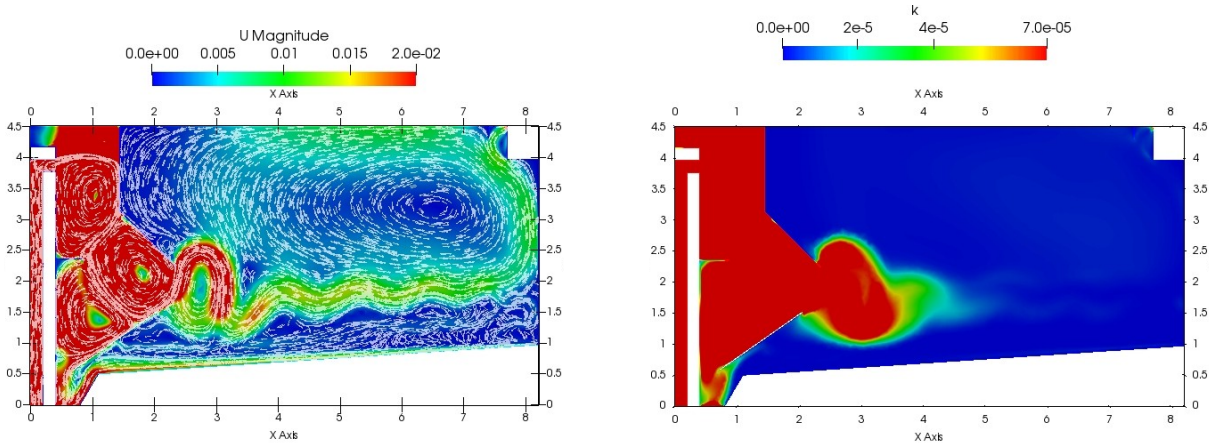

Figure 10.6
Left: U magnitude contour Right: k contour
rev3_refined9

rev4_refined9

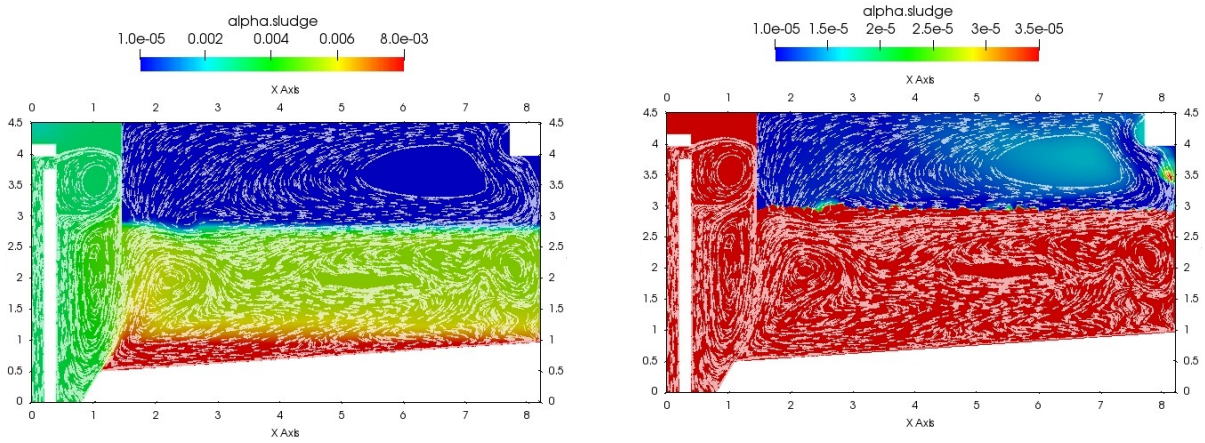

Figure 10.7
Alpha sludge contour (Left High TSS scale / Right Low TSS scale)
rev4_refined9

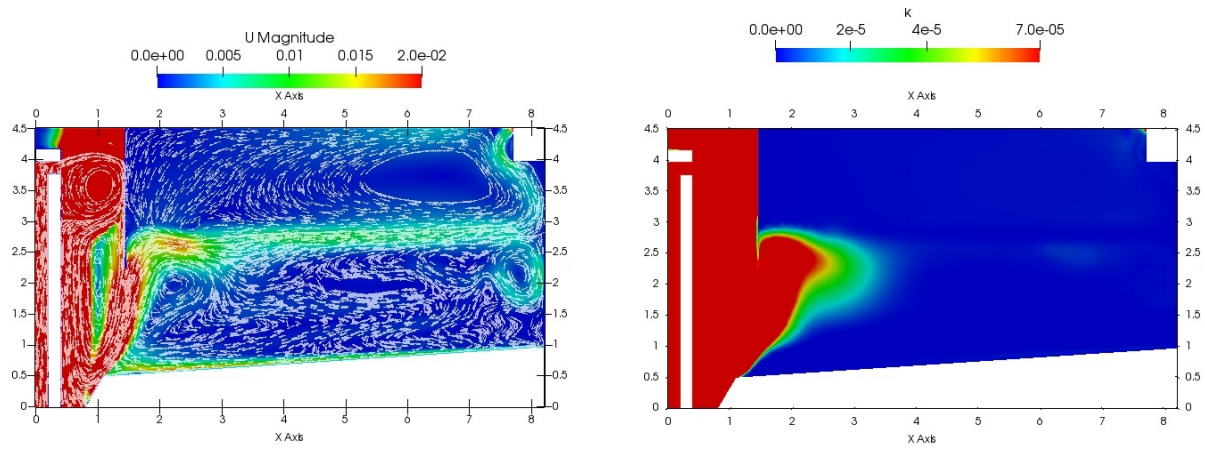

Figure 10.8
Left: U magnitude contour Right: k contour
rev4_refined9

rev5_refined9

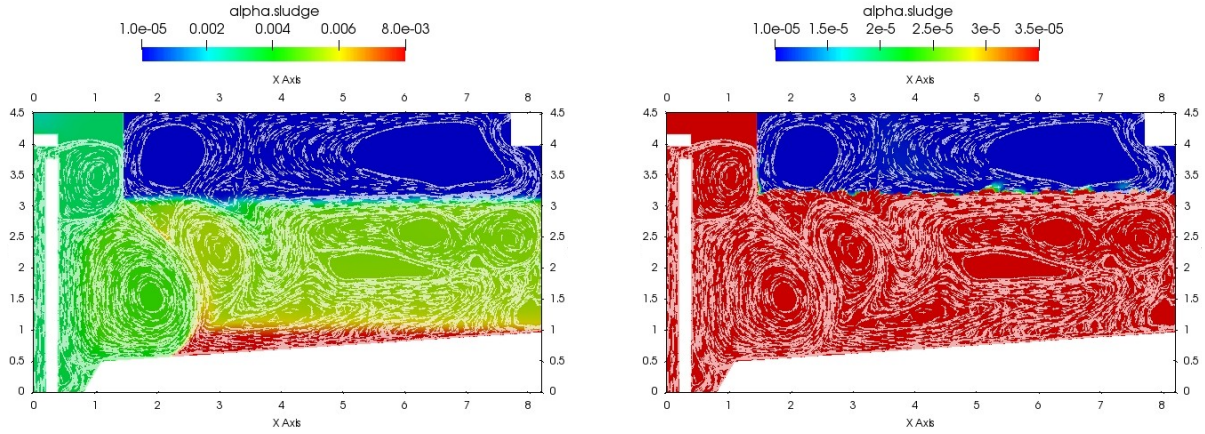

Figure 10.9
Alpha sludge contour (Left High TSS scale / Right Low TSS scale)
rev5_refined9

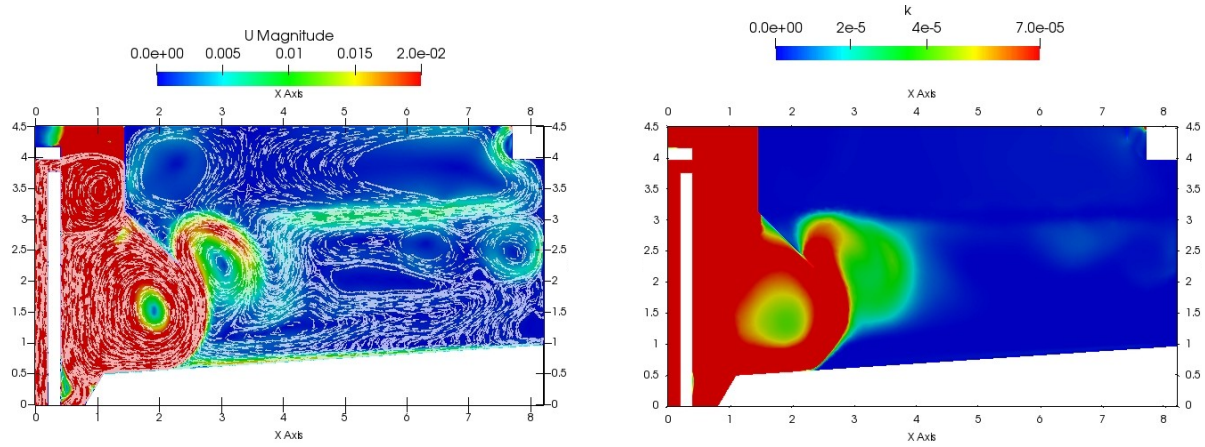

Figure 10.10
Left: U magnitude contour Right: k contour
rev5_refined9

rev6_refined10

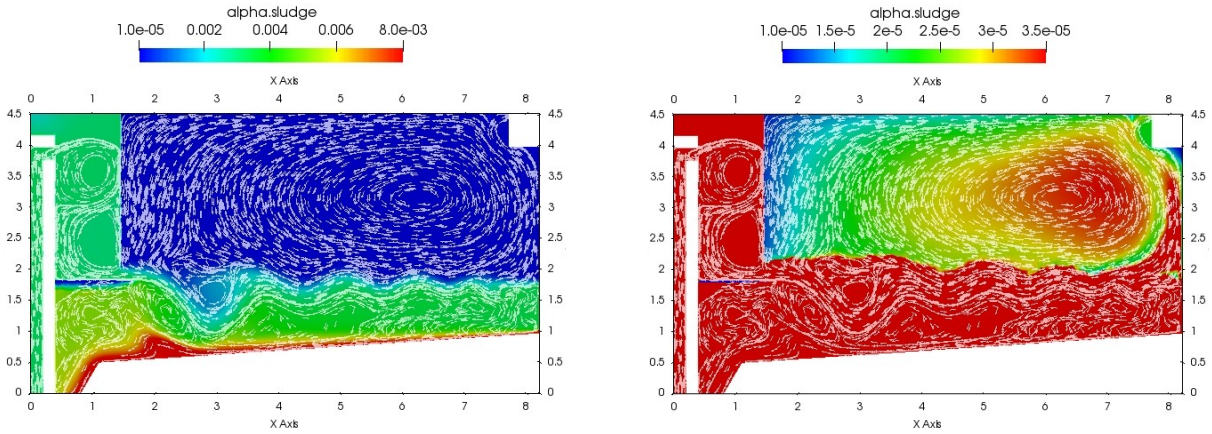

Figure 10.11
Alpha sludge contour (Left High TSS scale / Right Low TSS scale)
rev6_refined10

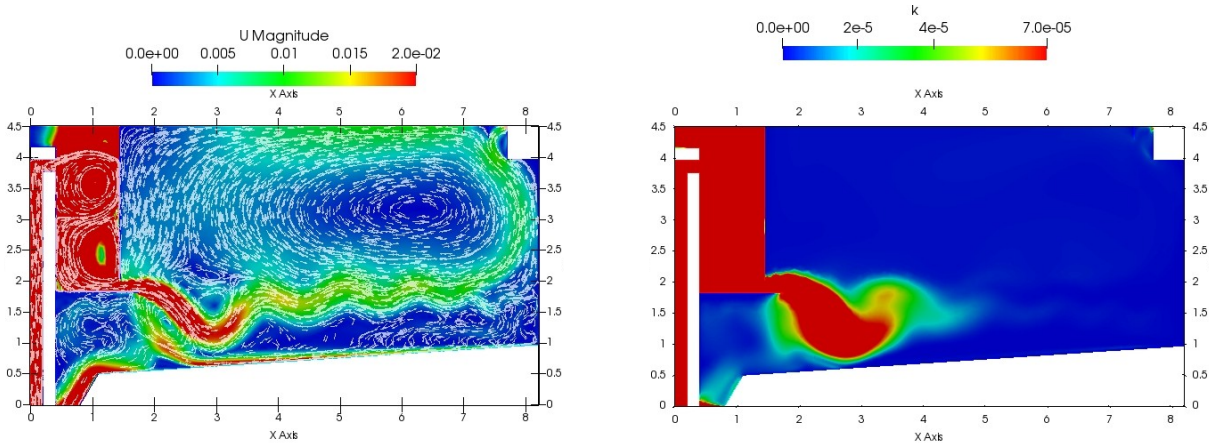

Figure 10.12
Left: U magnitude contour Right: k contour
rev6_refined10

rev7_refined10

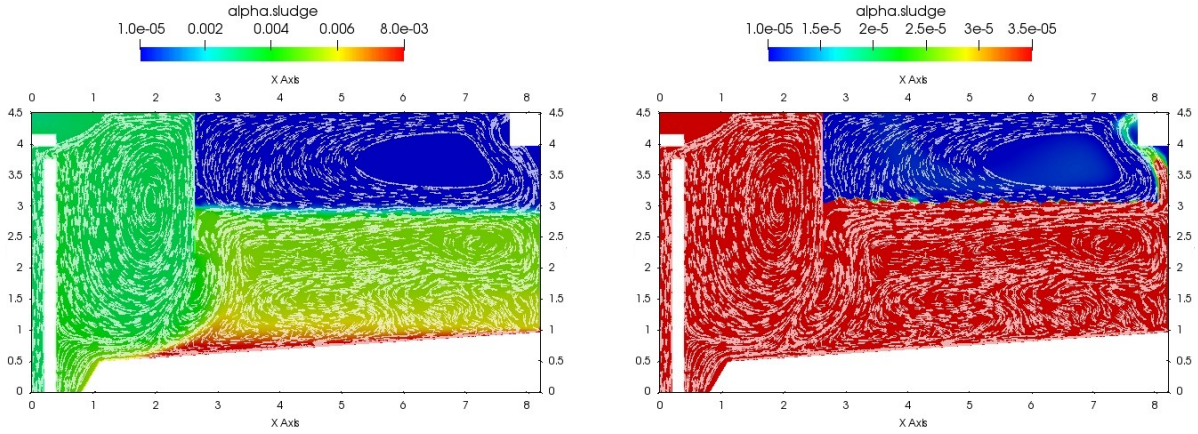

Figure 10.13
Alpha sludge contour (Left High TSS scale / Right Low TSS scale)
rev7_refined10

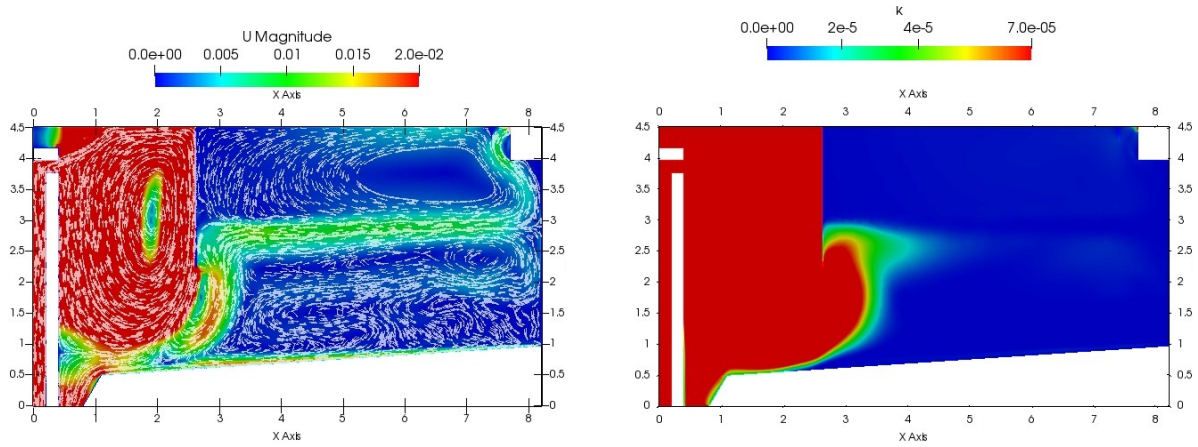

Figure 10.14
Left: U magnitude contour Right: k contour
rev7_refined10

rev6_1_refined10

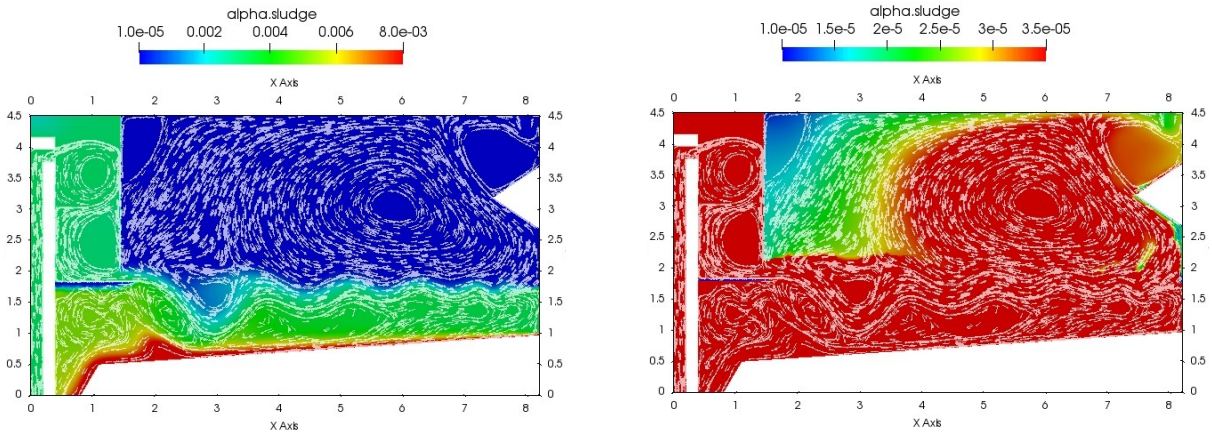

Figure 10.15
Alpha sludge contour (Left High TSS scale / Right Low TSS scale)
rev6_1_refined10

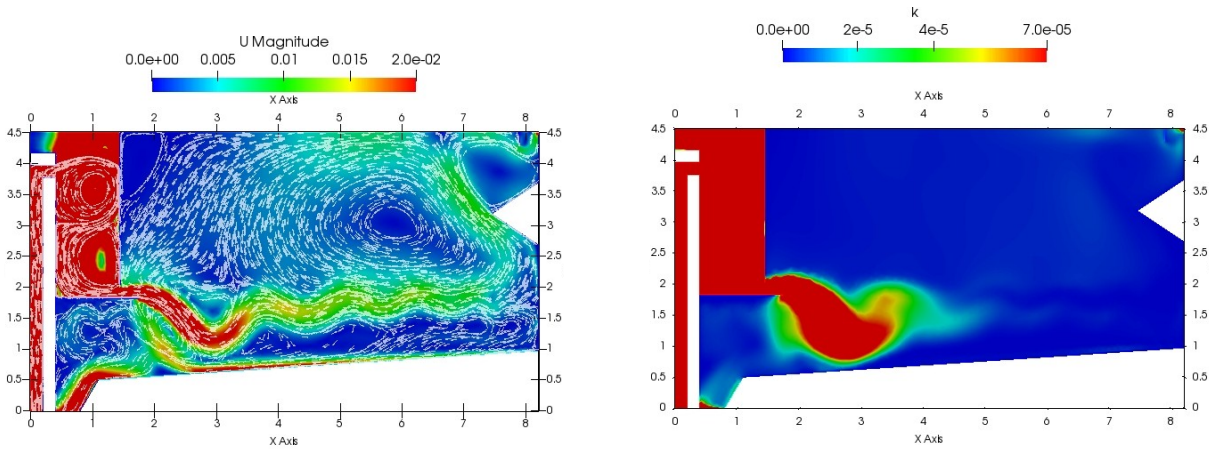

Figure 10.16
Left: U magnitude contour Right: k contour
rev6_1_refined10

rev6_2_refined10

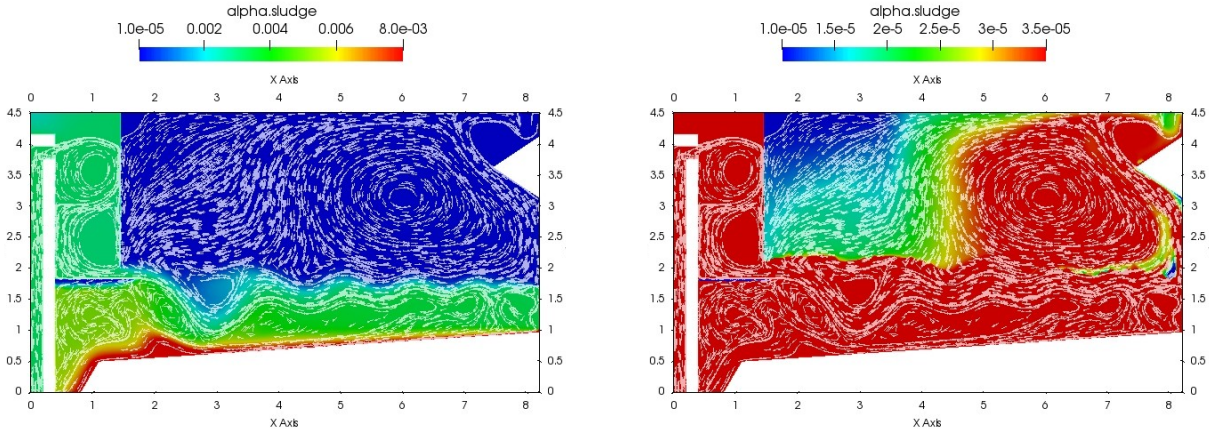

Figure 10.17
Alpha sludge contour (Left High TSS scale / Right Low TSS scale)
rev6_2_refined10

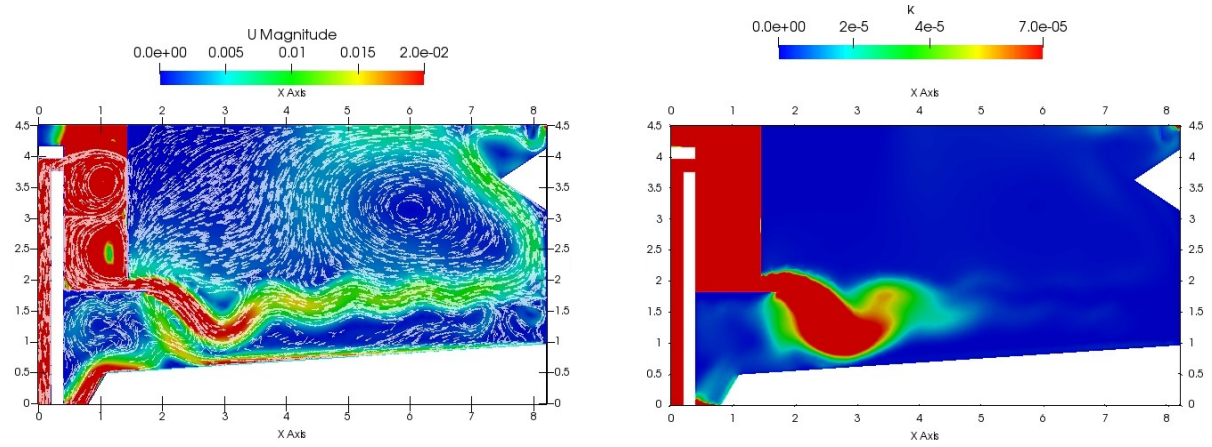

Figure 10.18
Left: U magnitude contour Right: k contour
rev6_2_refined10

rev6_3_refined10

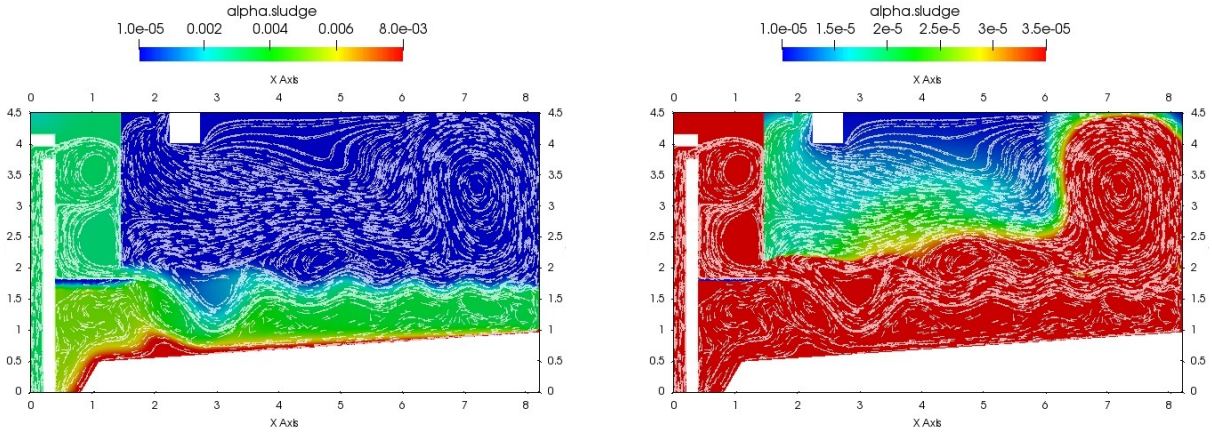

Figure 10.19
Alpha sludge contour (Left High TSS scale / Right Low TSS scale)
rev6_3_refined10

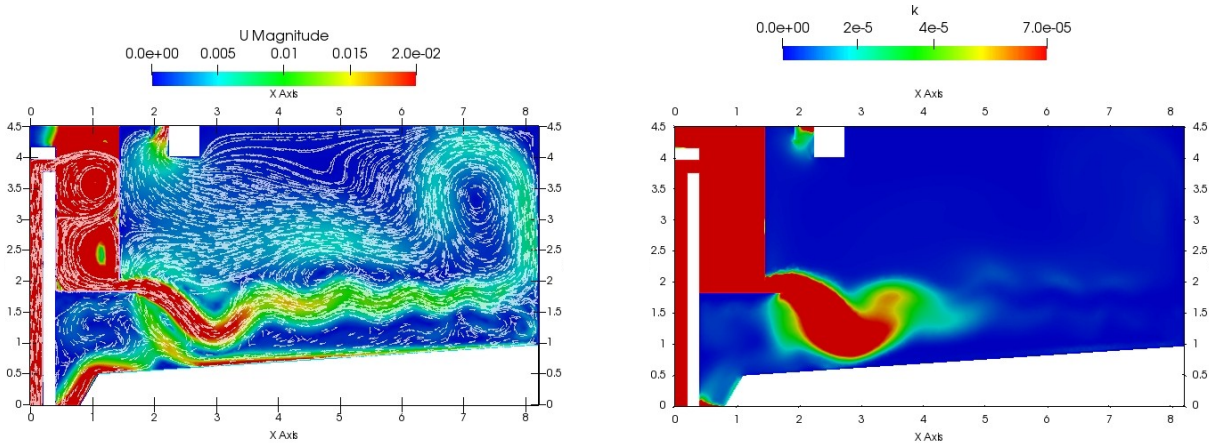

Figure 10.20
Left: U magnitude contour Right: k contour
rev6_3_refined10

rev9_refined10

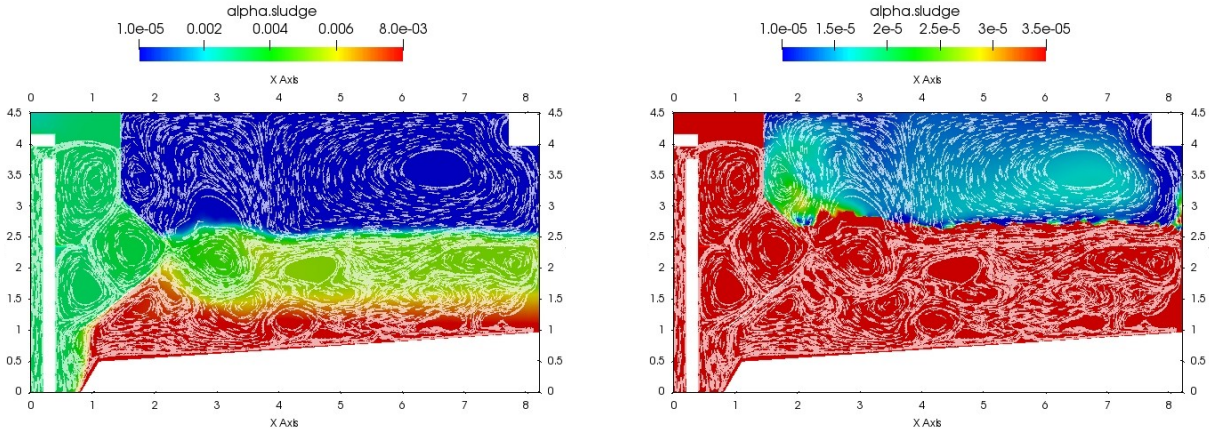

Figure 10.21
Alpha sludge contour (Left High TSS scale / Right Low TSS scale)
rev9_refined10

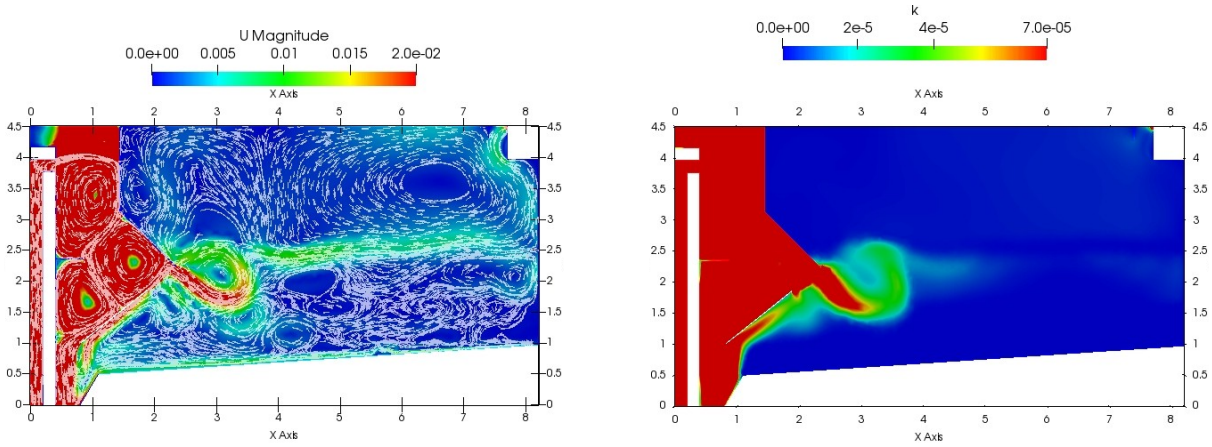

Figure 10.22
Left: U magnitude contour Right: k contour
rev9_refined10

rev10_refined10

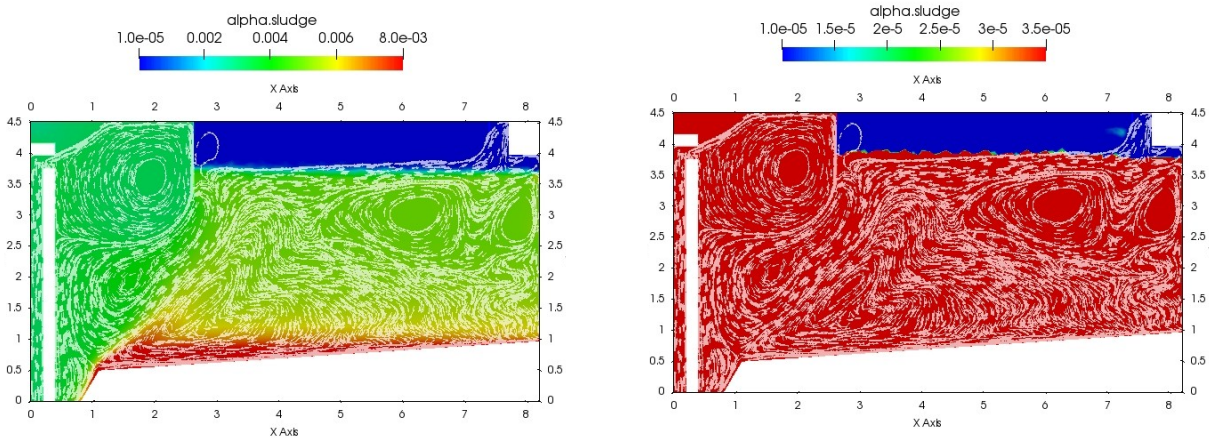

Figure 10.23
Alpha sludge contour (Left High TSS scale / Right Low TSS scale)
rev10_refined10

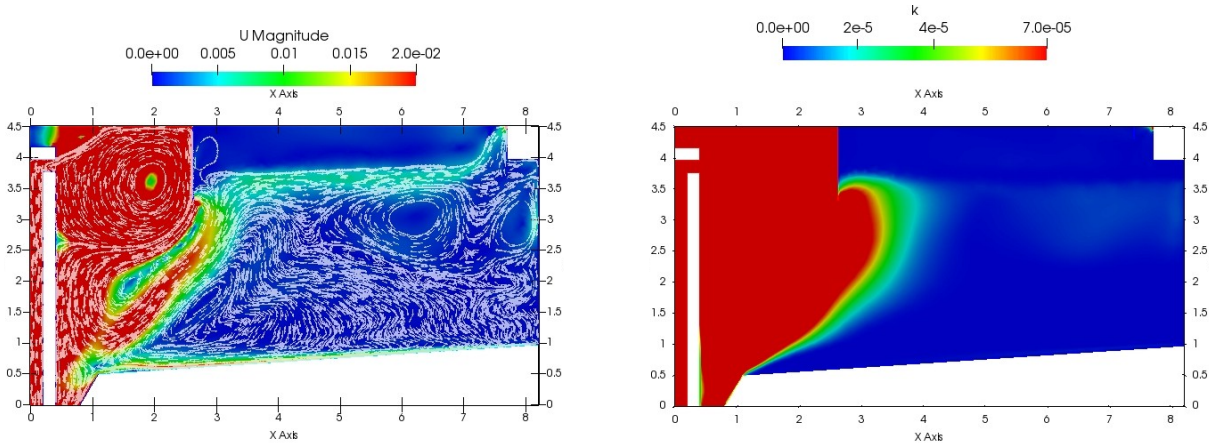

Figure 10.24
Left: U magnitude contour Right: k contour
rev10_refined10

rev11_refined10

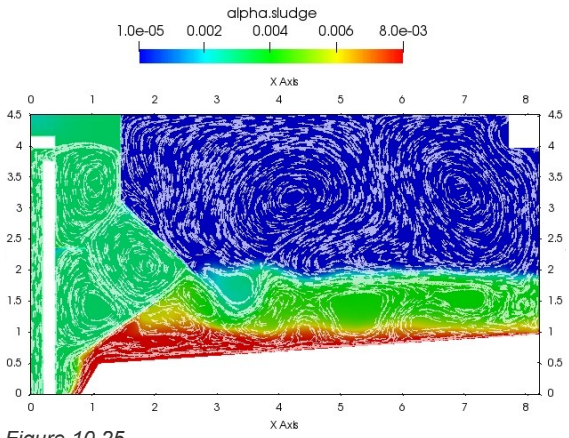

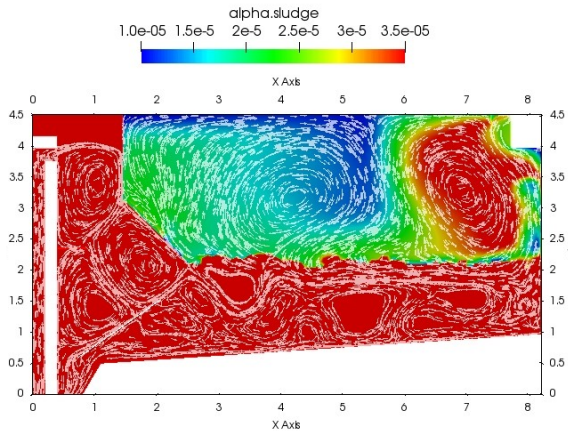

Figure 10.25
Alpha sludge contour (Left High TSS scale / Right Low TSS scale)
rev11_refined10

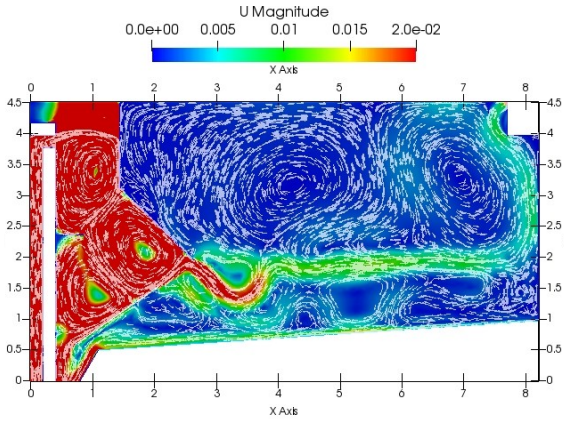

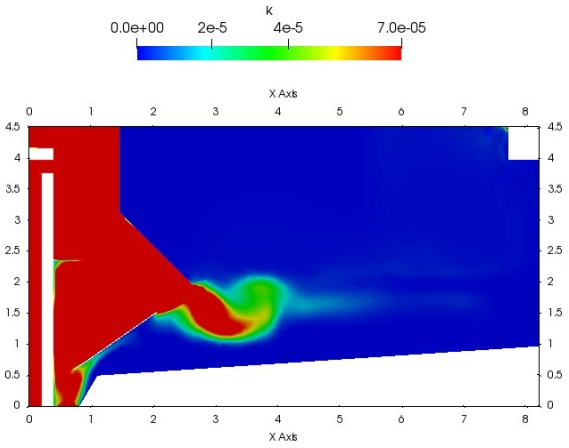

Figure 10.26
Left: U magnitude contour Right: k contour
rev11_refined10

rev11_2_refined10

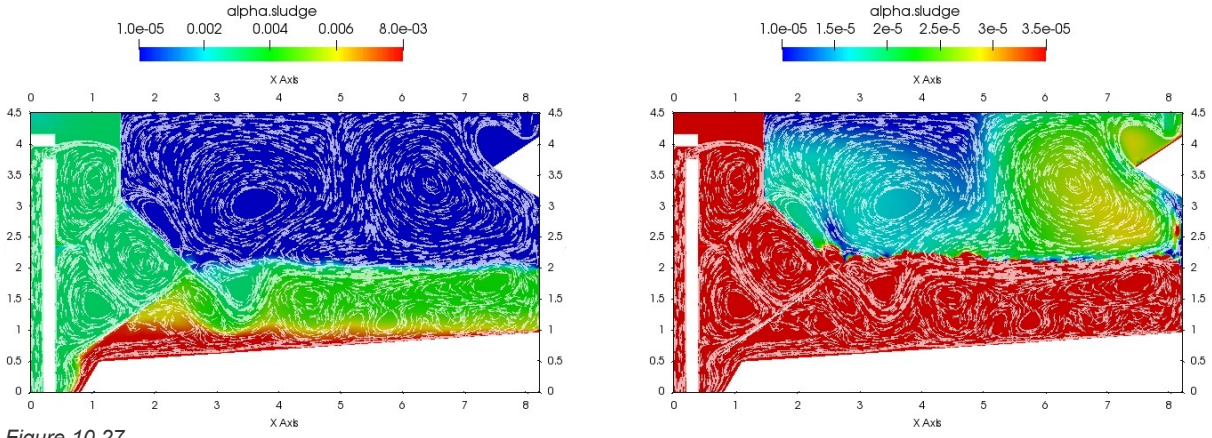

Figure 10.27
Alpha sludge contour (Left High TSS scale / Right Low TSS scale)
rev11_2_refined10

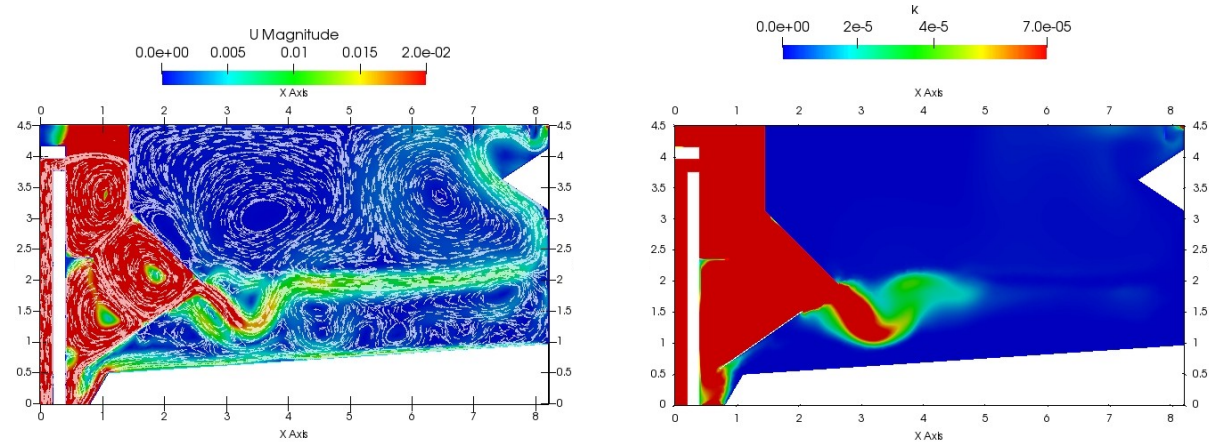

Figure 10.28
Left: U magnitude contour Right: k contour
rev11_2_refined10

rev11_3_refined10

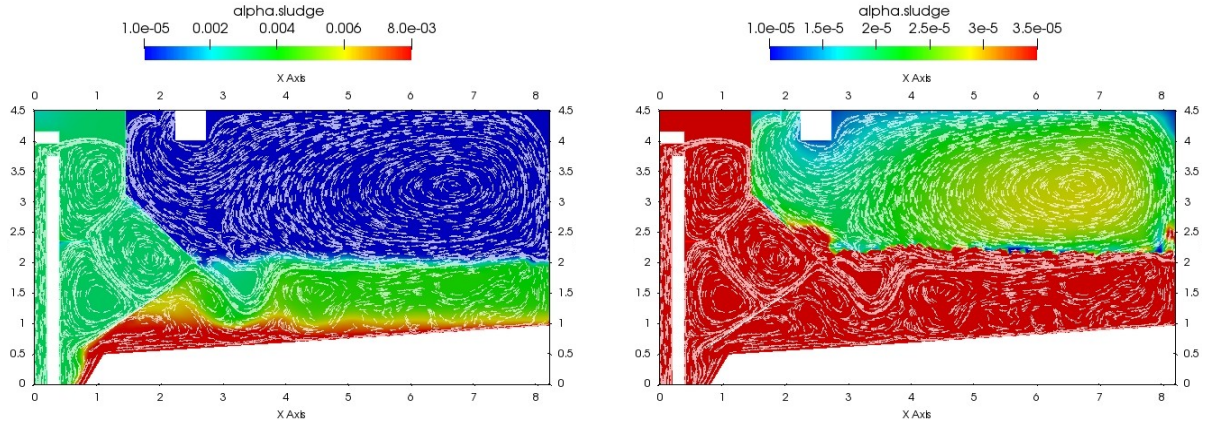

Figure 10.29
Alpha sludge contour (Left High TSS scale / Right Low TSS scale)
rev11_3_refined10

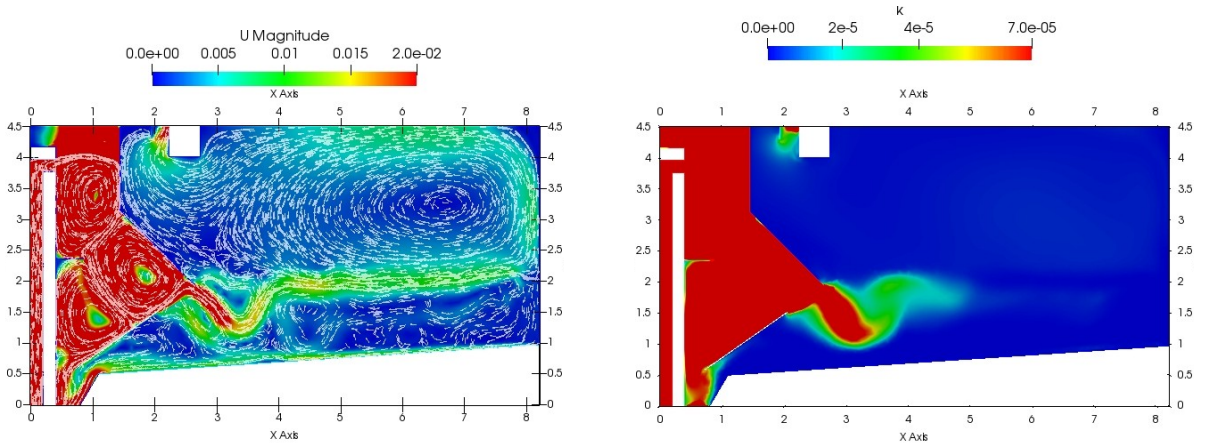

Figure 10.30
Left: U magnitude contour Right: k contour
rev11_3_refined10

rev11_4_refined10

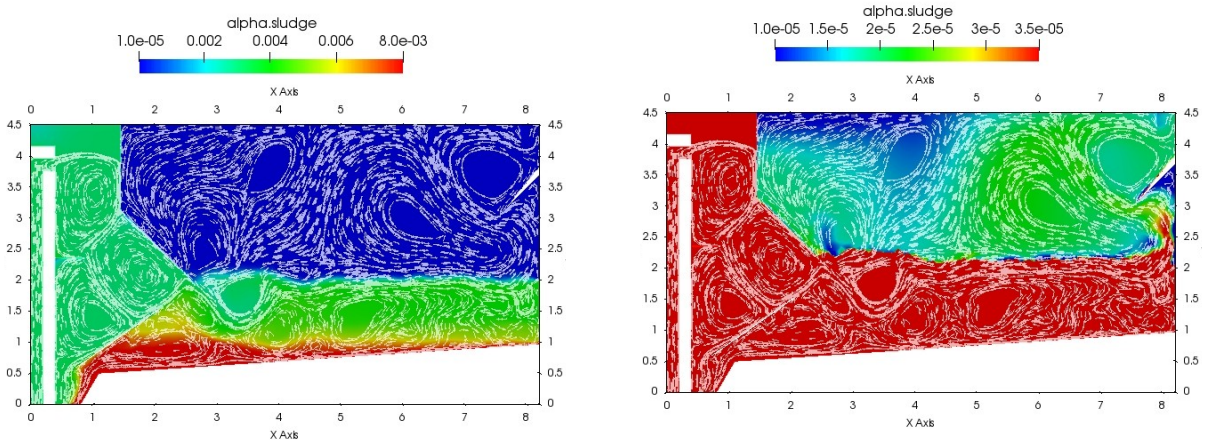

Figure 10.31
Alpha sludge contour (Left High TSS scale / Right Low TSS scale)
rev11_4_refined10

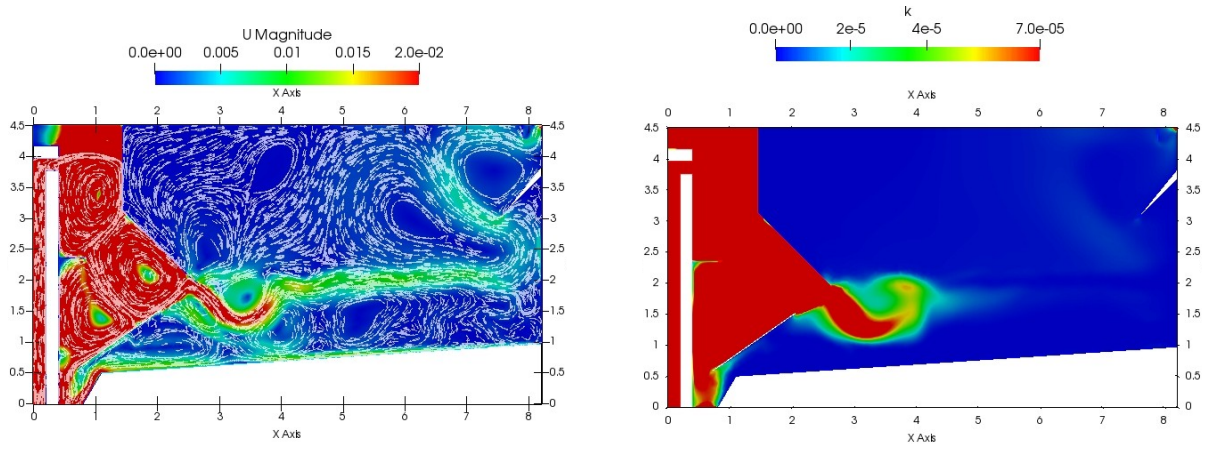

Figure 10.32
Left: U magnitude contour Right: k contour
rev11_4_refined10

rev11_5_refined10

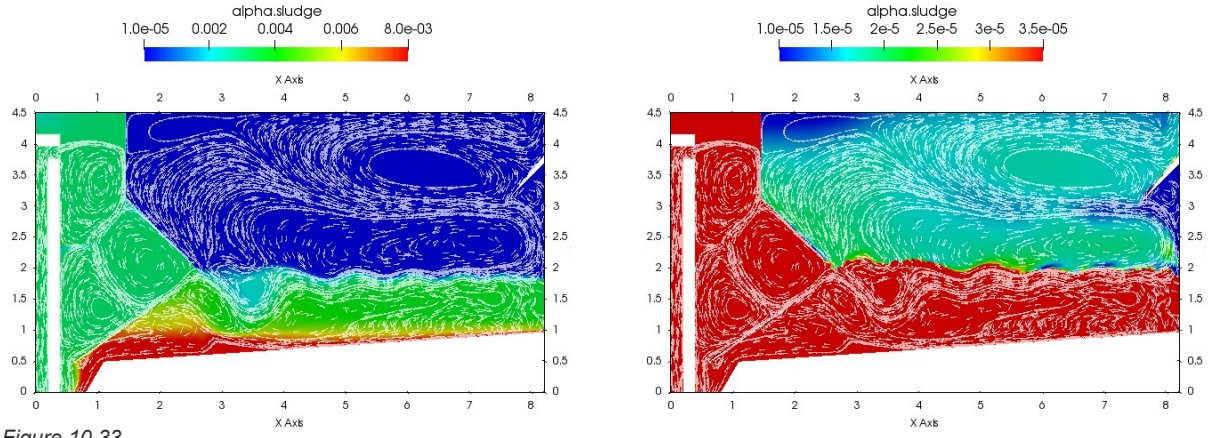

Figure 10.33
Alpha sludge contour (Left High TSS scale / Right Low TSS scale)
rev11_5_refined10

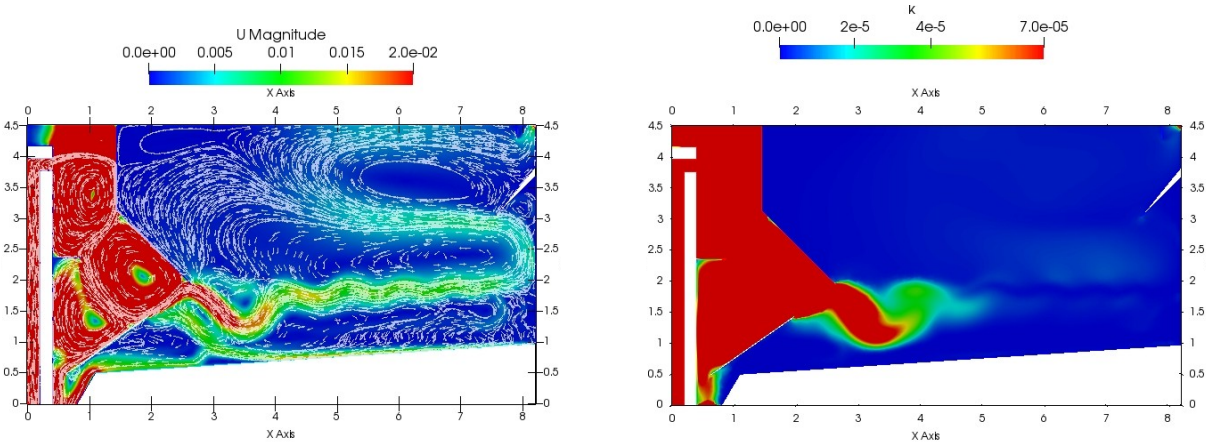

Figure 10.34
Left: U magnitude contour Right: k contour
rev11_5_refined10

rev12_refined10

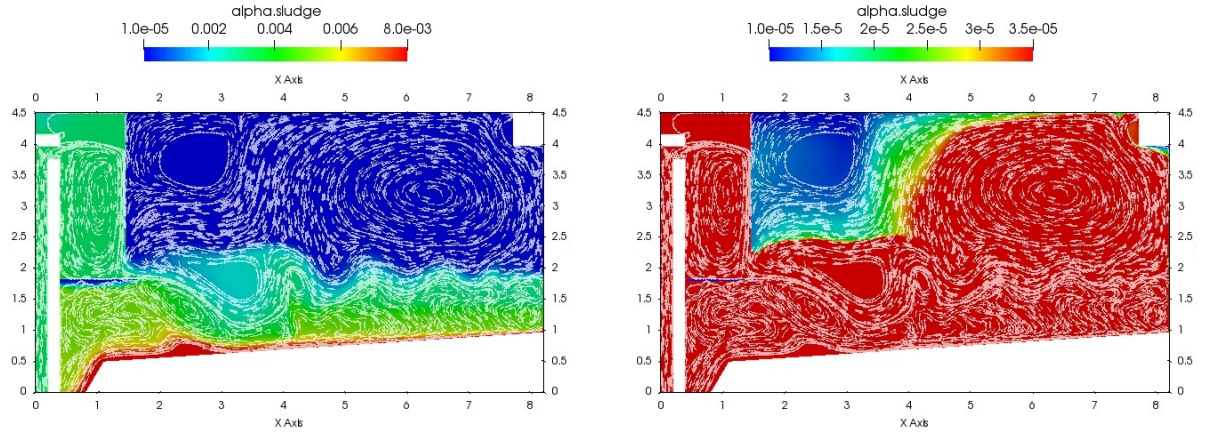

Figure 10.35
Alpha sludge contour (Left High TSS scale / Right Low TSS scale)
rev12_refined10

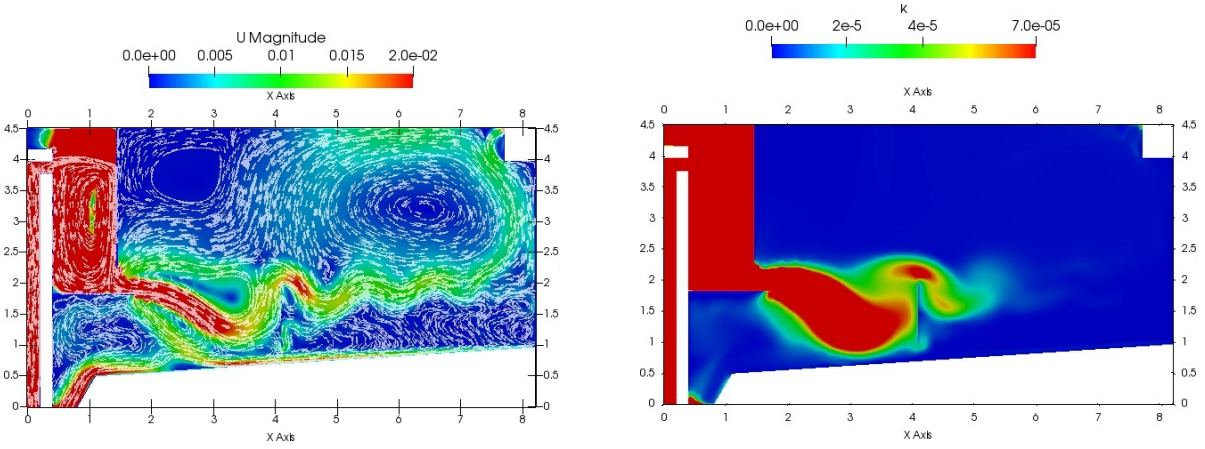

Figure 10.36
Left: U magnitude contour Right: k contour
rev12_refined10

rev12_1_refined10

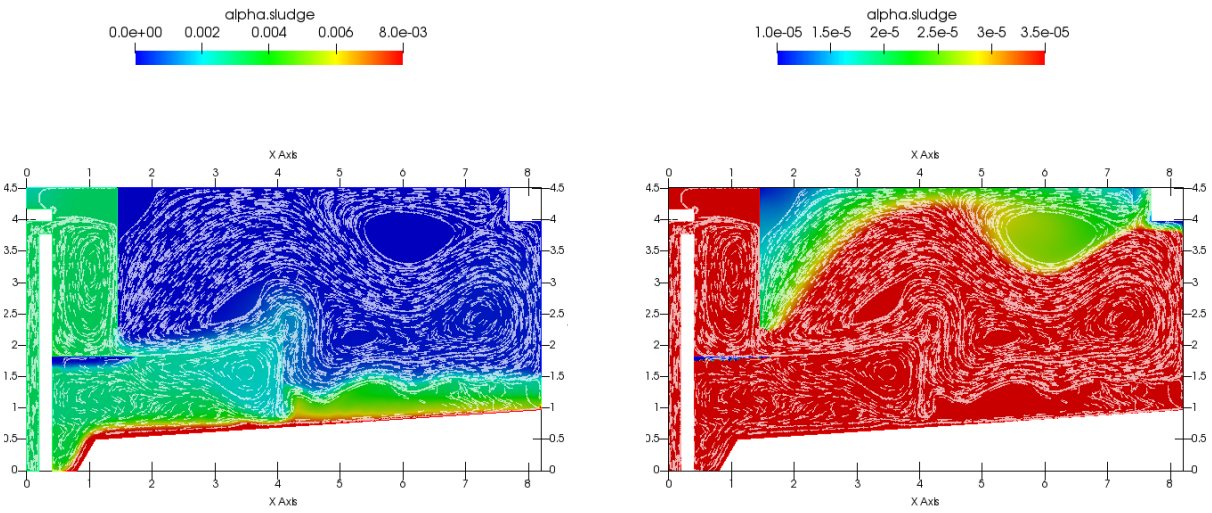

Figure 10.37
Alpha sludge contour (Left High TSS scale / Right Low TSS scale)
rev12_1_refined10

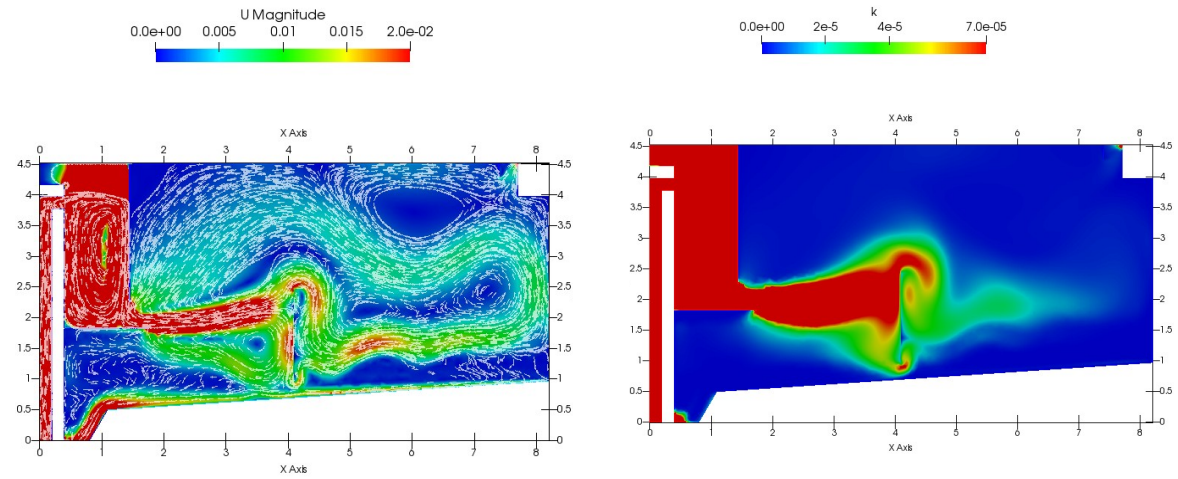

Figure 10.38
Left: U magnitude contour Right: k contour
rev12_1_refined10

11. ANNEX II: Mass balance calculation

The fluxes thought the model patches has been calculated with the openFoam tool: *postProcessing/FlowratePatch:*

Sum of flow through cell faces (m3/s): $flowRatePatch = \int_A \vec{u}\, d\vec{A}$

Total Suspended Solids (TSS) mass balance has been calculated as follows:

$$Total\ TSS\ flux\,(kg/h) = \rho_{sludge}\, Q \frac{1}{A} \int_A \alpha\, d\vec{A}$$

In case of "Inlet" and "Outlet_Sludge" patches, as velocity is imposed as a boundary condition as a uniform value ⇒ Q=constant, so:

$$Total\ TSS\ flux\,(kg/h) = \rho_{sludge} \frac{1}{A} \int_A Q\, \alpha\, d\vec{A} = \rho_{sludge} \frac{1}{A} Q \int_A \alpha\, d\vec{A}$$

In "Outlet_Water" patch, the boundary conditions imposed are not specified as a fixed velocity, so , this implies that $\rho_{sludge} \frac{1}{A} \int_A Q\, \alpha\, d\vec{A} \neq \rho_{sludge} \frac{1}{A} Q \int_A \alpha\, d\vec{A}$

In any case according to the calculations with data extracted from the analysis with paraview, the difference between considering variable velocity or constant velocity across "Outlet_Water" patch, is less than 0.4% for effluent TSS, which implies an error <0.002% in the sludge recirculation TSS. So considering the small error, this calculation is followed to verify the solid mass balance.

12. ANNEX III: Geometry and meshing example

```
/*********************************************************************
 *
 *  Gmsh Gemometry and mesh circular clarifier 9-03-2019
 *
 *
 *
 *********************************************************************/
SetFactory("OpenCASCADE");

// Clarifier general dimensions:

m = 1;


Pendiente_Tolva=1.7;
Pendiente_Dec=1/15;

R_Total=8.2*m;
R_Campana=1.45*m;
H_Campana=2.68*m;
Ap_Campana=0.21*m;
Esp_Campana=0.01*m;
R_T_in=0.2*m;
Esp_Col=0.2*m;
Bp_tolva=0.4*m;
D_T_Fango=0.25*m;
D_T_Agua=0.3*m;
H_Ver=0.5*m;
B_Ver=0.5*m;
H_Lam=0.035*m;
D_Def=0.3*m;
Sub_Def=0.2*m;
Esp_Def=0.01*m;
Hi_tolva=(2*D_T_Fango);
Bi_tolva=Hi_tolva/Pendiente_Tolva;
H_Recta=3.5*m;

R_pend_Dec=R_Total-R_T_in-Esp_Col-Bp_tolva-Bi_tolva;
H_Total=(2*D_T_Fango)+(R_pend_Dec*Pendiente_Dec)+H_Recta;


Lc1 = 0.1;
Lc2 = 0.005;

i=1;

```

```
Desp_mall1=0.025;
Desp_mall2=0.05;//0.05 //Inlet Area
Desp_mall3=0.15; //Carification area
Desp_mall4=0.0;//Central symmetry axis



// Then we define some points and some lines using these variables:
// We use i variable to introduce new points, in between in an easy way

//Geometry
Point(i) = {0   ,0      ,0      , Lc1}; //Point(1)
i=i+1;
Translate {R_T_in, 0, 0} {  Duplicata { Point{i-1}; } }                          //Point(2)
i=i+1;
Translate {0,H_Total-0.3-Esp_Col-R_T_in, 0} {  Duplicata { Point{i-1}; } }       //Point(3)
i=i+1;
Translate {Esp_Col,0, 0} {  Duplicata { Point{i-1}; } }                          //Point(4)
i=i+1;
p1=newp;                                                                         //Last point + 1
Point(p1) = {R_T_in+Esp_Col,H_Total+H_Lam-H_Campana,0   , Lc1};                  //Point(5)
i=i+1;

//Points 6 and 8 define influent well lower baffle diameter
Translate {1.2*R_Campana-Esp_Col-R_T_in,0, 0} {  Duplicata { Point{i-1}; } }    //Point(6)
i=i+1;
Translate {0,-Esp_Campana, 0} {  Duplicata { Point{i-1}; } }                    //Point(7)
i=i+1;
Translate {-(1.2*R_Campana-Esp_Col-R_T_in),0, 0} {  Duplicata { Point{i-1}; } } //Point(8)
i=i+1;
Translate {Esp_Col,0, 0} {  Duplicata { Point{2}; } }                            //Point(9)
i=i+1;
Translate {Bp_tolva,0, 0} {  Duplicata { Point{i-1}; } }                         //Point(10)
i=i+1;
Translate {Bi_tolva,Hi_tolva, 0} {  Duplicata { Point{i-1}; } }                  //Point(11)
i=i+1;
Translate {R_pend_Dec,R_pend_Dec*Pendiente_Dec, 0} {Duplicata {Point{i-1}; }}    //Point(12)
i=i+1;
Translate {0,H_Recta-(2*H_Campana/3), 0} {  Duplicata { Point{i-1}; } }          //Point(13)
i=i+1;
Translate {-1.5*B_Ver,H_Ver, 0} {  Duplicata { Point{i-1}; } }                   //Point(14)
i=i+1;
Translate {1.5*B_Ver,H_Ver, 0} {  Duplicata { Point{i-1}; } }                    //Point(15)
i=i+1;
Translate {0,(2*H_Campana/3)-(2*H_Ver), 0} {  Duplicata { Point{i-1}; } }        //Point(16)
i=i+1;
```

```
Translate {0,H_Lam, 0} {  Duplicata { Point{i-1}; } }                          //Point(17)
i=i+1;
Translate {-D_Def,0, 0} {  Duplicata { Point{i-1}; } }                         //Point(18)
i=i+1;
Translate {0,-Sub_Def, 0} {  Duplicata { Point{i-1}; } }                       //Point(19)
i=i+1;
Translate {-Esp_Def,0, 0} {  Duplicata { Point{i-1}; } }                       //Point(20)
i=i+1;
Translate {0,Sub_Def, 0} {  Duplicata { Point{i-1}; } }                        //Point(21)
i=i+1;
Marca=newp;
Point(Marca) = {R_Campana       ,H_Total+H_Lam  ,0      , Lc1};                //Point(22)
i=i+1;
Translate {0,-(H_Campana-Ap_Campana), 0} {  Duplicata { Point{i-1}; } }        //Point(23)
i=i+1;
Translate {-Esp_Campana,0, 0} {  Duplicata { Point{i-1}; } }                   //Point(24)
i=i+1;
Translate {0,H_Campana-Ap_Campana, 0} {  Duplicata { Point{i-1}; } }           //Point(25)
i=i+1;
Marca=newp;
Point(Marca) = {0,H_Total+H_Lam ,0, Lc1};                                      //Point(26)
//Printf(" Marca=%g", Marca); This is used to print in the screen the actual poin number
i=i+1;
Translate {0,-H_Lam-D_Def, 0} {  Duplicata { Point{i-1}; } }                   //Point(27)
i=i+1;
Translate {R_T_in+Esp_Col,0, 0} {  Duplicata { Point{i-1}; } }                 //Point(28)
i=i+1;
Translate {0,-Esp_Col, 0} {  Duplicata { Point{i-1}; } }                       //Point(29)
i=i+1;
Translate {-(R_T_in+Esp_Col),0, 0} {  Duplicata { Point{i-1}; } }              //Point(30)
i=i+1;
Translate {0,-R_T_in, 0} {  Duplicata { Point{i-1}; } }                        //Point(31)
i=i+1;


ult_P=newp-1;
//This is used to print in the screen the actual poin number
Printf(" Numero de puntos contorno exterior ult_P=%g", ult_P);



k=1;
//Internal point to make the structured meshAhora creamos los puntos internos para el mallado estructurado

k=k+1;
Translate {-Desp_mall1,Desp_mall4, 0} {  Duplicata { Point{k}; } }             //Point 32
```

```
k=k+1;
Translate {-Desp_mall1,Desp_mall1, 0} {  Duplicata { Point{k}; } }              //Point 33
k=k+1;
Translate {Desp_mall1,Desp_mall1, 0} {  Duplicata { Point{k}; } }               //Point 34
k=k+1;
Translate {Desp_mall1,Desp_mall1, 0} {  Duplicata { Point{k}; } }               //Point 35
k=k+1;
Translate {Desp_mall1,Desp_mall1, 0} {  Duplicata { Point{k}; } }               //Point 36
k=k+1;
Translate {Desp_mall1,-Desp_mall1, 0} {  Duplicata { Point{k}; } }              //Point(37)
k=k+1;
Translate {Desp_mall1,-Desp_mall1, 0} {  Duplicata { Point{k}; } }              //Point(38)
k=k+1;
Translate {Desp_mall1,Desp_mall1, 0} {  Duplicata { Point{k}; } }               //Point(39)
k=k+1;
Translate {-Desp_mall1,Desp_mall1, 0} {  Duplicata { Point{k}; } }              //Point(40)
k=k+1;
Translate {-Desp_mall1,Desp_mall1, 0} {  Duplicata { Point{k}; } }              //Point(41)
k=k+1;
Translate {-Desp_mall1,Desp_mall1, 0} {  Duplicata { Point{k}; } }              //Point(42)
k=k+1;
Translate {-Desp_mall1,-Desp_mall1, 0} {  Duplicata { Point{k}; } }             //Point(43)
k=k+1;
Translate {-Desp_mall1,0, 0} {  Duplicata { Point{k}; } }                       //Point(44)
k=k+1;
Translate {-Desp_mall1,Desp_mall1, 0} {  Duplicata { Point{k}; } }              //Point(45)
k=k+1;
Translate {-Desp_mall1,-Desp_mall1, 0} {  Duplicata { Point{k}; } }             //Point(46)
k=k+1;
Translate {-Desp_mall1,-Desp_mall1, 0} {  Duplicata { Point{k}; } }             //Point(47)
k=k+1;
Translate {Desp_mall1,-Desp_mall1, 0} {  Duplicata { Point{k}; } }              //NUEVO 48
k=k+1;
Marca=newp-1;
Printf(" Marca=%g", Marca);
Translate {Desp_mall1,-Desp_mall1, 0} {  Duplicata { Point{k}; } }              //Point(49)
k=k+1;
Translate {-Desp_mall1,-Desp_mall1, 0} {  Duplicata { Point{k}; } }             //Point(50)
k=k+1;
Translate {-Desp_mall1,-Desp_mall1, 0} {  Duplicata { Point{k}; } }             //Point(51)
k=k+1;
Translate {Desp_mall1,-Desp_mall1, 0} {  Duplicata { Point{k}; } }              //Point(52)
k=k+1;
Translate {Desp_mall1,-Desp_mall1, 0} {  Duplicata { Point{k}; } }              //Point(53)
k=k+1;
Translate {-Desp_mall1,-Desp_mall1, 0} {  Duplicata { Point{k}; } }             //Point(54)
```

```
k=k+1;
Translate {-Desp_mall1,-Desp_mall1, 0} {  Duplicata { Point{k}; } }             //Point(55)
k=k+1;
Translate {0,-Desp_mall1, 0} {  Duplicata { Point{k}; } }                       //Point(56)
k=k+1;
Translate {Desp_mall4,Desp_mall1, 0} {  Duplicata { Point{k}; } }               //Point(57)
k=k+1;
Translate {Desp_mall1,Desp_mall1, 0} {  Duplicata { Point{k}; } }               //Point(58)
k=k+1;
Translate {Desp_mall1,-Desp_mall1, 0} {  Duplicata { Point{k}; } }              //Point(59)
k=k+1;
Translate {Desp_mall4,-Desp_mall1, 0} {  Duplicata { Point{k}; } }              //Point(59)
k=k+1;
Translate {Desp_mall4,-Desp_mall1, 0} {  Duplicata { Point{k}; } }              //Point(60)
k=k+1;


ult_P1=newp-1;
Printf(" Ultimo numero de punto contorno  mallado estructurado ult_P1=%g", ult_P1);


//We create another inside layer to control size of internal mesh

k=ult_P+1;
//Ahora creamos otra capa mas para controlar el mallado interior
//Translate {Desp_mall2,Desp_mall2, 0} {  Duplicata { Point{k}; } }             //Point 61
//k=k+1;
Translate {-Desp_mall2,0, 0} {  Duplicata { Point{k}; } }                       //Point 62
k=k+1;
Translate {-Desp_mall2,Desp_mall2, 0} {  Duplicata { Point{k}; } }              //Point 63
k=k+1;
Translate {Desp_mall2,Desp_mall2, 0} {  Duplicata { Point{k}; } }               //Point 64
k=k+1;
Translate {Desp_mall2,Desp_mall2, 0} {  Duplicata { Point{k}; } }               //Point 65
k=k+1;
Translate {Desp_mall3,Desp_mall2, 0} {  Duplicata { Point{k}; } }               //Point 66
k=k+1;
Translate {Desp_mall3,-Desp_mall3, 0} {  Duplicata { Point{k}; } }              //Point 67
k=k+1;
Translate {Desp_mall3,-Desp_mall3, 0} {  Duplicata { Point{k}; } }              //Point 68
k=k+1;

Translate {Desp_mall3,4*Desp_mall3, 0} {  Duplicata { Point{k}; } }             //Point 69
k=k+1;
Translate {-Desp_mall3,4*Desp_mall3, 0} {  Duplicata { Point{k}; } }            //Point 70
k=k+1;
```

```
231
232   Translate {-2*Desp_mall3,4*Desp_mall3, 0} {  Duplicata { Point{k}; } }          //Point 71
233   k=k+1;
234   Translate {-2*Desp_mall3,4*Desp_mall3, 0} {  Duplicata { Point{k}; } }          //Point 72
235   k=k+1;
236   Translate {-2*Desp_mall3,-Desp_mall2, 0} {  Duplicata { Point{k}; } }           //Point 73
237   k=k+1;
238   Translate {-2*Desp_mall3,0, 0} {  Duplicata { Point{k}; } }                     //Point 74
239   k=k+1;
240   Translate {-2*Desp_mall2,0, 0} {  Duplicata { Point{k}; } }                     //Point 75
241   k=k+1;
242   Translate {-Desp_mall2,-Desp_mall2, 0} {  Duplicata { Point{k}; } }             //Point 76
243   k=k+1;
244   Translate {-Desp_mall2,-Desp_mall2, 0} {  Duplicata { Point{k}; } }             //Point 77
245   k=k+1;
246   Translate {Desp_mall2,-Desp_mall2, 0} {  Duplicata { Point{k}; } }              //Point 78
247   k=k+1;
248   Translate {Desp_mall2,-Desp_mall2, 0} {  Duplicata { Point{k}; } }              //Point 79
249   k=k+1;
250   Translate {-Desp_mall3,-Desp_mall2, 0} {  Duplicata { Point{k}; } }             //Point 80
251   k=k+1;
252   Translate {-Desp_mall3,-Desp_mall3, 0} {  Duplicata { Point{k}; } }             //Point 81
253   k=k+1;
254   Translate {Desp_mall3,-Desp_mall3, 0} {  Duplicata { Point{k}; } }              //Point 82
255   k=k+1;
256   Translate {Desp_mall3,-Desp_mall2, 0} {  Duplicata { Point{k}; } }              //Point 83
257   k=k+1;
258   Translate {-Desp_mall2,-Desp_mall2, 0} {  Duplicata { Point{k}; } }             //Point 84
259   k=k+1;
260   Translate {-Desp_mall2,-Desp_mall2, 0} {  Duplicata { Point{k}; } }             //Point 85
261   k=k+1;
262   Translate {Desp_mall2,-Desp_mall2, 0} {  Duplicata { Point{k}; } }              //Point 86
263   k=k+1;
264   Translate {Desp_mall2,Desp_mall2, 0} {  Duplicata { Point{k}; } }               //Point 87
265   k=k+1;
266   Translate {Desp_mall2,Desp_mall2, 0} {  Duplicata { Point{k}; } }               //Point 88
267   k=k+1;
268   Translate {Desp_mall2,-Desp_mall2, 0} {  Duplicata { Point{k}; } }              //Point 89
269   k=k+1;
270   Translate {Desp_mall2,-Desp_mall2, 0} {  Duplicata { Point{k}; } }              //Point 90
271   k=k+1;
272   Translate {Desp_mall2,0, 0} {  Duplicata { Point{1}; } }                        //Point(91)
273   k=k+1;
274
275
276   ult_P2=newp-1;
```

```
// Print in scereen for reference
Printf(" Ultimo numero de punto mallado interno ult_P2=%g", ult_P2);


// Rotate all the generated points in order to be able to use wedge boundary conditions in openFoam
For i In {1:ult_P2}
  Rotate {{0, 1, 0}, {0, 0, 0}, -Pi/180} {
  Point{i};
  }
EndFor


//Macro create lines see tutorial t5.geo y t8.geo
Macro CrearLineas
        l1 = newl; // "newl" gives number+1, where number is last existing line
        Line(l1) = {t,t+1};
Return


// We can use a `For' loop to generate lines:
fin=ult_P-1;
For t In {1:fin}
  // We call the macro:
  Call CrearLineas ;
EndFor

//This is the last line that closes the bucle
Line(fin+1) = {fin+1,1}; //Create a newline

ult_L=newl-1;

Printf(" Numero de lineas contorno exterior ult_L=%g", ult_L);


//**********************IMP LINES CAN NOT BE DUPLICATED OTHERWISE IT GOES TO ERROR

// We can use a `For' loop to generate lines:

inicio=ult_P+1;
fin=ult_P1-1;
For t In {inicio:fin}
  // We call the macro:
  Call CrearLineas ;
EndFor

ult_L1=newl-1;
```

```
Printf("Ultimo numero de linea contorno mallado estructurado ult_L1=%g", ult_L1);



//Create the lines that conects external lines and the lines for the estructured
// mesh in order to be able to generate the estructured mesh
fin=ult_P-1;
Macro CrearLineas1
        l1 = newl; Line(l1) = {t,t+fin};
        thelines[t] = newl ;
Return

For t In {2:fin}
  // We call the macro:
  Call CrearLineas1 ;
EndFor

ult_L2=newl-1;
Printf(" Ultimo numero de linea contorno mallado estructurado ult_L2=%g", ult_L2);



// We can use a `For' loop to generate lines:

inicio=ult_P1+1;
fin=ult_P2-1;
For t In {inicio:fin}
  // We call the macro:
  Call CrearLineas ;
EndFor

//This is the last line that closes the internal bucle
l1=newl;
Line(l1) = {ult_P2, ult_P1+1}; //genero la linea nueva

ult_L3=newl-1;
Printf(" Ultimo numero de linea contorno interno ult_L3 =%g", ult_L3);


//Lines to close the internal loop
l1=newl;
Line(l1) = {ult_P1, 1}; //new line
l1=newl;
Line(l1) = {1, ult_P2}; //new line
l1=newl;
Line(l1) = {ult_P1+1, ult_P+1}; //new line
```

```
369
370  L_bucle_intermedio_1=newl-3;
371  L_bucle_intermedio_2=newl-2;
372  L_bucle_intermedio_3=newl-1;
373
374
375  Printf(" Las lineas de cierre del bucle intermdio son %g, %g y %g", L_bucle_intermedio_1,L_bucle_intermedio_2,
     L_bucle_intermedio_3);
376
377
378
379  //*******************************Loops and areas for structured mesh
380
381  //*******************************
382
383
384  index=newll;
385  Printf(" newLine=%g", index);
386  i=2;//1;
387  j=i+ult_L1-1;
388  k=i+ult_L-1;
389  cont=1;
390  Printf(" Area inicio mallado estructurado=%g", cont);
391
392  For t In {index:index+(2*ult_L)-8}
393          //Printf(" i=%g", i);
394          //Printf(" j=%g", j);
395          //Printf(" k=%g", k);
396          //Printf(" t=%g", j+1);
397
398
399          If (i!=(ult_L-5)) //Me salto el area que caeria en el eje
400                  Curve Loop(t) = {i,j,k,j+1};
401                  Plane Surface(cont) = {t};
402                  cont=cont+1;
403          EndIf
404          i=i+1;
405          j=j+1;
406          k=k+1;
407          t=t+1;
408
409
410  //in each round 2 number are used one for the "curve loop" and the other for the "Palne surface"
411
412  EndFor
413  cont=cont-1;
```

```
414
415  Printf(" Area fin mallado estructurado=%g", cont);
416
417
418
419
420  //Internal area
421  //Create a vector with lines number that I'm going to use in cueve loop
422  //Index start in 0
423
424  j=0;
425  For k In {ult_L2+1:ult_L3}
426          //Printf(" k=%g", k);
427          CL_array[j]=k;
428          j=j+1;
429  EndFor
430
431  //We use previous vector to make the loop
432  t=newll;
433
434  cont1=cont+1;
435  Curve Loop(t) = CL_array[];
436  Plane Surface(cont1) = {t};
437  Printf(" Area interna central=%g", cont1);
438
439
440
441  //Middle area with hole
442
443
444  j=0;
445  For k In {ult_L+1:ult_L1}
446          CL_array0[j]=k;
447          //Printf(" CL_array0[%g]=%g",j, CL_array0[j]);
448          j=j+1;
449  EndFor
450
451  For k In {ult_L3+1:ult_L3+2}
452          CL_array0[j]=k;
453          //Printf(" CL_array0[%g]=%g",j, CL_array0[j]);
454          j=j+1;
455  EndFor
456
457  //This loop goes in reverse direction
458  r=ult_L3-1;
459  For k In {ult_L2+1:ult_L3-1}
```

```
460         CL_array0[j]=r;
461         //Printf(" CL_array0[%g]=%g",j, CL_array0[j]);
462         r=r-1;
463         j=j+1;
464 EndFor
465
466 CL_array0[j]=ult_L3+3;
467 //Printf(" CL_array0[%g]=%g",j, CL_array0[j]);
468
469
470
471 //We use previous vector to make the loopp
472 t=newll;
473 cont2=cont1+1;
474 Curve Loop(t) = CL_array0[];
475
476 Plane Surface(cont2) = {t};
477 Printf(" Curve loop%g", t);
478 Printf(" Area interna intermedia cont2=%g", cont2);
479
480
481
482
483
484 //*******************************Mesh with transfinite
485
486 // Instead of using the umber of point to divide each line we use a size of division
487 // To do this we need to know the coordenates of each point
488 // This is done: c[] = Point{1}; // c[] contains the coordinates 1,2,3
489 // Coordenate over we fi x the distance, 0=x, 1=y, 2=z
490
491
492 //Mesh of external and middle lines
493 inicio=ult_L+1;
494 For i In {inicio:ult_L1}
495
496         j=i+1;
497         delta=0.05*m;           //Mesh size
498         If (i==40+2)
499                 delta=0.02*m;   //Mesh size
500         EndIf
501         If (i==41+2)
502                 delta=0.02*m;   //Mesh size
503         EndIf
504         If (i==44+2)
505                 delta=0.005*m;  //Mesh size
```

```
506         EndIf
507         If (i==43+2)
508                 delta=0.02*m;   //Mesh size
509         EndIf
510         If (i==45+2)
511                 delta=0.02*m;   //Mesh size
512         EndIf
513         If (i==46+2)
514                 delta=0.02*m;   //Mesh size
515         EndIf
516         If (i==47+2)
517                 delta=0.02*m;   //Mesh size
518         EndIf
519         If (i==48+2)
520                 delta=0.02*m;   //Mesh size
521         EndIf
522         c1[] = Point{i}; c2[] = Point{j};
523         Ndiv=Round(Sqrt(((c1[0]-c2[0])^2)+((c1[1]-c2[1])^2))/delta);
524
525         Transfinite Curve{i} = Ndiv Using Progression 1; //Bump 0.15;
526         Transfinite Curve{i-ult_L+1} = Ndiv Using Progression 1; //Bump 0.15;
527 EndFor
528
529
530 //Mesh of conexion lines between external and middle lines, fix the thisness of mesh
531 j=2;
532 k=j+ult_L-1;
533 par=1;
534
535 For i In {ult_L1+1:ult_L2}
536
537         If (par==2)
538                 par=par-2;
539         EndIf
540
541         delta=0.01*m;           //Mesh size
542         c1[] = Point{j}; c2[] = Point{k};
543
544         Ndiv=3;
545         Transfinite Curve{i} = Ndiv Using Progression 1; //Bump 0.15;
546         par=par+1;
547
548 EndFor
549
550
551 //Internal lines meshing
```

```
inicio=ult_L2+1;
fin=ult_L3;
Printf(" inicio=%g", inicio);
Printf(" fin=%g", fin);

j=ult_P1+1;
k=j+1;

For i In {inicio:fin}

        delta=0.1*m;            //Mesh size
        If (i==98+5)
                delta=0.02*m;   //Mesh size
        EndIf
        If (i==99+5)
                delta=0.005*m;  //Mesh size
        EndIf

        If (i==100+5)
                delta=0.02*m;   //Mesh size
        EndIf
        If (i==101+5)
                delta=0.02*m;   //Mesh size
        EndIf
        If (i==102+5)
                delta=0.02*m;   //Mesh size
        EndIf

        c1[] = Point{j}; c2[] = Point{k};
        Ndiv=Round(Sqrt(((c1[0]-c2[0])^2)+((c1[1]-c2[1])^2))/delta);
        Transfinite Curve{i} = Ndiv Using Progression 1; //Bump 0.15;

        j=j+1;
        If (j==ult_P2)
                k=ult_P1+1;
        EndIf
        If (j<ult_P2)
                k=j+1;
        EndIf
EndFor

For k In {1:cont}

        Transfinite Surface{k};
        Recombine Surface {k};
EndFor
```

```
598
599
600   //We make the strusion to generate the sector
601   fin=cont2;
602   For k In {1:fin}
603
604           Extrude {{0, 1, 0}, {0, 0, 0}, (Pi/90)} {
605                   Surface{k}; Layers{1}; Recombine;
606           }
607   EndFor
608
609
610
611
612   //We Define the surfaces and the phisycal volumen
613
614   //+
615   Physical Surface("Inlet") = {220, 191, 250, 33};
616   //+
617   Physical Surface("Inlet_pipe") = {29+1};
618   //+
619   Physical Surface("Column") = {34+1, 39+1, 59+1, 152+1, 158, 147+2};
620   //+
621   Physical Surface("Outlet_Sludge") = {64+1};
622   //+
623   Physical Surface("Outlet_Water") = {100};
624   //+
625   Physical Surface("Free_Surface") = {125, 105, 145};
626   //+
627   Physical Surface("Out_Wall") = {79+1};
628   //+
629   Physical Surface("Weir_Wall") = {84+1, 89+1, 95};
630   //+
631   Physical Surface("Deflectora") = {114+1, 109+1, 109+1+10};
632   //+
633   Physical Surface("Pend_Dec") = {74+1};
634   //+
635   Physical Surface("Tolva") = {69+1};
636   //+
637   Physical Surface("Campana") = {134+1, 140, 129+1, 54+1, 44+1, 49+1};
638   //+
639   Physical Surface("Simetry_Plane1") = {1, 2, 3, 4, 5, 6, 7, 8, 9, 10, 11, 12, 13, 14, 15, 16, 17, 18, 19, 20, 21, 22, 23,
      24, 25, 26, 27, 28, 29};
640   //+
641   Physical Surface("Simetry_Plane2") = {84, 89, 94, 79, 74, 69, 124, 119, 114, 109, 104, 99, 59, 54, 49, 64, 44, 39, 34,
      192, 251, 157, 152, 148, 144, 139, 134, 129, 161};
```

```
642  //+
643  Physical Volume("fluidVolume") = {1, 2, 3, 4, 5, 6, 7, 8, 9, 10, 11, 12, 13, 14, 15, 16, 17, 18, 19, 20, 21, 22, 23, 24,
     25, 26, 27, 28, 29};
644
645
646  //IMP after export the mesh a ASCII 2 with the name "DecCircular_rev6_1_refined10.msh" execute
647  //Merge "DecCircular_rev6_1_refined10.msh";
648  //Coherence Mesh;
```

Erratum

In page 25, Figure 5.1 must be replaced by the following figure:

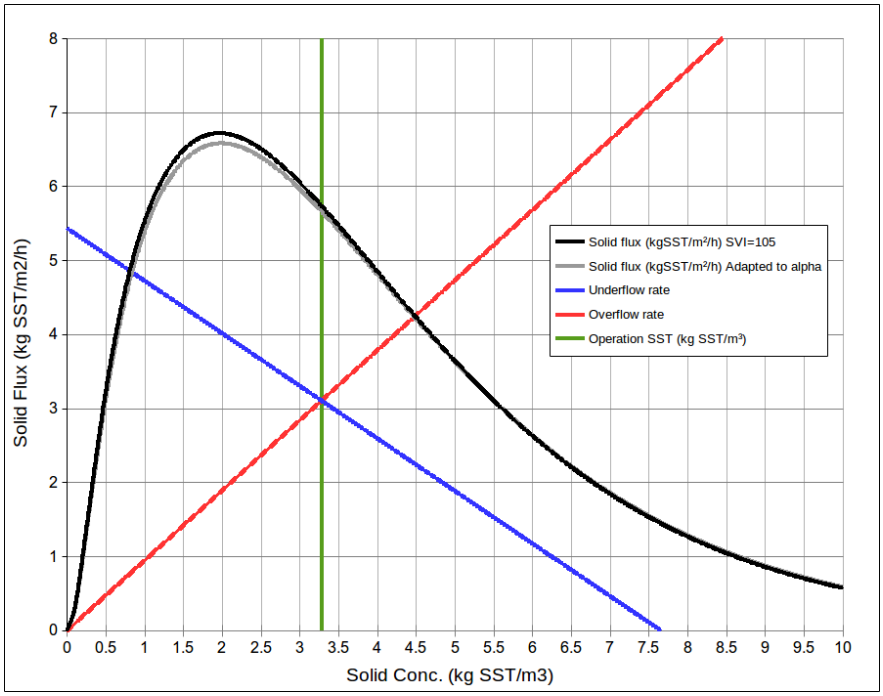

In page 24 the following test

"As it is shown in Figure 5.1 the system is operating very close to the critical condition, so the safety margin is almost zero. Under these conditions, depending on the hydraulic structures design the system can suffer a failure condition, with the lack of capacity for enough sludge removal."

must be replaced by:

"As it is shown in Figure 5.1 the system is operating below the critical condition. Under these conditions, according to solid flux theory the system should not suffer a critical failure due to under-sizing."